N° Ordre...../Institut/UMBB/2019

REPUBLIQUE ALGERIENNE DEMOCRATIQUE ET POPULAIRE
MINISTERE DE L'ENSEIGNEMENT SUPERIEUR ET DE LA RECHERCHE SCIENTIFIQUE
UNIVERSITE M'HAMED BOUGARA-BOUMERDES

Institut de **G**énie **E**lectrique et **E**lectronique

Thèse de Doctorat

Présenté par :
DJAFRI Kahina

En vue de l'obtention du diplôme de **DOCTORAT** en :
Filière : Génie Electrique et Electrotechnique
Option : ***Télécommunications***

TITRE : Contribution to the Study and Design of Miniaturized Microstrip Antennas

Devant le jury composé de :

Mr	DAHIMENE	Abdelhakim	Professeur	UMBB	Président
Mr	CHALLAL	Mouloud	Professeur	UMBB	Rapporteur
Mr	AKSAS	Rabia	Professeur	ENP	Co-Rapporteur
Mr	KIMOUCHE	Hocine	Professeur	EMP	Examinateur
Mr	TOUNSI	Mohamed Lamine	Professeur	USTHB	Examinateur

Année Universitaire 2018/2019

To my parents,

To my brothers,

To my sisters,

To my friends.

Kahina Djafri

Acknowledgments

All gratitude is due to ALLAH for giving me the strength, courage, and commitment that enabled me to start and finish this research work.

I want to express my sincere gratitude and appreciation to my advisors Prof.CHALLAL Mouloud and Prof. AKSAS Rabia for their continuous support, encouragement and guidance throughout the accomplishment of this work.

I would like to express my sincere gratitude to Prof. ROMEU Jordi at Communication Signal and System laboratory of Universitat Politecnica de Catalunya, Barcelona, Spain for his guidance and support during the 45 days (from 1^{st} June to 15 July 2017) fruitful internships accomplished in the CommSensLab laboratory under his guidance.

I would like to extend my sincere gratitude to the dissertation committee composed of Prof. DAHIMENE Abdelhakim, Prof. KIMOUCHE Hocine and Prof.TOUNSI Mohamed Lamine for devoting their time to review this thesis and advising me with valuable suggestions.

I am deeply thankful to Prof. AZRAR Arab and Dr. DEHMAS Mokrane for their encouragement, useful advices and support throughout this research work.

I am deeply thankful to my colleague and friend Mrs MOUHOUCHE Faiza for her encouragement, support during fabrication and measurements of the prototypes throughout my research.

Finally, I would like to deeply thank my family for all of their overall encouragement and provided support.

Kahina Djafri

ملخص

تتنـاول هذه الأطروحـة دراسة و تصميـم هوائيات مستوية مصغرة. الجزء الأول يشرح كيفية تصميم ,تحليل و قياس هوائيـات مصغرة, أحادية القطب وثنـائية التردد ذات شكل حلقي منحدرة من شكـل كسري (fractal). الجـزء الثاني يعرض تحليـل و تصميـم هوائيـات مصغـرة ثلاثيـة التـردد. الجزء الأخير يشـرح كيفية تصميـم هوائيـة مصغرة على شكل حرف U للتطبيـق في المجال الطبـي " تنظيـر القولـون" . نتائـج المحـاكـاة و القيـاسات التي تـم الحصول عليها متوافقة فيما بينها ، الشيء الذي يثبت صحة أداء الهوائيـات المقترحـة.

الكلمـات المفتـاح: تصغيـر، هوائـي فركتالـي ، هوائي متعـدد التـردد ، التطبيقـات اللاسكليـة، RFID , WiMAX , WLAN.

Résumé

Cette thèse porte sur l'étude, la conception et l'implémentation d'antennes planaires miniaturisées. La première partie présente la conception, l'analyse et le test d'antennes monopoles compactes à géometrie fractale pour une application à double bande. La deuxième partie traite la conception, l'analyse et réalisation d'antennes compactes tri-bande pour les applications sans fil. La dernière partie est dédiée à la conception d'une antenne compacte à fente en forme de "U" et à cavité pour une application de coloscopie. Les résultats de mesure et de simulations ont montré un bon accord validant ainsi les différentes configurations proposées et les procédures de conception adoptées.

Mot-clés : Miniaturisation, antenne fractale, antenne multibande, applications san fil, WLAN, WiMAX, RFID.

Abstract

This thesis focuses on the study, design and implementation of miniaturized planar antennas. The first part presents the design, analysis and test of compact fractal shaped monopole antennas for dual-band application. The second part deals with design, analysis and implementation of compact tri-band antennas for wireless applications. The last part is dedicated to the design of compact U-slot antenna backed by a cavity for colonoscopy application. The measured and simulation results have shown good agreement which validate the different proposed configurations and the adopted design procedures.

Keywords: Miniaturization, fractal antenna, multi-band antenna, wireless applications, WLAN, WiMAX, RFID.

List of Symbols

ϵ_r	Relative permittivity
Z_c	Characteristic impedance
k	Wave number
k_0	Free space wave number
(r, θ, ϕ)	Spherical coordinate system
Af	Array factor
U_0	Radiation intensity of an isotropic antenna
U_{max}	Maximum radiation intensity
D_0	Maximum Directivity
P_{rad}	Radiated power
$E_{r,\theta,\phi}$	Electric field intensity
$E^t_{r,\theta,\phi}$	Total electric field intensity
a	Diameter of the sphere enclosing the antenna
λ	Wavelength.
λ_0	Free-space wavelength.
R_r	Radiation resistance
R_m	Material losses resistance
η_s	Efficiency of the system
η_a	Efficiency of the antenna
Q_s	System quality factor
Q_a	Antenna quality factor
Q_m	Matching network quality factor
f_r	resonant frequency
c	Speed of light in free space
h	Substrate height
W	Patch width
t	thickness of metallic strip
C	Capacitance
L	Inductance
L_{eff}	Effective length

S_{11}	Return loss
f_h	upper cut off frequency
f_l	lower cut off frequency
f_c	Central frequency of the band

List of Abbreviations

RFID	Radio-Frequency Identification
Wi-Fi	Wireless Fidelity
LTE	Long-Term Evolution
WiMAX	Worldwide Interoperability for Microwave Access
DGS	Defected Ground Structure
DMS	Defected Microstrip Structure
EM	Electromagnetic
SRR	Split Ring Resonator
DRA	Dielectric Resonator Antenna
TLM	Transmission line method
CM	Cavity model
VSWR	Voltage standing wave ratio
MPA	Microstrip patch antenna
MTM	Metamaterials
DNG	Double-negative material
ENG	Epsilon negative material
MNG	μ-negative material
SRR	Split ring resonator
SMA	SubMiniature version A connector
VNA	Vector Nework Analyser
LTCC	Low-Temperature Co-fired Ceramic
CPW	Coplanar Waveguide
ACS	Asymmetrical Coplanar Strip
BW	Impedance Bandwidth

Author's publication list

- **Journal Papers**

1. Guardiola M, **Djafri K**, Challal M, Miguel A, Ballester G, Fernandez-Esparrach G, Camara O and Romeu J, *Design and Evaluation of an Antenna Applicator for a Microwave Colonoscopy System*, IEEE Transactions on Antennas and Propagation, Jan 2019, DOI: 10.1109/TAP.2019.2896703

2. **Djafri K**, Challal M, Aksas R, Mouhouche F and Dehmas M, *Miniaturized Concentric Hexagonal Fractal Rings based Microstrip Patch Antenna for WLAN/WiMAX Application*, Radioengineering, Apr 2019, Vol.28 Issue 1, p39-44,DOI: 10.13164/re.2019.0039

3. **Djafri K**, Challal, Dehmas M, Mouhouche F and Aksas R,*A Compact ACS-Fed Tri-band Microstrip Monopole Antenna for WLAN/WiMAX Applications*, Advanced Electromagnetic, Nov 2018, DOI:10.7716/aem.v7i5.853.

4. **Djafri K**, Challal M, Aksas R and Romeu J, *A Compact Dual-Band Planar Monopole Antenna using Fractal Rings and a Y-Shaped Feeding Transmission Line*, Frequenz: Journal of RF-Engineering and Telecommunications, Apr 2018. DOI.org/10.1515/freq-2018-0097 .

5. **Djafri K**, Challal M, Azrar A, Dehmas M, Aksas R, Mouhouche F. *Compact dual-band fractal hexagonal ring monopole antenna for RFID and GSM applications*. Microw OptTechnol Lett . Mar 2018; $1-4$. DOI:10.1002/mop.31497.

- **Conference Proceedings**

1. **Djafri K**, Challal M, Mouhouche F, Dehmas M and , Aksas R, *Miniaturized multi-band shorted antenna for wireless communication applications* , International Conference on Electronics and Electrical Engineering ($IC3E'18$),November 12-13, 2018, University of Bouira, Algeria.

2. **Djafri K**, Challal M, Mouhouche F, Dehmas M and , Aksas R, *Miniaturization using Combinations of First Order Hexagonal Fractal Shaped Rings* , International Conference on Electronics and Electrical Engineering ($IC3E'18$),November 12-13, 2018, University of Bouira, Algeria.

3. **Djafri K**, Challal M, Dehmas M, Mouhouche F, Aksas R and Romeu J, *A novel miniaturized dual-band microstrip antenna for WiFi/WiMAX applications*, ICEE-B , International Conference on Electrical Engineering-Boumerdes, Boumerdes, ALGERIE, 2017, https://ieeexplore.ieee.org/document/8192084/.

4. **Djafri K**, Challal M, Aksas R, Mouhouche F and Dehmas M, *Miniaturized Concentric Fractal Rings Microstrip Patch Antenna for Wireless Applications*, International Conference on Automatic control, Telecommunication and Signals, Anaba, ALGERIE, 2017.

5. **Djafri K**, Challal M, Aksas R, Mouhouche F and Dehmas M, *A Compact ACS-Fed Tri-band Microstrip Monopole Antenna for WLAN/WiMAX Applications*, International Conference on Electronics and New Technologies, Msila, ALGERIE, 2017.

- **Other works**

  - Dehmas M, Azrar A, F Mouhouche , **K Djafri** and Challal M. *Compact dual band slotted triangular monopole antenna for RFID applications*.Microw Opt Technol Lett 2018;60:432 â 436. https://doi.org/10.1002/mop.30984.

  - F Mouhouche, Azrar A, Dehmas M, and **K Djafri** . *Compact dual band slotted triangular monopole antenna for RFID applications*.Microw Opt Technol Lett 2018;60:432 â 436. https://doi.org/10.1002/mop.30984.

  - A Boutadjar, M Challal ,SD Bennani,F Mouhouche and **K Djafri**. *Design and fabrication of a novel quadruple-Band monopole antenna using a U-DGS and open-Loop-Ring resonators*. Advanced Electromagnetics, 2017, vol. 6, no 3, p. 59-63.

  - **K. Djafri**, F. Mouhouche, F. Guichi and F. Fertas, *Review on Compact Microstrip Antennas: Multiband, Wideband and UWB Applications,* IJEEES - International Journal of Electronic and Electrical Engineering Systems, vol. 1, No. 1, pp. 5-8, Mar. 2018.

  - M. Challal, F. Mouhouche, **K. Djafri** and A. Boutejdar, *Quad-band Microstrip Patch Antenna for WLAN/WiMAX/C/X Applications,* IEEE â 2017 5th International Conference on Electrical Engineering â ICEE-B, 29-31 October 2017, Boumerdes, Algeria. DOI: 10.1109/ICEE-B.2017.8192065.

Contents

List of Figures

List of Tables

Chapter 1

Introduction and Microstrip Antenna Overview

Contents

1.1 Introduction

1.1.1 Motivation

Nowadays, wireless communication devices including tablets, laptops, cellular mobile phones, satellite phones and receivers, radio-frequency identification (RFID) systems are continuously required to be downsized. Therefore, the demand for miniaturization of the electronic elements has been increased drastically. The most crucial element composing all communication equipments is the antenna and it is critical in deciding the quality of radio communication. It assures the transmission and reception of radio waves and therefore it design for any wireless device must be done carefully. At resonance, the antenna dimension must be around half of wavelength. Hence the lower resonant frequency is, the larger the size of the antenna will be. In addition to the need for miniaturization, antenna with broadband and multi-band characteristics are of great interest due to the fast growing of wireless applications and communication standards.

Microstrip antennas are very attractive candidates suitable for wireless devices owing to their unique characteristics such as low-profile nature, light weight, ease of integration with associated electronics, conformal to any surface, low cost and mechanically robust. Nevertheless, in their basic forms, microstrip antennas have some limitations compared to conventional microwave antennas, such as narrow impedance bandwidth (typically of around

1%),somewhat lower gain ($\approx 6dB$), poor power capability ($\approx 100W$), poor polarization purity, poor scan performance, and excitation of surface waves. Many ways have been developed to overcomes most of these drawbacks. By the emerging of many new standards for wireless communications including RFID, Wi-Fi, fourth generation/Long-Term Evolution (LTE), Worldwide Interoperability for Microwave Access (WiMAX) which are working in the frequency range of 700 MHz to 6 GHz, the main limitation of microstrip antenna is its physical size. For this reason, much effort has been devoted to the development of antenna miniaturization techniques. Therefore, new techniques for designing compact and multiband antenna need to be investigated, which is the key motivation of this thesis work.

1.1.2 Contributions and Thesis Organization

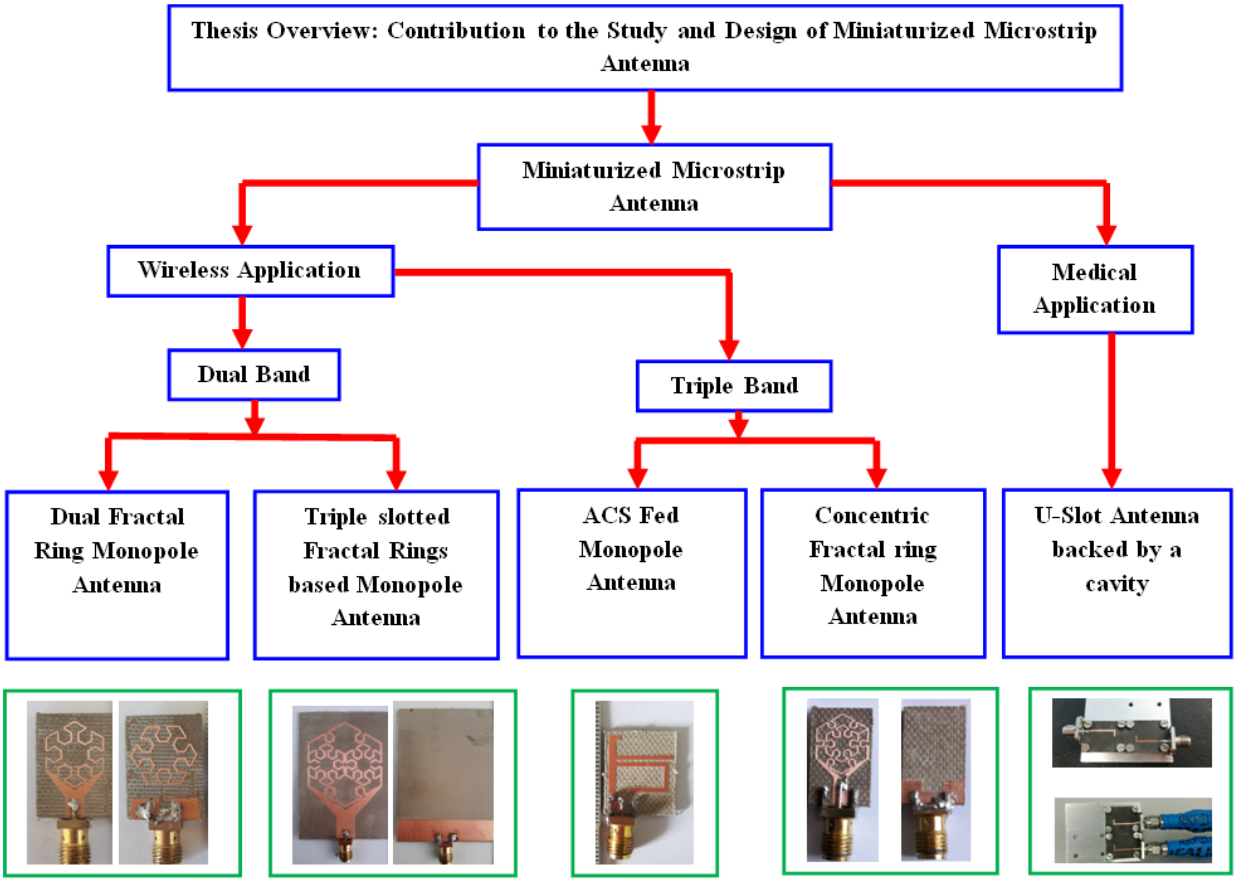

Figure 1.1: Dissertation overview

The outlines of the thesis and authors contributions are organized as follows:

Chapter two In this chapter, most of miniaturization techniques applied to the field of microstrip antennas will be presented and summarized.

Chapter three will present the detailed procedure to design miniaturized antenna start-

ing from the conventional circular patch. The theory of a circular patch will be quickly reviewed as well. The derived hexagonal ring monopole antenna will be the basic antenna which will serve as the zero iteration to generate the first order hexagonal fractal ring monopole antenna.

Chapter four will present two novel miniaturized dual band monopole antennas printed on an FR4 substrate with the dielectric constant of 4.3, a thickness of 1.6 and a loss tangent of 0.017. A detailed study of the proposed compact antennas along with their experimental results will be presented.

Chapter five This chapter will discuss two different compact triple band monopole antennas. The fist design will be based on the ACS feeding technique to reduce the antenna size and a the antenna will be attached to two branches to excite multiple resonances. The second design will be based on two concentric fractal rings connected to each other. The position of the connection will be optimized to tune the resonant frequencies to the desired bands. The measured and simulated results will be compared to validate the proposed antennas.

Chapter six will investigate the design, analysis and implementation of miniaturized microstrip antenna for a colonoscopy application. The proposed antenna element used in the applicator is a cavity-backed U-slot fed by an inverted L-shape microstrip line. The U-shaped slot is selected to meet the reduced size requirements of the intended application and it is backed by a cavity to enhance the isolation between array elements. The slot is printed on RT/Duroid 5880 substrate having a relative permittivity of 2.2 and a thickness of 0.127 mm which is very flexible and could be easily conformed onto a cylindrical surface. An L-shape microstrip line printed on the back side of the substrate is used to excite the slot and the cavity is filled by a lossy foam with relative permittivity of 2.1. To validate the proposed design, measured and simulated results will be compared and will be discussed in details.

Chapter seven will summarize the contributions presented in this thesis and will provide some suggestions for further research.

Chapter 2

Microstrip Antenna Miniaturization: State of the Art

Contents

2.1 Introduction

Antenna miniaturization has been studied extensively for over 70 years [1, 2, 3]. It is found that by decreasing the size of the antenna the bandwidth and the radiation efficiency are also decreased. Thus, there is a size limitation for which the antenna radiation characteristics are no more acceptable. Besides, recently many antenna size reduction methods have been proposed in literature [4], [5].

In the remaining sections of this chapter, the limits of antenna size and main microstrip patch antenna (MPA) miniaturization techniques will be discussed.

2.2 The Microstrip Antenna

Microstrip antennas consist of very thin metallic patch printed on a grounded substrate with a thickness h. A basic rectangular microstrip antenna is presented in Figure 2.1.

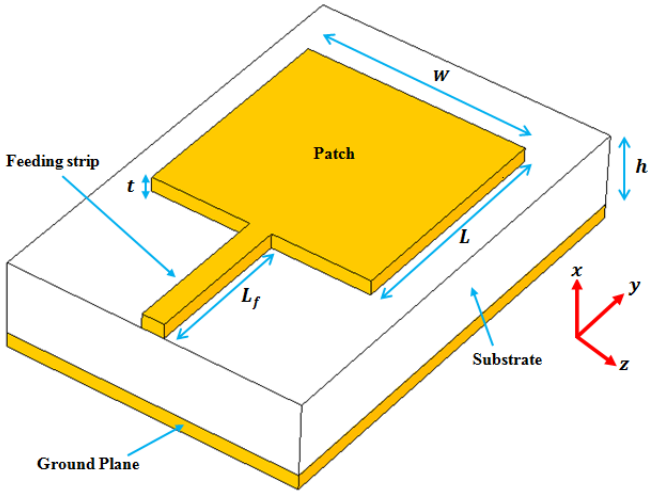

Figure 2.1: Microstrip antenna

For a rectangular shaped patch, the length L is usually $\lambda_0/3 \leq L \leq \lambda_0/2$. The radiation pattern of the patch depends on the current distribution on the patch. The shape of the patch, the feeding technique and the substrate characteristics are chosen to satisfy the requirements of a specific application [6].

The shape of patch can take different geometrical forms such as rectangular, circular , triangular, elliptical, square and any other configuration. More complex patterns based on regular shapes have been introduced to meet the requirements of a certain applications. Consequently, the choice of the shape depends on specific limitations such as size, radiation pattern, gain , bandwidth etc. Basically, the operating modes of the antenna depends on the patch dimensions, the substrate characteristics as well as the feeding configuration.

Several dielectric materials can be used for substrate in the antenna design. Their relative dielectric constant are generally in the range $2.2 \leq \epsilon_r \leq 12$. The most suitable ones for good radiation performances are thick with lower relative permittivity because they ensure better radiation efficiency, larger bandwidth, loosely bound fields for radiation into space, but at the expense of larger element size. Thin substrates with higher dielectric constant are desirable for microwave circuitry because they need tightly bound fields to minimize unwanted radiation and coupling. However they are considered less efficient and they have relatively narrow bandwidth due to their great losses. Hence, better compromise have to

be found between the antenna radiation performances and circuit design since microstrip antennas are integrated with other microwave circuitry.

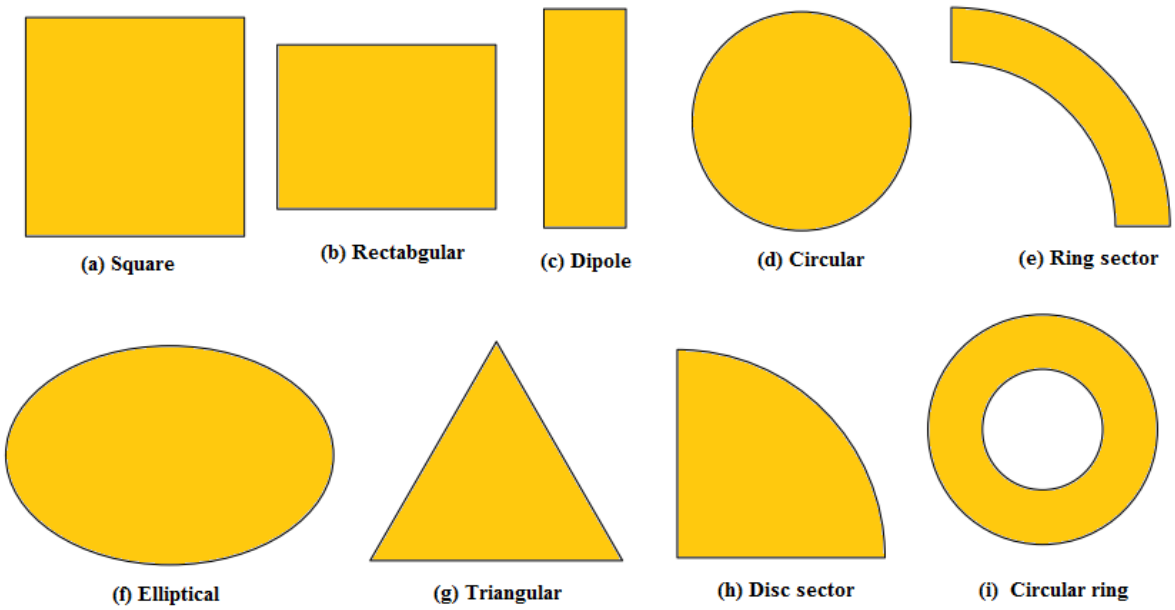

Figure 2.2: Representative shapes of microstrip antennas

2.2.1 Feeding Structures

The feed must transfer efficiently energy from the transmission system to the antenna. Various feeding techniques are used to feed microstrip antenna. The feeding structure affects significantly the bandwidth, operating modes, spurious radiation, surface waves and antenna geometry. Accordingly, the design of the feeding play an important role in the radiation performances. The most popular feeding configurations are the microstrip line, coaxial probe, aperture coupling, and proximity coupling as can be seen in Figure 2.3.

Figure 2.3(a) shows a probe feeding structure. The coaxial inner conductor is connected to the patch through the substrate and the outer conductor is soldered to the ground plane. The impedance matching between the radiating patch and the coaxial cable is achieved by adjusting the location of the feed point. However, this feeding structure presents certain limitations including the increase in spurious radiation, surface waves, input inductance for antennas with thick substrates and not suitable for arrays owing to the great number of solder points.

In the aim of simplifying the design and reducing the cost, the microstrip antenna can be fed by means of a coplanar strip as illustrated in Figure 2.3(b). The feeding strip can be directly connected or coupled to the edge of the patch. This feeding configuration is

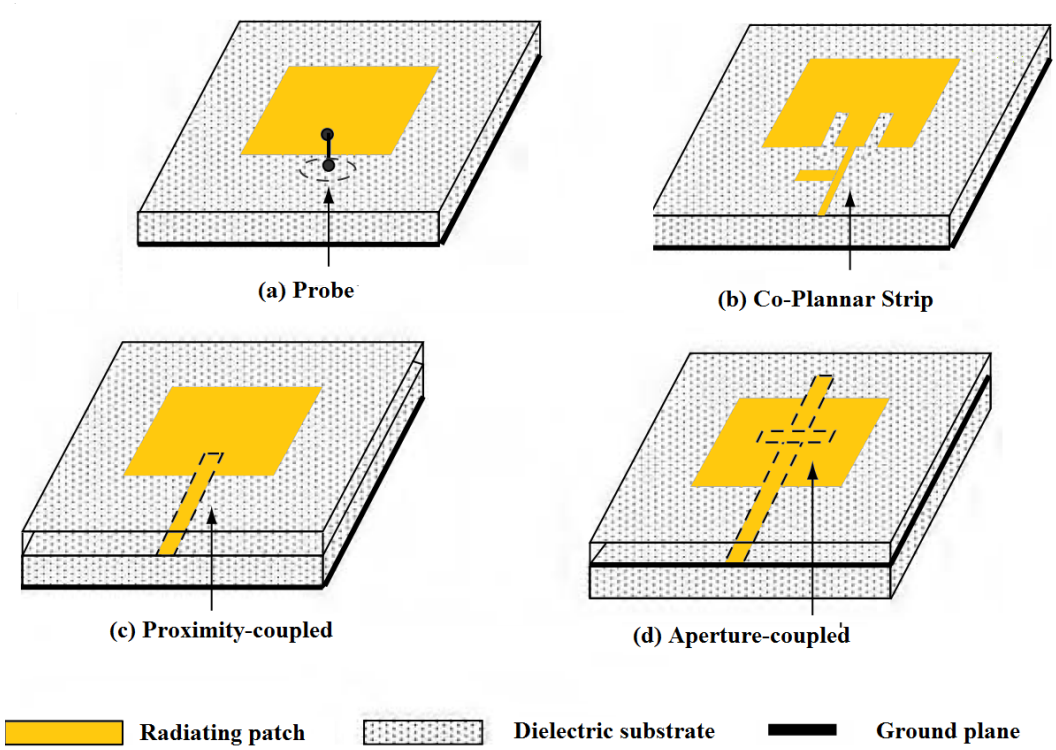

Figure 2.3: Feeding structures used in microstrip antenna [7]

suitable for array applications. Impedance matching is achieved by notching the patch near the feeding (inset fed) strip or placing a matching-network (using stubs).

The proximity coupling depicted in Figure 2.3(c) has the largest bandwidth (as high as 13 percent), is relatively easy to model and has low spurious radiation among the four feeding configurations. However its fabrication is somewhat more difficult. The feeding stub length and the width-to-line ratio of the patch can be used to control the match [8].

The aperture coupling depicted in Figure 2.3(d) has a notable features which are wider bandwidth and high polarization purity. Two substrate separated by a common ground plane are used. A microstrip feed line printed on the lower substrate is electromagnetically coupled to the patch through a slot printed in the common ground plane [9]. The slot can have any shape and size, and these parameters are used to improve the bandwidth. Typically matching is performed by controlling the width of the feed line and the length of the slot. However, this feeding configuration has higher fabrication complexity and cost than single-layered structures.

2.2.2 Modeling Techniques

Microstrip patch antenna are modeled using the transmission line model (TLM), cavity model (CM) and full wave model (which include integral equations and Moment method). The

analytical methods TLM and CM provide more physical insight to the operating mechanism whereas the numerical methods gives more accurate results . In the reminder of this chapter the radiation characteristics of a rectangular patch antenna (the most studied geometry) will be reviewed using the TLM.

Basically, in the TLM, the microstrip antenna is considered as two slots, separated by a low-impedance Z_c transmission line of length L.

2.2.3 Fringing effects

Due to the finite dimensions of the antenna along the length and the width, the field at the edges of the patch undergoes fringing. Figure 2.4 presents the fringing along the length for the two radiating slots. Same effect applies along the width and this effect influences the resonant frequency of the antenna. The amount of the fringing is a function on the patch dimensions as well as the substrate height. Because of fringing fields, the patch behaves as if it has a slightly larger dimension hence semi-empirical factors are usually introduced to obtain these effective dimensions. These factors vary from patch to patch [6].

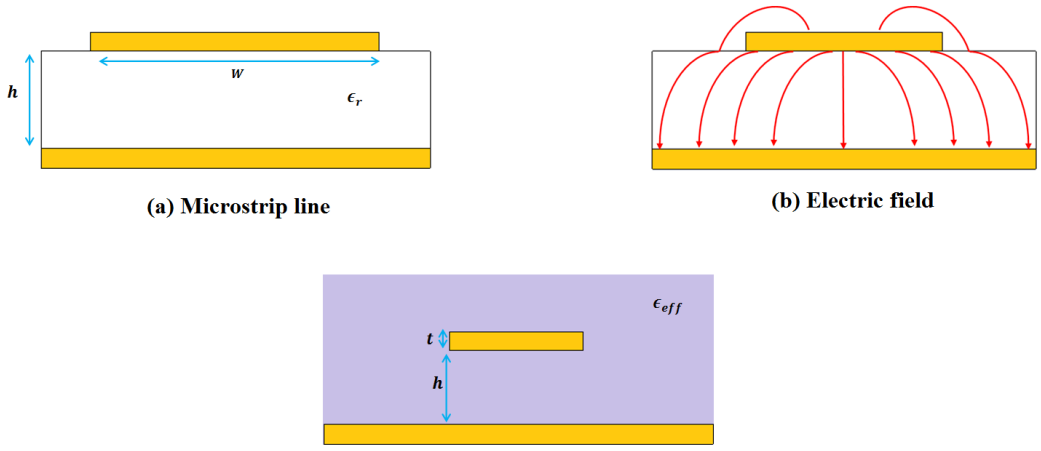

Figure 2.4: Fringing Effect and effective dielectric constant

Figure 2.4 shows the field lines in an non-homogenous medium composed generally by air and substrate. Typically most of the field lines lie in the substrate and parts exit in air . Since part of the waves travel in the substrate and part in air, an effective dielectric constant ϵ_{eff} is introduced to account for fringing and wave propagation in the line. Accordingly, the effective dielectric constant is defined as the dielectric constant of the uniform dielectric material so that the line of Figure 2.4 (b) has identical electrical characteristics, particularly

propagation constant, as the actual line of Figure 2.4 (c). For lower frequencies the effective dielectric constant is given by [10]:

$W/h >> 1$

$$\epsilon_{eff} = \frac{\epsilon_r + 1}{2} + \frac{\epsilon_r - 1}{2}\left[1 + 12\frac{h}{W}\right]^{-1/2} \tag{2.1}$$

2.2.4 Resonant frequency, effective length and effective width

Because of the fringing effect, the antenna dimensions look greater than its physical dimensions. This is presented in Figure 2.5 for the principal plane E (x-y) where the length of the antenna has been extended by ΔL on each side. A common and a practical approximation of the fringing distance ΔL is given by:

$$\Delta L = 0.412h\frac{(\epsilon_{eff} + 0.3)\left(\frac{W}{h} + 0.264\right)}{(\epsilon_{eff} - 0.258)\left(\frac{W}{h} + 0.8\right)} \tag{2.2}$$

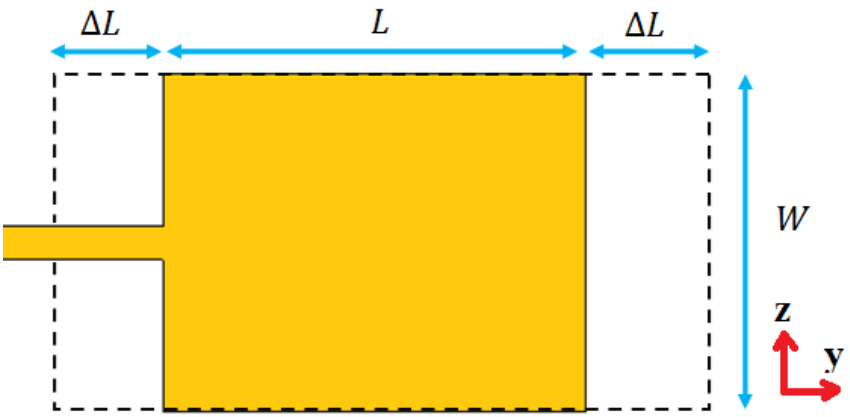

Figure 2.5: Effective and physical length of a microstrip antenna

Because the the patch length is extended by ΔL at each end, the effective length L_{eff} becomes:

$$L_{eff} = L + 2 \times \Delta L \tag{2.3}$$

The resonant frequency for the dominant mode TM_{010} is given by:

$$f_r = \frac{c}{2L_{eff}\sqrt{\epsilon_{eff}}} \tag{2.4}$$

For an efficient radiator, a practical width that leads to good radiation efficiencies is given by [10]:

$$W = L\sqrt{\frac{\epsilon_r}{\epsilon_r + 1}} \tag{2.5}$$

2.2.5 Radiated Field and Directivity

As the microstrip antenna is considered as two radiating slots, The total radiating field is electric far-field radiated by one slot times the array factor (two slots separated by a distance L_{eff}. The electric far field radiated by a slot is given by:

$$E_\theta \approx E_r \approx 0 \tag{2.6}$$

$$E_\Phi = j\frac{k_0 hW E_0 e^{-jk_0 r}}{2\pi r}\left\{sin\theta\frac{sin(X)}{X}\frac{sin(Z)}{Z}\right\} \tag{2.7}$$

$$X = \frac{k_0 h}{2}sin\theta cos\phi \tag{2.8}$$

$$Z = \frac{k_0 W}{2}cos\theta \tag{2.9}$$

Where (r, θ, ϕ) are the spherical coordinates of the observation point, k_0 is the free space wave number and E_0 is a constant. The array factor Af of two identical elements separated by a distance L_{eff} is given:

$$Af = 2cos\left(\frac{k_0 L_{eff}}{2}sin\theta sin\phi\right) \tag{2.10}$$

Thus the total radiated field by the two slots is

$$E_\phi^t = 2 \times j\frac{k_0 h E_0 e^{-jk_0 r}}{2\pi r}\left\{sin\theta\frac{sin(X)}{X}\frac{sin(Z)}{Z}\right\} \times cos\left(\frac{k_0 L_{eff}}{2}sin\theta sin\phi\right) \tag{2.11}$$

For small values of h ($k_0 h << 1$) equation 2.11 reduces to:

$$E_\phi^t \approx j\frac{2V_0 e^{-jk_0 r}}{\pi r}\left\{sin\theta\frac{sin(\frac{k_0 W cos\theta}{2})}{cos\theta}\right\} \times cos\left(\frac{k_0 L_{eff}}{2}sin\theta sin\phi\right) \tag{2.12}$$

where $V_0 = E_0 h$ is the voltage across the slot. It can deduced that the expression of the electric filed in the E-plane $(x - y)$ ($\theta = 90°, 0° \leq \phi \leq 90°, 270° \leq \phi \leq 360°$) can be whiten as:

$$E_{\phi}^{t} \approx j\frac{k_0 W V_0 e^{-jk_0 r}}{\pi r}\left\{\frac{sin(\frac{k_0 hcos\phi}{2})}{\frac{k_0 hcos\phi}{2}}\right\} \times cos\left(\frac{k_0 L_{eff}}{2}sin\phi\right) \tag{2.13}$$

The expression of the field in the H-plane $(x-z)$ $(\phi = 0°, 0° \leq \theta \leq 180°)$ can be written as :

$$E_{\phi}^{t} \approx j\frac{k_0 W V_0 e^{-jk_0 r}}{\pi r}\left\{sin\theta\frac{sin(\frac{k_0 Wcos\theta}{2})}{\frac{k_0 Wcos\theta}{2}}\frac{sin(\frac{k_0 hsin\theta}{2})}{\frac{k_0 hsin\theta}{2}}\right\} \tag{2.14}$$

The directivity of the antenna is one of the most important figures-of-merit whose definition is given by

$$D_0 = \frac{U_{max}}{U_0} = \frac{4\pi U_{max}}{P_{rad}} \tag{2.15}$$

where U_0 is the radiation intensity of an isotropic antenna, U_{max} is the maximum radiation intensity and P_{rad} is the radiated power.For a microstrip antenna , the directivity is given by :

$$D_0 = \left(\frac{2\pi W}{\lambda_0}\right)^2 \frac{\pi}{I} \tag{2.16}$$

where

$$I = \int_0^{\pi}\int_0^{\pi}\left[\frac{sin(\frac{k_0 Wcos\theta}{2}}{cos\theta}\right]^2 sin^3 cos^2\left(\frac{k_0 L_{eff}}{2}sin\theta sin\phi\right) d\theta d\phi \tag{2.17}$$

The directivity of a microstrip antenna can be also expressed asymptotically as

$$D_0 = \begin{cases} 6.6 = 8.2dB, & \text{W« } \lambda_0 \\ 8(\frac{W}{\lambda_0}), & \text{W» } \lambda_0 \end{cases} \tag{2.18}$$

2.2.6 Impedance bandwidth, efficiency and gain

The frequency range for which the antenna is well matched to its feed is defined as its impedance bandwidth. The impedance bandwidth can be defined in terms of return loss ($|S_{11}|$) or a voltage standing wave ratio (VSWR) over a frequency range. The well-matched impedance bandwidth must totally cover the required operating frequency range for some specified level, such as $VSWR = 2$ or a return loss $|S_{11}|$of less than 10 dB. The fractional bandwidth of a microstrip antenna can be whitten as

$$FBW = \frac{f_h - f_l}{f_c} \tag{2.19}$$

where f_h and f_l are the upper and the lower cut off frequency of the frequency range respectively and f_c is the central frequency of the band. In addition, the antenna bandwidth is inversely proportional to the antenna quality factor Q_a and is given by

$$FBW = \frac{1}{Q_a} \tag{2.20}$$

The FBW can be also expressed using $VSWR$ as

$$FBW = \frac{VSWR - 1}{Q_a\sqrt{VSWR}} \tag{2.21}$$

The radiation efficiency of an antenna is defined as the power radiated over the input power. It can also be expressed in terms of the quality factors, which for a microstrip antenna can be written as

$$\eta_a = \frac{Q_a}{Q_{rad}} \tag{2.22}$$

Q_{rad} is the quality factor due to radiation. The total qualy ty factor Q_a is given by [10]

$$\frac{1}{Q_a} = \frac{1}{Q_{rad}} + \frac{1}{Q_c} + \frac{1}{Q_d} + \frac{1}{Q_{SW}} \tag{2.23}$$

where Q_c , Q_d and Q_{SW} account for quality factors associated with losses caused by conductivity of the patch, substrate dielectric and surface wave, respectively. The gain of the antenna is given by :

$$G = \eta_a D_0 \tag{2.24}$$

2.3 Fundamental limits of antenna size

It has been established that by reducing the antenna dimensions the quality factor, the gain as well as the bandwidth of the antenna are negatively affected. This fact has been first introduced by Wheeler in 1940 . He established the relation between the antenna volume and the maximum achievable power which is the inverse of the quality factor Q [1]. Wheeler defined an electrically small antenna as one whose maximum dimension is less than $\frac{\lambda}{2\pi}$. This

relation is often expressed as:

$$ka < 1 \tag{2.25}$$

where $k = \frac{2\pi}{\lambda}$ is the wave number [radians per meter], λ is free space wavelength [meter], a is the radius of sphere enclosing the maximum dimension of the antenna (meters).

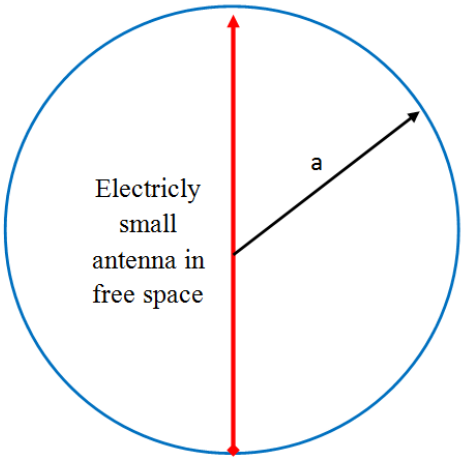

Figure 2.6: Sphere enclosing an electrically small radiating element.

In 1948, by using spherical wave functions Chu [2] has extended the analysis done by Wheeler and he found that, for an antenna with a maximum dimension of $2a$, the antenna can operates in broad bandwidth with a gain equal to or less than $4a/\lambda$. To achieve a gain higher than this value, the quality factor Q_a increases at an considerable rate. Thus, the antenna that has potentially the broadest bandwidth, which exhibits an omnidirectional radiation pattern, corresponds to an infinitesimally small dipole.

In 1987, Fujimoto, Henderson, Hirasawa and James summarized the different approaches used to design small antenna. Furthermore, they have given a survey for the theoritical limits of electrically small antennas (ESA). They also established that an ESA enclosed in a given volume has a minimum value of Q_a which limits the bandwidth of the ESA. Accordingly, the higher the antenna Q_a the smaller the impedance bandwidth.

The amount of conductor, dielectrics and other materials losses out of radiation loss defines the SMA efficiency which can be expressed as:

$$\eta_a = \frac{R_r}{R_r + R_m} \tag{2.26}$$

It is well known that there is a theoretical lower limit on the quality factor Q_a that can be achieved for a small antenna. For an ESA which can be enclosed in a sphere of radius a, the theoretical lower bound on the antenna Q_a is given by [11]:

$$Q_a = \frac{1}{ka} + \frac{1}{(ka)^3} \tag{2.27}$$

It is worth to mention that equation 2.27 is valid for a lossless antenna. It can be clearly seen from the equation that decreasing the size of an antenna results in an increase in its Q.It can be concluded from the above mentioned equations that the quality factor of the antenna can be decreased at the expense of its gain and efficiency. Consequently, the miniaturization of the antenna is to find a better compromise between size, bandwidth and gain.

Basically microstrip patch antenna (MPA) are miniaturized by using two different principles. The first is based on changing the material properties of the substrate in the aim of decreasing the effective wavelength in the substrate. The second is simply based on reshaping the antenna radiating element such that its electrical size gets increased (controlling the current path). In the reminder in this chapter, a review of the most used techniques of size reduction will be discussed and detailed.

2.4 Main Techniques for Antenna Miniaturization

2.4.1 Material Loading

Since the resonant frequency of an MPA is inversely proportional to the dielectric constant of the substrate, then it can be downsized by using substrate with high permittivity ϵ_r. However, using such substrates increase the level of surface wave which leads to lower bandwidth and decrease the radiation efficiency.

Different material have been investigated as well as configurations to reduce the size of an MPA. In [12] an experimental study of MPAs printed on moderately thick $(0.02-0.03\lambda_0)$ substrates with relative permittivities of 10 and 13 have been studied experimentally. It was found that the measured input impedances are similar to those of antennas on thinner substrates with lower permittivity. However, deformation of the radiation pattern in E-plane has been observed which mainly due to the diffraction of the surface wave at the substrate edges.

Ceramic substrates for MPA miniaturization have been extensively investigated. In [13] various types of ceramic substrates have been used to design different miniaturized MPAs. A low-temperature co-fired ceramic (LTCC) substrate of $\epsilon_r = 100$ has been used to fabricate a square MPA. A size reduction of MPA dimension of a factor of 8 was achieved as compared

with that of a conventional patch printed on an FR4 substrate. However, the substrate was chosen to be relatively thick ($0.031\lambda_0$) to enhance the antenna bandwidth. Accordingly, the antenna had a fractional bandwidth of 7.2% and a gain of 2.8 dBi at 1.88 GHz. A textured ceramic substrate, which was a mixture of LTCC and Stycast, was also used to fabricate another MPA. The resulted substrate had an effective permittivity of 23.5. The MPA fabricated on this substrate was 2.5 times smaller than the conventional MPA printed on an FR4 substrate. The measured gain of the antenna was 3 dBi with a fractional bandwidth of about 9.1%.

Ceramic substrates and modified engineered substrates can offer significant reduction in the patch size. However, this method of miniaturization has major drawbacks such as the cost of such substrates as well as reduction of the obtained bandwidth.

2.4.2 Defected Ground Structure (DGS)

DGS refers to the insertion of defect in the ground plane of a circuit at microwave frequencies. The defect can have any geometrical shape including dumbbell-shaped [14], concentric ring shaped [15], fractal shape [16], split-ring resonators [17], meander line [18], U-shaped [19], trapezoidal [20], V-shaped [21], H-shaped, cross-shaped [22] and square heads connected with U slots as can be seen in Figure 2.7. Furthermore, the DGS can comprise either one defect (unit cell) or several defects arranged in periodic or non periodic configurations. The geometry and the number of the defects embedded in the ground plane depend the application.

The propagation of electromagnetic (EM) microwave is stopped by the presence of a DGS over a certain range of frequency leading to a filtering behavior. Hence , the DGS is modeled by an RLC circuit. Many DGS configurations have been studied with different applications and some of these are discussed below.

Basically, the DGS perturbs the electromagnetic field around the defect. Capacitive effect (C) is the result of the trapped electromagnetic field while the surface currents around the defect gives rise to an inductive effect (L). Consequently, this results in resonant characteristics of a DGS. In [17] a split circle resonator loaded in circular microstrip patch antenna to reduce the size of the antenna. The conventional circular microstrip patch antenna resonates at 6.11 GHz, while after introducing the complementary split ring resonator (SRR), the same antenna resonates near 6.11 GHz with reduced size. The antenna effective footprint

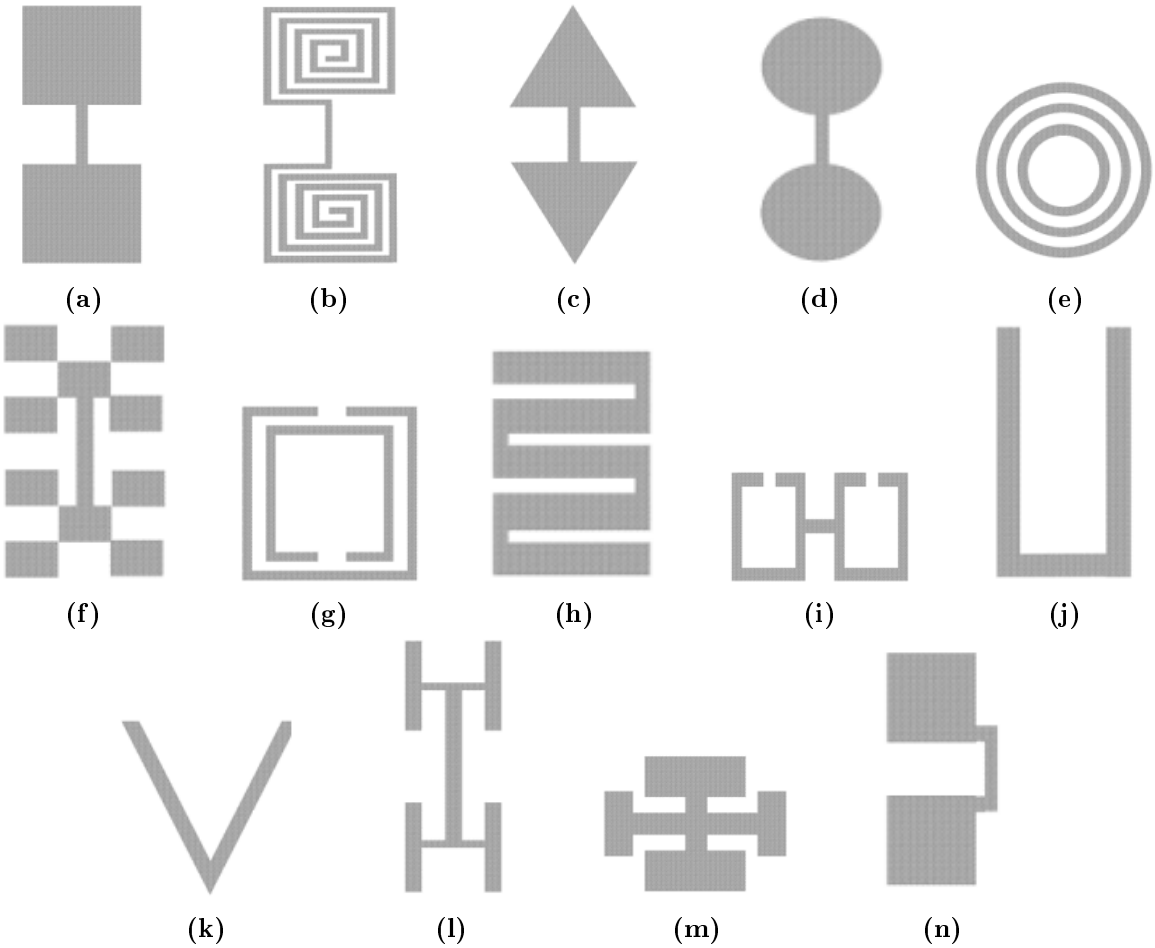

Figure 2.7: Different geometries DGS :(a) Dumbbell-shaped (b) Spiral-shaped (c) Arrow head dumbbell (d) Circular head dumbbell (e) Concentric ring shaped (f) Fractal (g) Split-ring resonators (h) Meander line (i) Open loop Dumbbell (j) U-shaped (k) V-shaped (l) H-shaped (m) Cross-shaped (n) Square heads connected with U slots.

is reduced by nearly 64 % compared to the conventional patch antenna with a gain of 5.04 dB.

A compact ring-shaped dielectric resonator antenna (DRA) loaded with a moon-shaped DGS has been studied in [23]. The moon-shaped DGS is acting as a radiator and also reduces the size of proposed antenna by an amount of 14.87 % (lower frequency band) and 48.77 % (upper frequency band) see Figure 2.8b.

In [19] a U-shape patch antenna for high gain and wide bandwidth has been presented. By introducing an inverted U-shape slot on the circular ground plane of diameter of 40 mm a controllable wide impedance bandwidth has been obtained. The simulated results have been confirmed experimentally. An impedance bandwidth for -10dB return loss about 100.35 % has been achieved by individually optimizing its parameters.

In [24] a wide band Microstrip antenna has been proposed for Ku band applications with circular shaped DGS.The antenna has an impedance bandwidth of 56.67 % ranging from 9.8

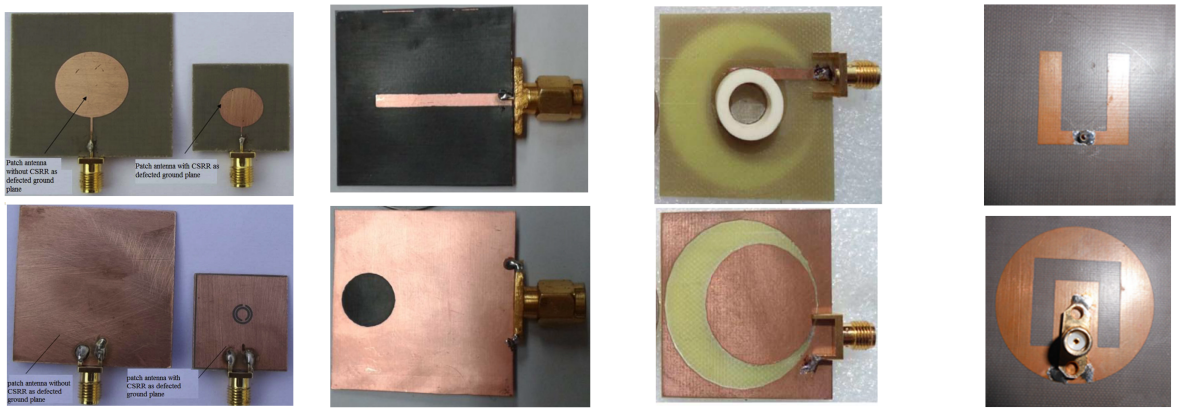

Figure 2.8: Antenna load with DGS:(a) [24] (b)[23], (c)[19] and (d) [24]

GHz to 17.55 GHz, which covers Ku-band and partially X-band. The antenna has shown good radiation characteristics within the entire band, and has a gain ranging from 5 dBi to 12.08 dBi.

2.4.3 Defected Microstrip Structure (DMS)

DMS refers to a defect inserted in the microstrip line. It is made by etching shaped slots in the microstrip line hence no leakage through the ground plane can take place. DMS are mostly used to enhance the performaces of various planar passive circuits and to filter certain spurious signals[25]. By etching slots in the antenna radiating patch,the current distribution is disturbed and the electrical length of the microstrip antenna gets lengthened. Consequently, the effective inductance and capacitance of the microstrip line is increased which influences the input impedance and current flow of the antenna and thus, reducing it size with respect to a certain resonant frequency. Accordingly, DMD presents an effective technique to reduce the circuit size without affecting any of the ground plane [25].

In [26] a spiral DMS is used to design a miniaturized microstrip antenna. The proposed design compared with a conventional one (without DMS slot) resonate at 2.69 GHz while the conventional antenna resonates at 5.8 GHz. The DMS is employed to shift the resonance frequency to 2.69 GHz consequently size reduction has been achieved. Figure 2.9 shows a size comparison between a conventional microstrip antenna and the antenna designed using DMS, and both resonating at 2.69 GHz. It can be seen that the patch size, as compared with the conventional one, is reduced by 78%.

In [27], a fractal shaped defected microstrip antenna has been designed (see Figure 2.10a).

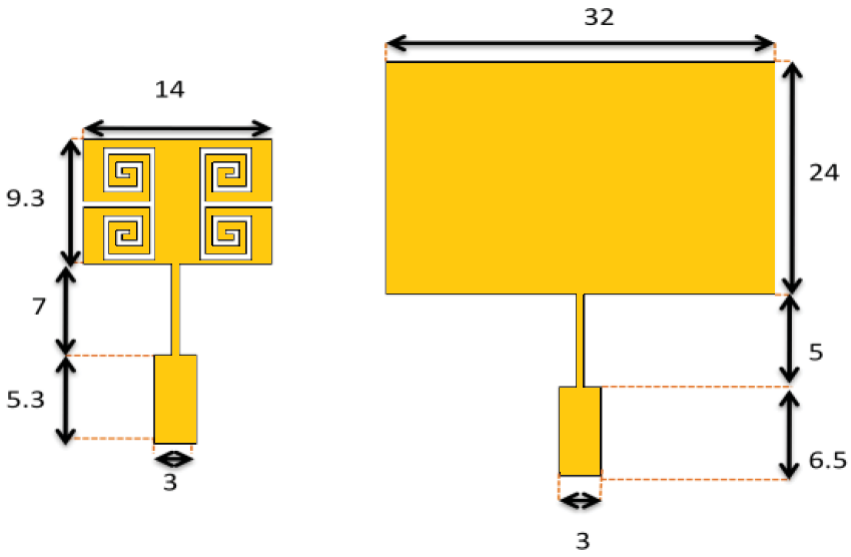

Figure 2.9: Dimensions (mm) for the 2.69 GHz antennas with and without DMS

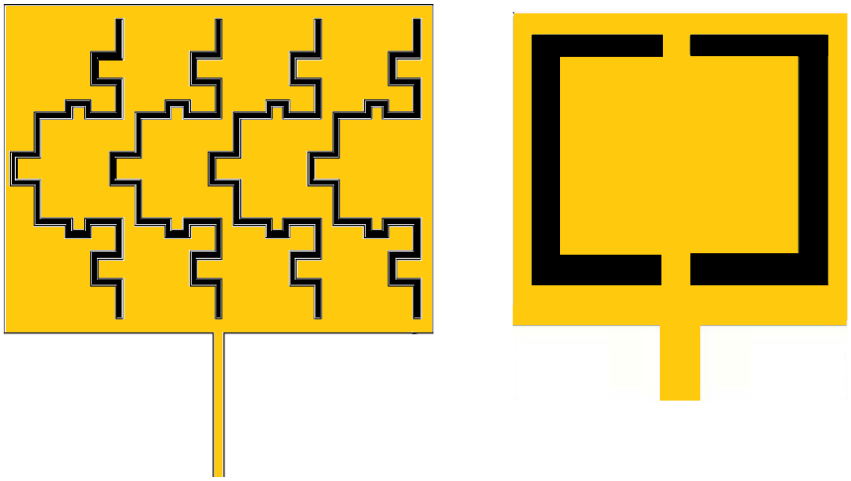

(a) **(b)**

Figure 2.10: DMS slots:(a) fractal[27] and (b) U-slot shape [28]

Using the defects, the surface current path is lengthened and thus the resonance frequency is significantly decreased. When compared with a conventional antenna which resonates at the same frequency, a reduction of about 85% is achieved in antenna size. In order to reduce the size and to improve the impedance bandwidth and radiation characteristics of a square patch antenna, U defected microstrip shapes and a small notch have been etched on radiating patch and on partial ground plane respectively (Figure 2.10b) [28].

A defected microstrip structure (DMS) which has a similar performance to the one-cell DGS, has been proposed in [29] (see Figure 2.11a). This DMS increases the associated inductance, and hence increase the electric length of the structure. This phenomenon is employed to reduce the physical dimensions of a rectangular patch antenna, without degrading its radiation pattern, as well as its VSWR at the resonant frequency. Moreover, by avoiding

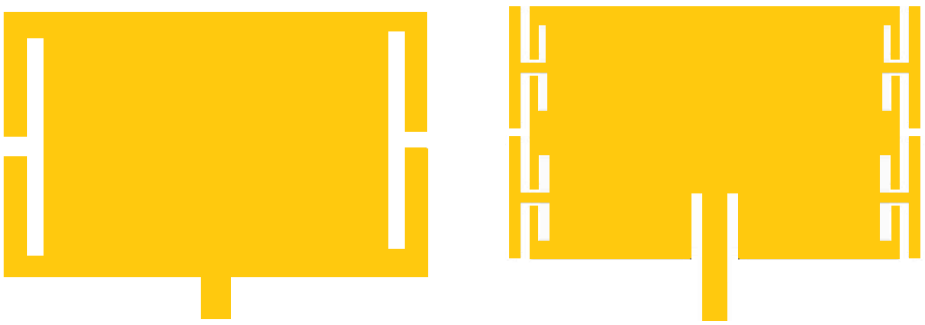

(a) (b)

Figure 2.11: DMS :(a) Simple spur-line[29] and (b) Slots with spur-line [30]

any etching in the ground plane, any increasing leakage through the plane which could interfere with another circuit of the system is not allowed. An area reduction factor of 22% was obtained. Two different techniques have been applied to a patch antenna in order to obtain a reduced size multiband radiator have been presented by [30]. A DMS and a spur-line are assembled together , as shown in Figure 2.11b, to obtain different resonances in an easy way, without affecting the performance of the antenna. Morever, 30% size reduction has been achieved.

2.4.4 Fractal Pattern

In the concern of miniaturization, fractal geometries are promising candidates which leads to more compact and more efficient designs than those derived from the traditional Euclidean geometry. Self similarity and space filling property are the two main characteristics of fractal geometries. More efficient manner of occupying an area is assured by the self similarity property while multiband and broad band characteristics are achieved by space filling feature. This effective use of space results in efficient energy coupling from excitation transmission lines to free space in smaller volume. Some compact antenna topologies based on fractal structures have been investigated based on conventional fractal curves: Koch, Minkowski, Hillbert, Sierpinski, tree, and so forth [33],[34],

The boundary of the patch (Figure 2.12) can be generated using fractal patterns. The resulted fractal patches are very compact, simple and can operate in broadband. Besides, the bandwidth can be improved to suite the Ultra Wide Band (UWB) [31] and even Super Wide Band (SWB) [5].

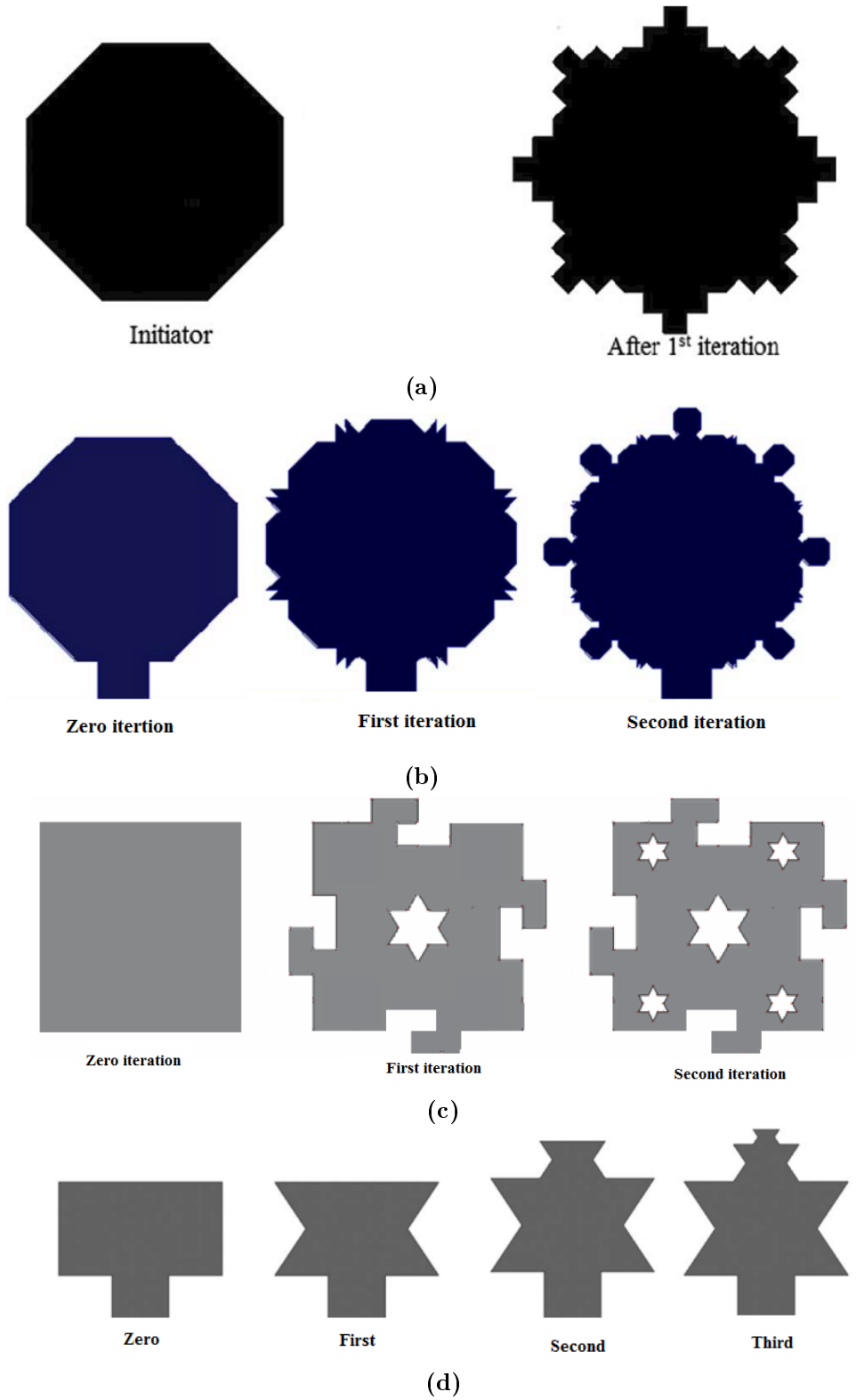

Figure 2.12: Fractal patches:(a) [31] (b) [32], (c) [5]and (d) [4]

2.4.5 Use of metamaterials

Metamaterials are artificial materials having electromagnetic properties which do not exist in nature. Using these type of materials to design antennas will improve their parameters like bandwidth, gain, efficiency. Furthermore, it is possible to reduce the antenna dimensions

as much as desired with these structures. In metamaterials, the real part of ϵ, μ or both of them are negative [35]. A material with only negative permittivity is called epsilon negative (ENG), whereas one with only negative permeability is referred to as a μ-negative (MNG) material. A material with both negative permittivity and permeability is called double-negative (DNG). Loading an antenna by metamaterial structures has been widely used for miniaturization as well as for radiation characteristics enhancement.

In [36], A miniaturized microstrip patch antenna loaded with a DNG metamaterial has been investigated. 50% size reduction has been achieved and the location of the operating frequency is tuned effectively by the resonance of the metamaterial; therefore a sub-wavelength resonance was produced by the help of metamaterials. A deformation of the radiation pattern has been also observed which is mainly due to miniaturization.

In [37], a rectangular shaped monopole antenna loaded with two split ring resonator (SRR) has been proposed for tri-band operation. The antenna covers the WiMAX (3.5/5.5GHZ) and WLAN (2.4/5.2/5.8 GHz) applications. By inserting two SRR slots with adequate dimensions, three operating bands have been obtained. Though the reported structure was simple, it has a relatively large size of $832mm^2$. In order to downsize the antenna dimensions, the authors in [38] have proposed two miniaturized antennas using difference metamaterial structure. The first antenna operates at three bands covering WiMAX, WLAN and GPS applications with a total size of $30 \times 30mm^2$. The second one was designed using interdigital capacitor and spiral inductor operating at 1.06 GHz, 1.8 GHz and 2.5 GHz with a size including the ground plane of $25 \times 25mm^2$. Even though, the reported antennas have small patch sizes, they still have relatively large size by including their ground planes.

A development of the performance microstrip patch antennas has been realized by using metamaterials left hand as the split ring resonator (SRRs) and Toothed SRRs in [39]. The two proposed models of the metamaterial antennas have been used to justify the radiation efficiency.The approach has shown that more efficient antenna, having interesting gain level, directivity, and frequencies band have been obtained. Furthermore antenna size reduction of 70% has been achieved.

Several MTM techniques have been investigated for MPA miniaturization. Although they have been successful in reducing the size, this has been at a substantial cost in terms of complex material use, very narrow operating bandwidths and low radiation efficiency.

2.4.6 Shorting post insertion

A common technique to reduce the overall size of a microstrip patch antenna is to insert one or more shorting posts. By inserting shorting post at a certain position , the resonant frequency of the microstrip antenna is reduced as well as multiband characteristic is achieved. This technique of size reduction is widely used because the shorted antenna can operate at the same resonant frequency, about half the size of the standard microstrip antenna [40].

The shorted MPA can be realized by connecting one end of the shorting post to the ground plane and the other one to the patch. The short can be performed by wrapping a copper strip around the edge of the antenna, or it may be simulated by shorting posts. However, the construction of shorting posts is much easier than wrapping a copper strip around the the antenna edge.

By loading of the microstrip antenna with shorting post, a change of polarization can be achieved [41]. The effect of the shorting pins depend on the number of the shorts, their position, diameters and the lengths (substrate thickness).

The shorting post is basically modeled as an inductance parallel to the LC resonant circuit describing the antenna without shorting post. The antenna with shorting pin can be viewed as resulting from the inductance (due to shorting post) in series with static capacitance of the patch configuration. Accordingly, Larger the inductive part smaller will be the resulting resonance frequency which leads to higher degree of miniaturization for a fixed operating frequency [42]. This technique has been proposed to reduce the antenna dimensions by decreasing its first resonant frequency and it has been used first by [43].

A single shorting post , in [43], is properly used to achieve maximum reduction in physical size of a circular MPA. The radius of circular patch has been reduced by a factor of three. In[44], a dual frequency circular MPA is designed by shorting the patch. It has been observed that the size of the antenna can be reduced by placing shorting post at the patch edge.

MPA can therefore be miniaturized using folding and shorting. However, this method comes at a cost of greatly decreasing the gain and directivity of the antenna. Moreover, this method complicates the geometry of the MPA at times and also makes it non-planar, which adds to the complexity of the structure and its conformity. However, when properly applied, this method has little effect on the efficiency of the antenna [45].

2.4.7 Antenna Feeding

A very attracting technique of miniaturization is to use the asymmetrical coplanar strip (ACS) feeding. This technique is analogous to Coplanar Waveguide (CPW) feed except it has a single lateral ground plane, known by ACS, compared to the dual lateral ground in the CPW. Many ACS-fed antennas have been reported in the aim of size reduction as well as for wide band applications [46][47][48].

In [49], an ACS-fed planar antenna with DGS and DMS slots for dual-band application has been presented. The reported antenna is composed of defect in both ground plane and radiating strip. The antenna has an overall dimension of $21 \times 15.35mm^2$ and resonates at 3.5 and 5.5 GHz.

The authors in [48] have proposed a compact uniplanar monopole antenna for tri-band operation. This antenna is loaded with two rectangular SRRs etched on the radiating patch to achieve tri-band resonant characteristic with a total size of $32 \times 12mm^2$. A dual-band meandered ACS-fed is comprised of an asymmetric ground plane, an ACS-fed structure, and a coupled meandered monopole-type of radiating elements that are designed to provide two desired operation bands. The antenna overall size is of $14.6 \times 17.5mm^2$.

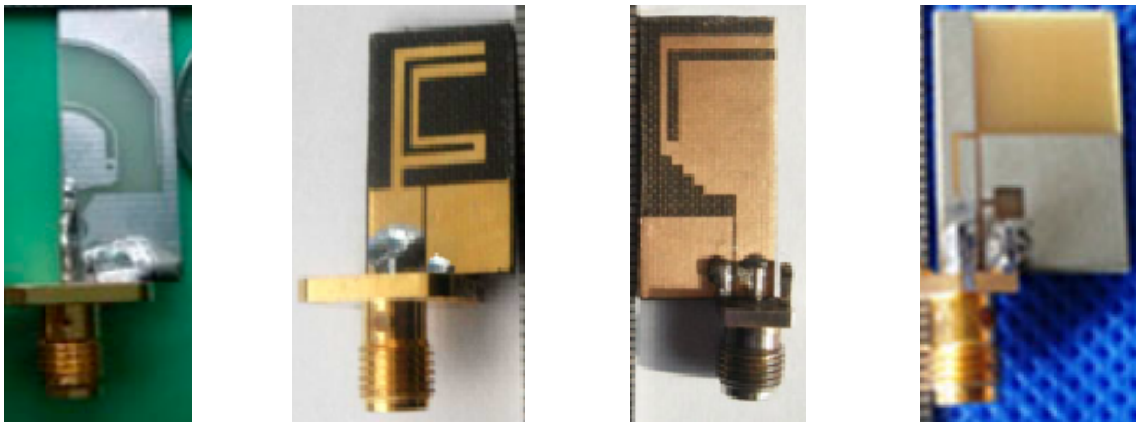

(a) **(b)** **(c)** **(d)**

Figure 2.13: ACS-fed antennas:(a) [47] (b)[50], (c)[48] and (d) [49]

2.5 Summary

The first part of this chapter gives the fundamental parameters of a microstrip antenna. A brief definition of a microstrip antenna was provided , then some of the important parameters

are presented in details. In the second part of the chapter, the limitations of small antennas and the effect of the antenna size on its characteristics such as bandwidth, efficiency and gain have been presented. Major techniques of size reduction applied to microstrip antennas have been presented in details and the advantages and drawbacks of each technique have been presented and discussed.

Bibliography

[1] Harold A Wheeler. Fundamental limitations of small antennas. *Proceedings of the IRE*, 35(12):1479–1484, 1947.

[2] Lan Jen Chu. Physical limitations of omni-directional antennas. *Journal of applied physics*, 19(12):1163–1175, 1948.

[3] James S McLean. A re-examination of the fundamental limits on the radiation q of electrically small antennas. *IEEE Transactions on antennas and propagation*, 44(5):672, 1996.

[4] Sarthak Singhal, Tushar Goel, and Amit Kumar Singh. Inner tapered tree-shaped fractal antenna for uwb applications. *Microwave and Optical Technology Letters*, 57(3):559–567, 2015.

[5] Babu Lal Shahu, Srikanta Pal, and Neela Chattoraj. A compact super wideband monopole antenna design using fractal geometries. *Microwave Rev*, 2:20–24, 2014.

[6] Vasiliki Paraforou. Design and full-wave analysis of supershaped patch antennas. 2013.

[7] Zhi Ning Chen and Michael Yan Wah Chia. *Broadband planar antennas: design and applications*. John Wiley & Sons, 2006.

[8] A Balanis Constantine et al. Antenna theory: analysis and design. *MICROSTRIP ANTENNAS, third edition, John wiley & sons*, 2005.

[9] Ramesh Garg, Prakash Bhartia, Inder J Bahl, and Apisak Ittipiboon. *Microstrip antenna design handbook*. Artech house, 2001.

[10] Da-Gang Fang. *Antenna theory and microstrip antennas*. CRC Press, 2009.

[11] Robert C Hansen. *Electrically small, superdirective, and superconducting antennas*. John Wiley & Sons, 2006.

[12] D Schaubert and K Yngvesson. Experimental study of a microstrip array on high permittivity substrate. *IEEE transactions on antennas and propagation*, 34(1):92–97, 1986.

[13] JS Kula, D Psychoudakis, W-J Liao, C-C Chen, JL Volakis, and JW Halloran. Patch-antenna miniaturization using recently available ceramic substrates. *IEEE Antennas and Propagation Magazine*, 48(6):13–20, 2006.

[14] Chul-Soo Kim, Jun-Seok Park, Dal Ahn, and Jae-Bong Lim. A novel 1-d periodic defected ground structure for planar circuits. *IEEE Microwave and guided wave letters*, 10(4):131–133, 2000.

[15] Debatosh Guha, Sujoy Biswas, Manotosh Biswas, Jawad Y Siddiqui, and Yahia MM Antar. Concentric ring-shaped defected ground structures for microstrip applications. *IEEE Antennas and Wireless Propagation Letters*, 5(1):402–405, 2006.

[16] Hai W Liu, Zheng F Li, and Xiao W Sun. A novel fractal defected ground structure and its application to the low-pass filter. *Microwave and Optical Technology Letters*, 39(6):453–456, 2003.

[17] Falguni Raval, YP Kosta, and Harshita Joshi. Reduced size patch antenna using complementary split ring resonator as defected ground plane. *AEU-International Journal of Electronics and Communications*, 69(8):1126–1133, 2015.

[18] Atallah Balalem, Ali R Ali, Jan Machac, and Abbas Omar. Quasi-elliptic microstrip low-pass filters using an interdigital dgs slot. *IEEE Microwave and wireless Components letters*, 17(8):586–588, 2007.

[19] Kaushik Mandal and Partha Pratim Sarkar. A compact low profile wideband u-shape antenna with slotted circular ground plane. *AEU-International Journal of Electronics and Communications*, 70(3):336–340, 2016.

[20] Reeta Devi and Dipak KR Neog. A compact elevated cpw-fed antenna with slotted

ground plane for wideband applications. *International Journal of Microwave and Wireless Technologies*, 9(10):2005–2011, 2017.

[21] Mrinal Kanti Mandal and Subrata Sanyal. A novel defected ground structure for planar circuits. *IEEE Microwave and Wireless Components Letters*, 16(2):93–95, 2006.

[22] Han-Jan Chen, Tsung-Hui Huang, Chin-Sheng Chang, Lih-Shan Chen, Na-Fu Wang, Yeong-Her Wang, and Mau-Phon Houng. A novel cross-shape dgs applied to design ultra-wide stopband low-pass filters. *IEEE Microwave and Wireless Components Letters*, 16(5):252–254, 2006.

[23] Anand Sharma and Ravi Kumar Gangwar. Compact dual-band ring dielectric resonator antenna with moon-shaped defected ground structure for w i max/wlan applications. *International Journal of RF and Microwave Computer-Aided Engineering*, 26(6):503–511, 2016.

[24] Mukesh Kumar Khandelwal, Binod Kumar Kanaujia, Santanu Dwari, Sachin Kumar, and AK Gautam. Analysis and design of wide band microstrip-line-fed antenna with defected ground structure for ku band applications. *AEU-International Journal of Electronics and Communications*, 68(10):951–957, 2014.

[25] Jian-Kang Xiao, Wen-Jun Zhu, and Jeffrey S Fu. New bandstop filter using simple. defected microstrip structure. *Microwave Journal*, 54(9), 2011.

[26] Elftouh Hanae, Naima Amar Touhami, and Mohamed Aghoutane. Miniaturized microstrip patch antenna with spiral defected microstrip structure. *Progress In Electromagnetics Research*, 53:37–44, 2015.

[27] Atefeh Kordzadeh and Farrokh Hojjat-Kashani. A new reduced size microstrip patch antenna with fractal shaped defects. *Progress In Electromagnetics Research*, 11:29–37, 2009.

[28] Ahmed Boutejdar, Mohammad Ahmad Salamin, Saad Dosse Bennani, et al. Design of compact monopole antenna using double u-dms resonators for wlan, lte, and wimax applications. *Telkomnika*, 15(4), 2017.

[29] Jose Alfredo Tirado-Méndez, Hildeberto Jardón-Aguilar, Flavio Iturbide-Sánchez, Israel Garcia-Ruiz, Victoria Molina-Lopez, and Rene Acevo-Herrera. A proposed defected microstrip structure (dms) behavior for reducing rectangular patch antenna size. *Microwave and optical technology letters*, 43(6):481–484, 2004.

[30] Jose A Tirado-Mendez, Hildeberto Jardon-Aguilar, Ruben Flores-Leal, and Arturo Rangel-Merino. Multiband reduced-size patch antenna by employing a modified dms-spur-line combo technique. *International Journal of RF and Microwave Computer-Aided Engineering*, 28(4):e21232, 2018.

[31] Shrivishal Tripathi, Akhilesh Mohan, and Sandeep Yadav. A multinotched octagonal shaped fractal uwb antenna. *Microwave and Optical Technology Letters*, 56(11):2469–2473, 2014.

[32] Shrivishal Tripathi, Akhilesh Mohan, and Sandeep Yadav. A compact octagonal-shaped fractal uwb antenna with s ierpinski fractal geometry. *Microwave and Optical Technology Letters*, 57(3):570–574, 2015.

[33] M Naser-Moghadasi, RA Sadeghzadeh, T Aribi, T Sedghi, and BS Virdee. Uwb monopole microstrip antenna using fractal tree unit-cells. *Microwave and Optical Technology Letters*, 54(10):2366–2370, 2012.

[34] MKA Rahim, MNA Karim, F Zubir, O Ayop, and NA Samsuri. Second iteration fractal koch planar log periodic antenna design. *Microwave and Optical Technology Letters*, 53(8):1869–1875, 2011.

[35] Filiberto Bilotti, Andrea Alu, and Lucio Vegni. Design of miniaturized metamaterial patch antennas with μ-negative loading. *IEEE Transactions on Antennas and Propagation*, 56(6):1640–1647, 2008.

[36] Anahita Ghaznavi Jahromi, Farzad Mohajeri, and Nooshin Feiz. Miniaturization of a rectangular microstrip patch antenna loaded with metamaterial. *World academy of Science, engineering and technology*, 7(4):668–671, 2013.

[37] D-L Jin, T-T Bu, J-S Hong, J-F Wang, and H Xiong. A tri-band antenna for wireless applications using slot-type srr. *Applied Computational Electromagnetics Society Journal*, 29(1), 2014.

[38] Maryam Rahimi, Ferdows B Zarrabi, Rahele Ahmadian, Zahra Mansouri, and Asghar Keshtkar. Miniaturization of antenna for wireless application with difference metamaterial structures. *Progress In Electromagnetics Research*, 145:19–29, 2014.

[39] Seif Naoui, Lassaad Latrach, and Ali Gharsallah. Metamaterials dipole antenna by using split ring resonators for rfid technology. *Microwave and Optical Technology Letters*, 56(12):2899–2903, 2014.

[40] H Sanad. Effect of the shorting posts on short circuit microstrip antennas. In *Antennas and Propagation Society International Symposium, 1994. AP-S. Digest*, volume 2, pages 794–797. IEEE, 1994.

[41] Tapas Chakravarty and Asok De. Design of tunable modes and dual-band circular patch antenna using shorting posts. *IEE Proceedings-Microwaves, Antennas and Propagation*, 146(3):224–228, 1999.

[42] Rebekka Porath. Theory of miniaturized shorting-post microstrip antennas. *IEEE Transactions on Antennas and Propagation*, 48(1):41–47, 2000.

[43] Rod Waterhouse. Small microstrip patch antenna. *Electronics letters*, 31(8):604–605, 1995.

[44] Chia-Luan Tang, Hong-Twu Chen, and Kin-Lu Wong. Small circular microstrip antenna with dual-frequency operation. *Electronics Letters*, 33(13):1112–1113, 1997.

[45] Muhammad Umar Khan, Mohammad Said Sharawi, and Raj Mittra. Microstrip patch antenna miniaturisation techniques: a review. *IET Microwaves, Antennas & Propagation*, 9(9):913–922, 2015.

[46] Saber Soltani, Mohammadnaghi Azarmanesh, Parisa Lotfi, and Gholamreza Dadashzadeh. Two novel very small monopole antennas having frequency band notch function using dgs for uwb application. *AEU-International Journal of Electronics and Communications*, 65(1):87–94, 2011.

[47] Xian-ping Xiong, Qian Liu, Yun Zhang, and Yong-lun Luo. Novel acs-fed monopole antenna for uwb applications with sharp selectivity notched band and additional bluetooth

band characteristics. *Journal of Electromagnetic Waves and Applications*, 28(18):2308–2317, 2014.

[48] Yingsong Li, Wenxing Li, and Qiubo Ye. Miniaturization of asymmetric coplanar strip-fed staircase ultrawideband antenna with reconfigurable notch band. *Microwave and Optical Technology Letters*, 55(7):1467–1470, 2013.

[49] Kalikuzhackal Abbas Ansal and Thangavelu Shanmuganantham. Compact acs-fed antenna with dgs and dms for wimax/wlan applications. *International Journal of Microwave and Wireless Technologies*, 8(7):1095–1100, 2016.

[50] Yingsong Li, Wenxing Li, and Raj Mittra. A compact acs-fed dual-band meandered monopole antenna for wlan and wimax applications. *Microwave and Optical Technology Letters*, 55(10):2370–2373, 2013.

Chapter 3

Design Procedure of Miniaturized Dual-Band Fractal Ring Monopole Antenna

Contents

3.1 Introduction

Fractal geometries applied to antenna design is a promising technique to meet the requirements of modern communication systems. Small size, multiband and broadband operations are major challenges of these systems. The main characteristics of fractal geometries are self-similarity and space filling. Self-similarity gives rise to multiband and broadband operations, whereas space filling offers the possibility of achieving antenna size reduction. Basically, fractal geometries are generated by repetition of a geometrical basic pattern with a number of iterations. Besides the conventional fractal geometries such as Koch , Sierpinski gasket and Hilbert curve[1], several patterns have been introduced for fractal antenna designs including X-shaped[2], hexagonal tree shaped [3], octagonal fractal shaped [4] and inner tapered tree shaped [5]. Fractal antenna designs based on a high number of iterations lead to complex structures whereas those using few iterations result in larger structure size.

In this chapter, a novel approach based on fractal concept for miniaturization will be proposed and studied. Firstly, a basic circular antenna will be designed and used to derive an hexagonal shaped patch antenna. Secondly, the resulted structure will be loaded with an hexagonal slot such that an hexagonal shaped ring patch antenna will be obtained. Finally, a fractal generation of a radiating ring is applied to the hexagonal ring. The four (04) structures, namely circular patch, hexagonal patch, hexagonal and fractal ring antennas will be studied in details in the following sections.

3.2 Circular Shaped Patch Antenna

The circular patch is one of the most used configuration in the antenna design. Besides its ease of analysis and fabrication, the circular shaped microstrip antenna has attractive radiation performances especially low cross polarization. Accordingly, this shape is selected in this section to design an antenna operating at 3.5GHz band dedicated to the WiMAX application. The antenna is designed and investigated by means of the full-wave commercial software CST Microwave Studio.

Based on the cavity model, the resonant frequencies $(f_r)_{mn0}$ supported by a circular patch of radius a are [6]

$$(f_r)_{mn0} = \frac{X'_{mn}c}{2\pi a_e\sqrt{\epsilon_r}} \tag{3.1}$$

where c is the speed of light in free-space, X'_{mn} represents the zeroes of the derivative of the Bessel function $J_m(x)$ and a_e is the effective radius given by

$$a_e = a\{1 + \frac{2h}{\pi a\epsilon_r}[ln(\frac{\pi a}{2h}) + 1.7726]\}^{1/2} \tag{3.2}$$

The first three values of X'_{mn} which represent the order of the resonant frequencies are given in ascending order

$$\begin{aligned} X'_{11} &= 1.8412 \\ X'_{21} &= 3.0542 \\ X'_{01} &= 3.8318 \end{aligned} \tag{3.3}$$

Therefore the resonant frequency f_0 for the dominant TM_{110} is expressed as

$$f_0 = \frac{1.8412c}{2\pi a_e \sqrt{\epsilon_r}} \tag{3.4}$$

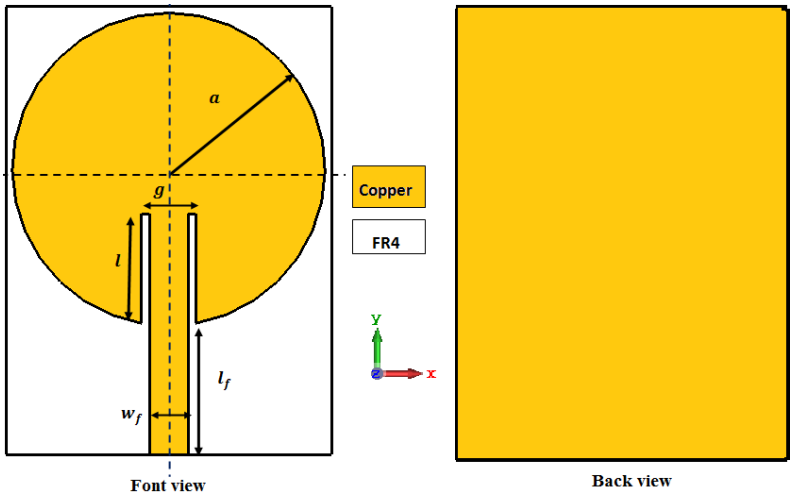

Figure 3.1: Schematic of a circular microstrip patch antenna

Using the two equations 3.2 and 3.4, the circular patch radius a operating at the frequency $f_0 = 3.5GHz$ is found to be equal to $11.64mm$. In the above equations, the operating frequency f_0 should be taken in Hertz (Hz) and the height of the substrate h should be taken in Centimeters (cm). An FR4 substrate of dimensions $25.3mm \times 34.8mm$ is taken and a wave port is used to feed the circular patch. The resulted circular microstrip patch antenna model designed is shown in Figure 3.1. As can be seen from the figure, an inset feedline is used to feed the radiating element, the notch geometry is chosen for the proper impedance matching. A 50Ω impedance microstrip line of length $l_f = 10mm$ and width $w_f = 3mm$ is used to feed the circular patch.

3.2.1 Reflection coefficient (S_{11})

Usually, the first design is not fully optimized and it is necessary to adjust the model to further refine the dimensions. Variation of reflection coefficient in dB with radius a of the circular patch is shown in Figure 3.2. It can be seen from the figure that the resonant frequency of the patch with a radius of 11.64 mm is of 3.66 GHz which is different from the desired frequency of 3.5GHz. This discrepancy is due to the fact that the design of the circular patch is based on the cavity model while the software used to simulate the antenna is based on full wave method of calculation (CST software). Hence, the radius must be increased to obtain a resonance at 3.5 GHz. It can be clearly noticed from this figure that for $a = 12.15mm$, the antenna resonates at the desired frequency. For better impedance

matching, the inset dimensions are varied and the simulated return loss results are shown in Figure 3.3. It can be concluded from the figure that for $l = 8.7mm$ and $g = 4.2mm$ good impedance matching is achieved. The simulated return loss of the designed antenna is shown in Figure 3.4. It can be seen that the antenna operates at 3.5 GHz with a return loss of $-46dB$ and a bandwidth of 151MHz (4.3%).

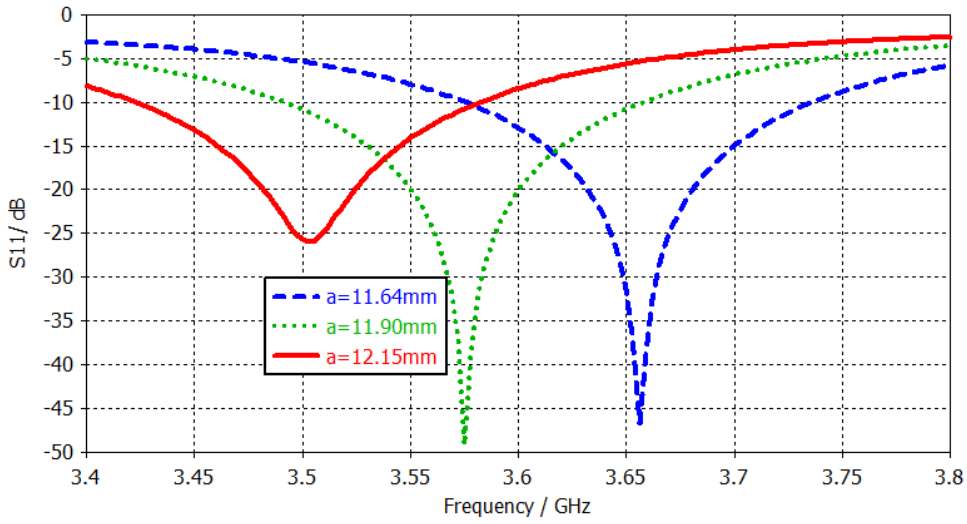

Figure 3.2: Simulated return loss of the circular antenna for different values of the radius a

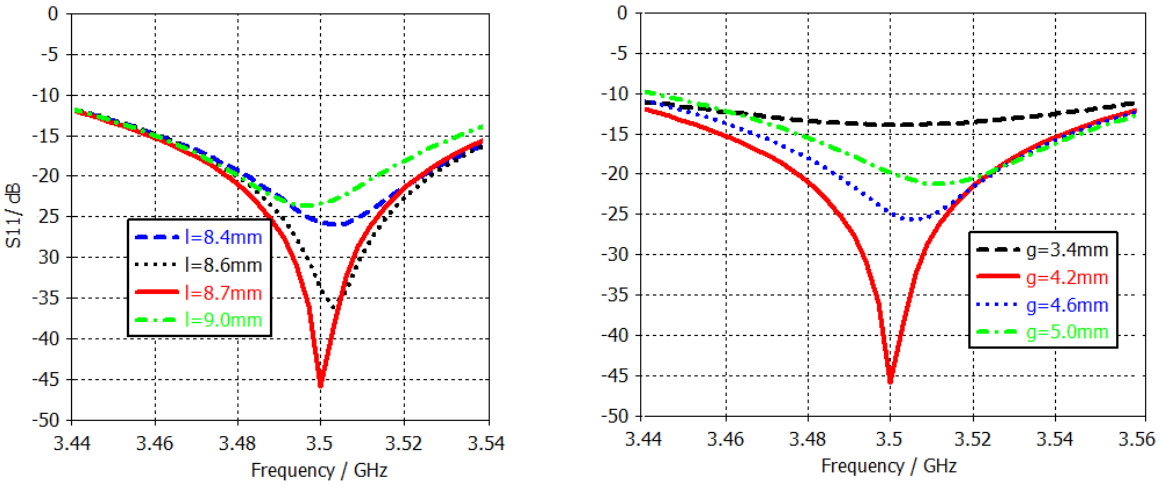

(a) **(b)**

Figure 3.3: Simulated reflection coefficients of circular antenna for different values of (a) length l and (b) width g of the inset

3.2.2 Current Distribution and Radiation Pattern

The excited surface current distribution for the operating frequency is simulated and it is shown in Figure 3.5. It can be clearly seen that the exited mode is the mode TM11 where the current zeros occur at two opposite points located on the disc periphery. Maximum current

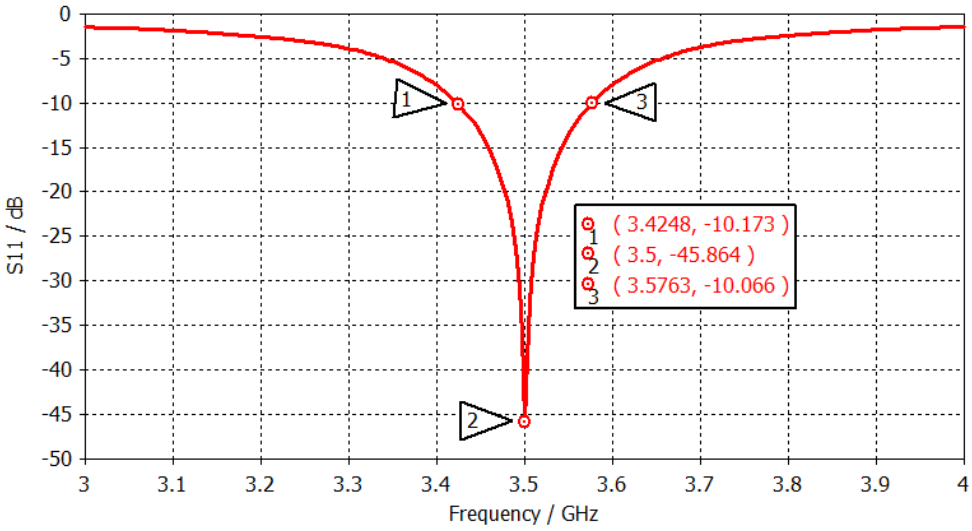

Figure 3.4: Simulated return losses of the circular microstrip patch antenna

density is seen at the center of the patch. Consequently, this mode is fully controlled by the circular patch radius.

Figure 3.6 represents the simulated E-plane (y-z-plane) and H-plane (x-z-plane) radiation patterns of the circular antenna at 3.5 GHz. It can be seen that the antenna maximum radiation occurs in the broadside direction which is primarily determined by the circular disc. The radiation pattern is omnidirectional in the H-plane while it is broadside in the E-plane where maximum directivity is 5.47dBi.

Since the main contribution of this work focuses on antenna miniaturization, monopole configuration presents a good candidate due to its radiation characteristics and size as compared to patch antenna. By using monopole structure, the antenna dimensions will be reduced to the half because in monopole configuration antennas are $\lambda/4$ radiator. In addition, the radiation pattern of the monopole antenna is dipole-like in the E-plane which covers both radiator side and ground plane side hemispheres hence more suitable for wireless applications such as WiMAX.

3.3 Design Procedure of Dual-Band Fractal Antenna

3.3.1 Circular Monopole antenna

Based on the circular patch presented in the previous section and by truncating the ground plane, a monopole antenna is derived. The resulted structure along with its dimensions is presented in Figure 3.7. It is seen in the figure that the radius of the circular radiating element is reduced to about half. Hence, the total achieved size reduction is around 69.2%

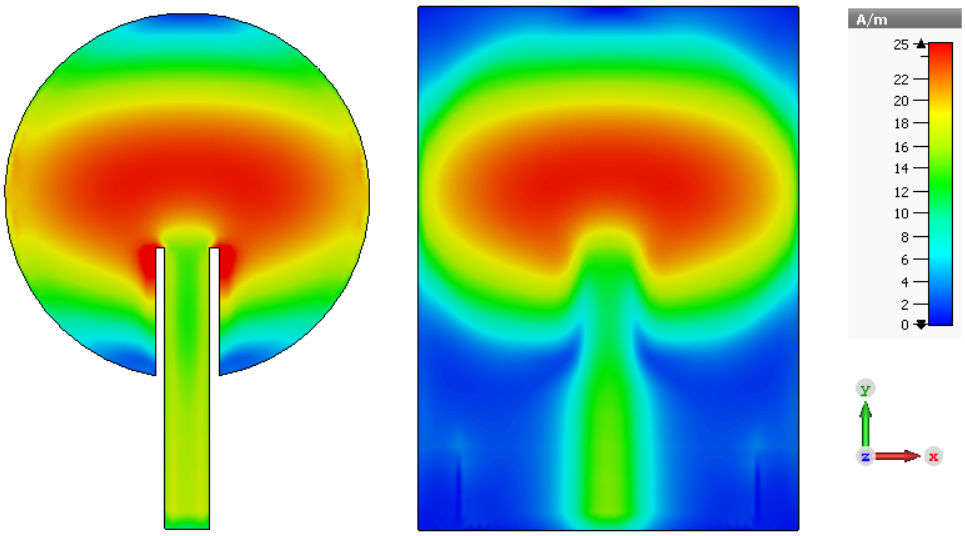

Figure 3.5: Simulated surface current plot at 3.5 GHz

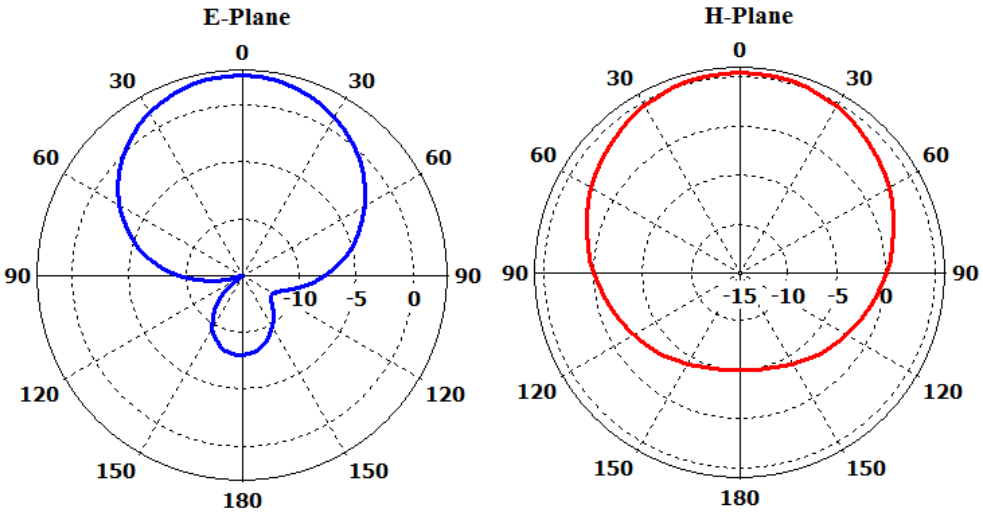

Figure 3.6: Simulated radiation pattern of Circular Patch Antenna at 3.5 GHz

which represents a significant miniaturization rate.

Besides antenna size reduction, the antenna bandwidth is as well extended. Therefore, the circular monopole antenna operates in a wide frequency band extending from 3.49 GHz to 8 GHz covering the 3.5 GHz band as shown in Figure 3.8. The simulated far-field of the circular monopole antenna is also depicted in Figure 3.8. It can be clearly seen from the result, the radiation pattern is omnidirectional in the H-plane (x-z plane) and bidirectional in the E-plane (y-z plane) with two nulls. Consequently, it can be concluded that the radiation characteristics have been been improved by truncation of the ground plane of a circular patch.

The antenna operates in a wide band with a compact size of $13.3 \times 20mm^2$. In addition, the antenna has an omnidirectional radiation pattern which make the design a good candidate

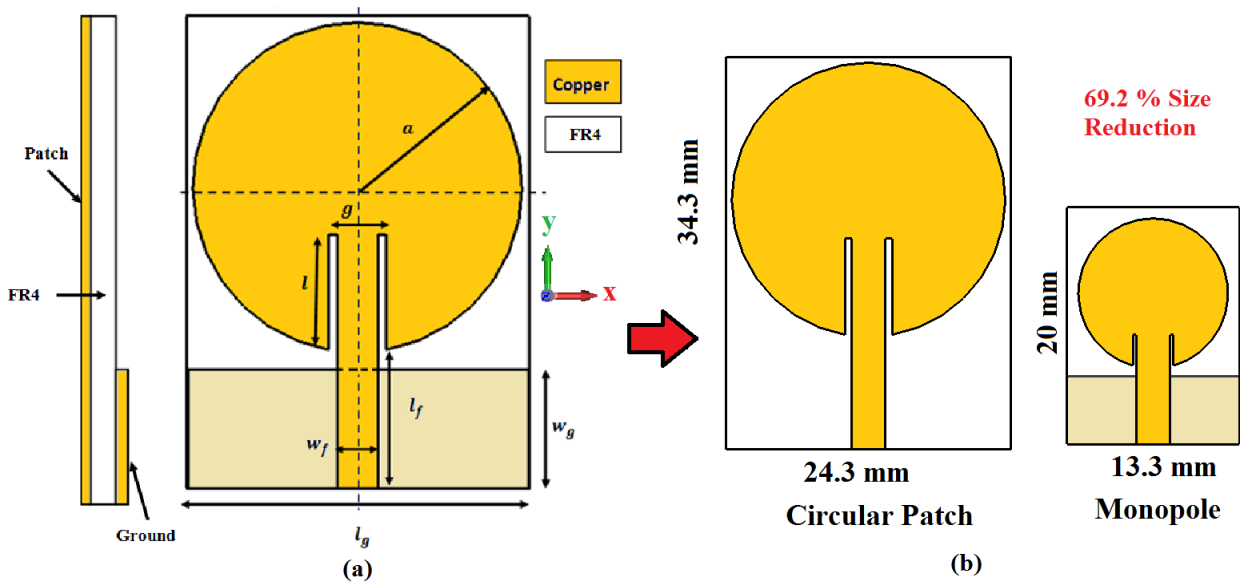

Figure 3.7: (a)Geometry of circular monopole antenna $W_g = 13.3mm, L_g = 6mm, a = 6.65mm, L_f = 6.7mm, W_f = 3mm$ and $g = 3.6mm$, (b) Comparison between monopole and circular patch configurations

for wireless communication application. To control the operating bandwidth as well as the resonant frequency of the antenna without changing its dimensions, a modified circular patch will be introduced. In what follows, the details of the so derived antenna will be presented.

3.3.2 Hexagonal Monopole Antenna

Based on the circular monopole antenna described in the previous section, an hexagonal shaped monopole antenna is derived and studied. The resulted structure is obtained by substituting the circular disk by an hexagonal polygon. It is noted that during the simulation of the hexagonal antenna, the matching was very sensitive to a small change of any parameter and it is difficult to achieve. For improving the impedance matching of the antenna, the feeding structure is changed from a simple microstrip line to a Y shaped transmission line as shown in Figure 3.9.

The simulated return losses of the structures are compared and presented in Figure 3.10. It can be noted that by introducing the hexagonal shape as a radiating element, with a simple feedline, the antenna resonant frequency is decreased from 4.2 GHz to 3.66 GHz while the S_{11} level is increased from -35dB to -25dB. To improve the antenna matching, the feedline is changed from a simple transmission line to a Y-shaped transmission line as can be seen in Figure 3.9. The introduction of the Y-transmission line has significantly improved the antenna impedance matching. The simulated current distribution for different configurations

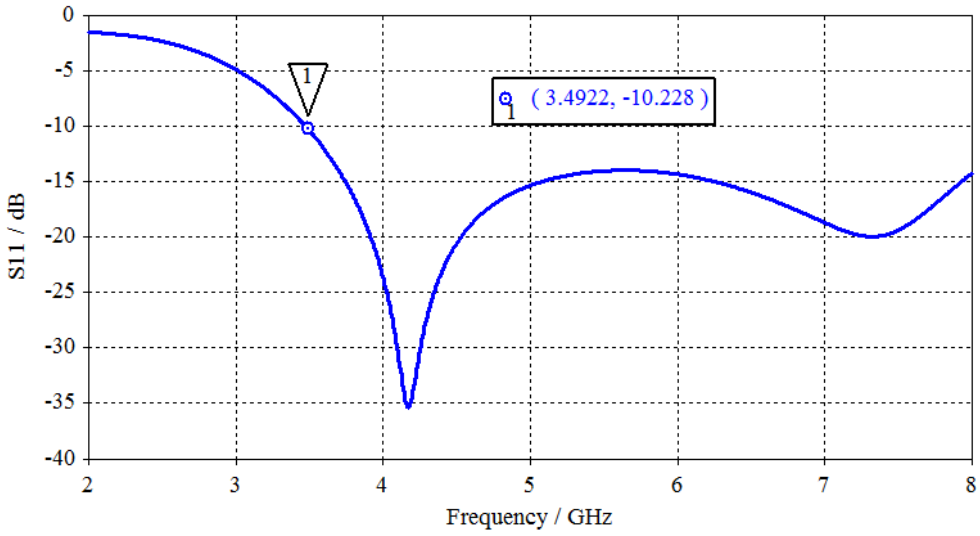

(a)

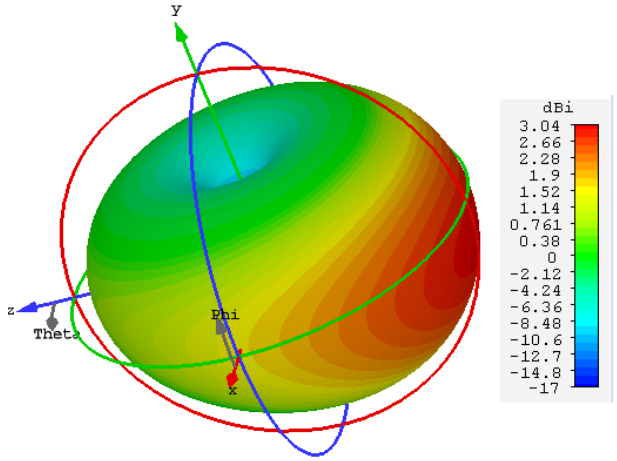

(b)

Figure 3.8: (a) Simulated return loss of the circular monopole antenna and (b) its radiation pattern at $f = 3.5GHz$

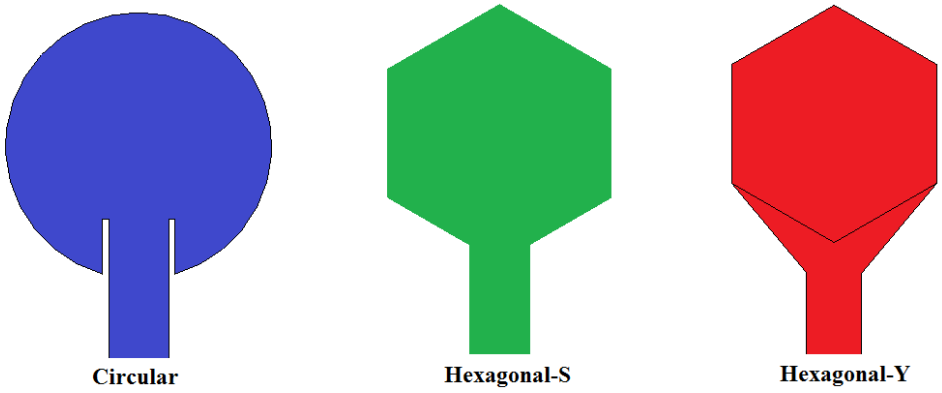

Figure 3.9: Circular patch, hexagonal patch with a simple transmission line and hexagonal patch with a Y transmission line

are presented in Figure 3.11. It is observed that, for all structures, strong electric current exists around the feedline and at the lowest part of the patch. It can be also seen that the hexagonal structure with Y feedline presents larger patch active area as compared to two

other designs.

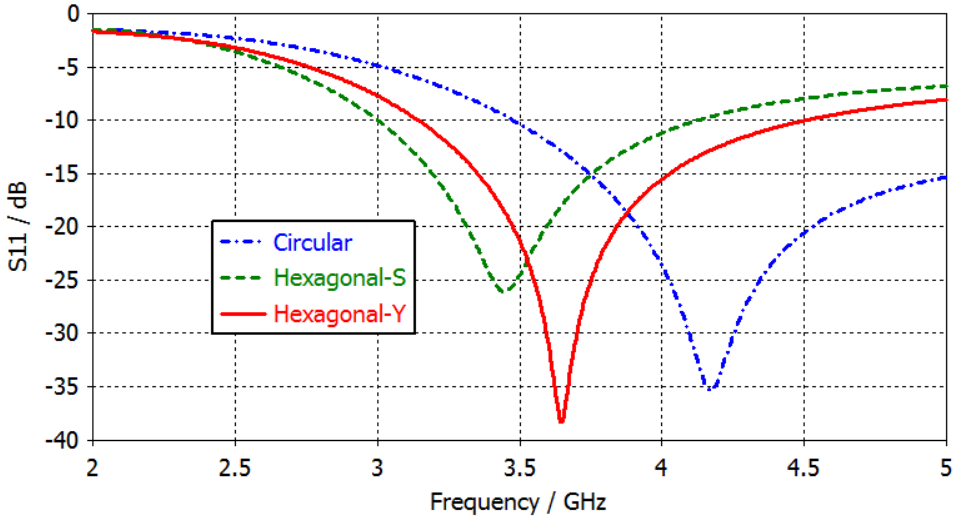

Figure 3.10: Simulated return losses for different antennas

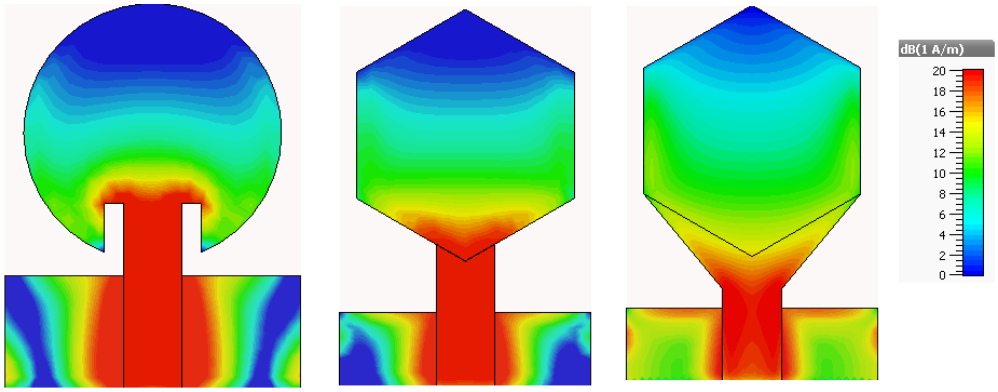

Figure 3.11: Simulated current distributions for different antennas

3.3.3 Hexagonal Ring Monopole Antenna

To further downsize the antenna dimension, the hexagonal monopole antenna described in the previous section is loaded with an hexagonal slot in the center of the patch. When the slot is etched from the patch, the resulted antenna is an hexagonal ring antenna as depicted in Figure 3.12a.

- **Effect of changing t**

The effect of varying the parameter t on return loss is given in Figure 3.13 . It can be observed from the figure that as the width of the hexagonal ring t decreases, the resonant frequency shifts towards lower frequencies. At the same time, the upper cut-off frequency of the operating band decreases significantly while the lower cut-off frequency decreases slightly. Accordingly, the bandwidth of the antenna decreases with the decrease of the parameter t.

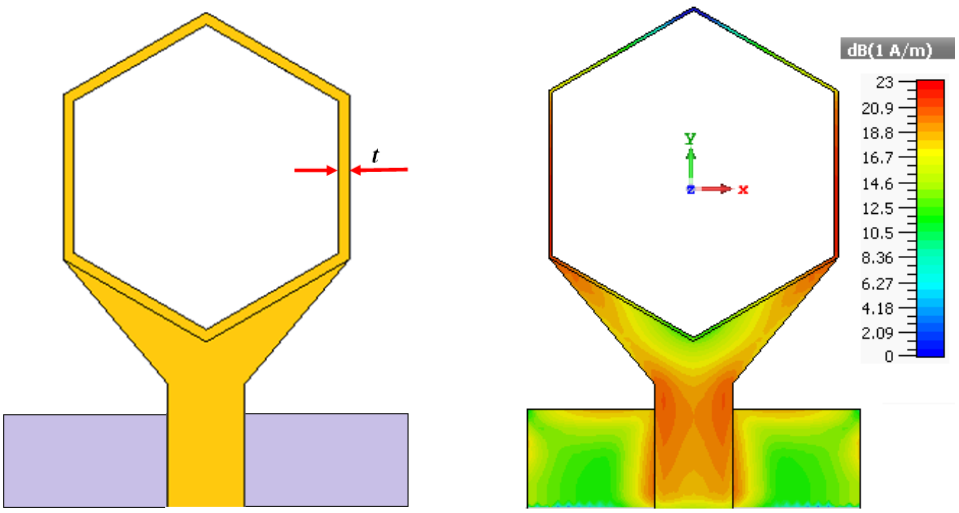

Figure 3.12: (a) Hexagonal ring monopole antenna structure and (b) its current distribution for $t = 0.3mm$ at its resonant frequency of $3.33GHz$

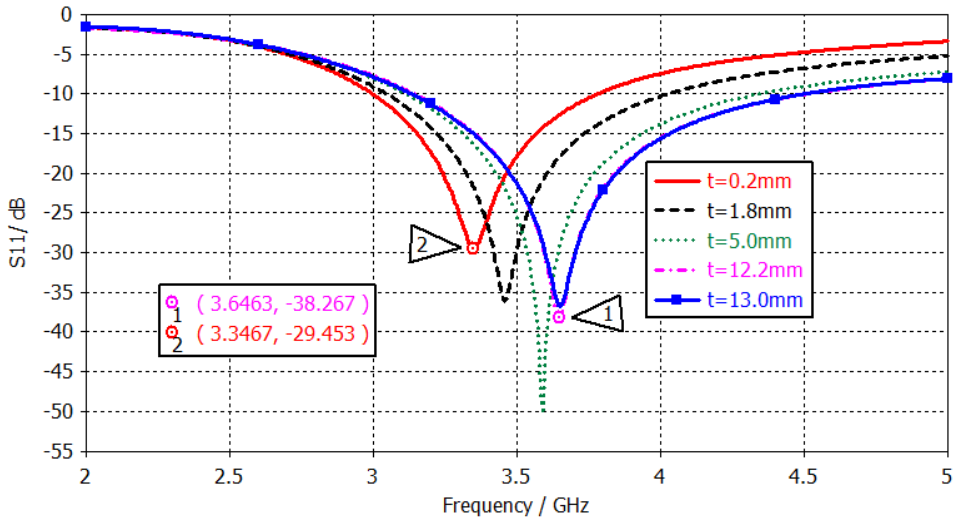

Figure 3.13: Simulated return losses for different antennas

3.3.4 Hexagonal Fractal Ring Monopole Antenna

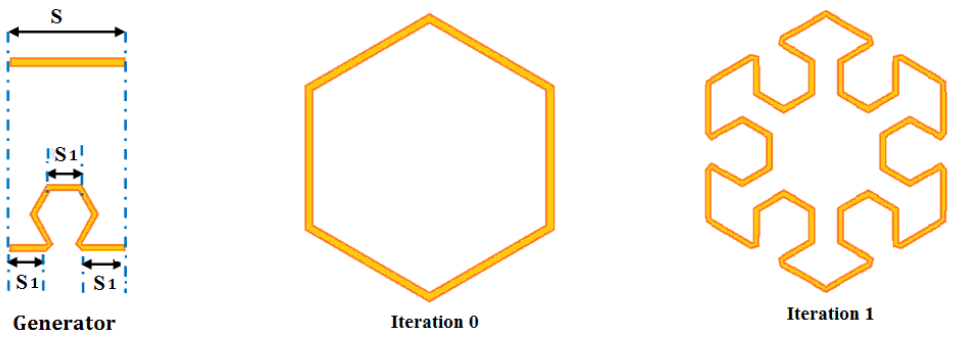

Figure 3.14: Hexagonal fractal ring generation procedure

The previous sections dealt with the design and development of compact monopole an-

tenna operating at a single frequency band. In this section, a fractal concept is effectively used to design a miniaturized antenna operating at two different frequency bands. The generation process of the fractal hexagonal ring is illustrated in Figure 3.14. The straight sides of the hexagonal ring are substituted with an open hexagonal rings with two extensions as shown in the same figure. The small generated open hexagonal rings have same side lengths S_1. The resulted structure is presented in Figure 3.15 which has same dimensions as the hexagonal ring described in the previous section.

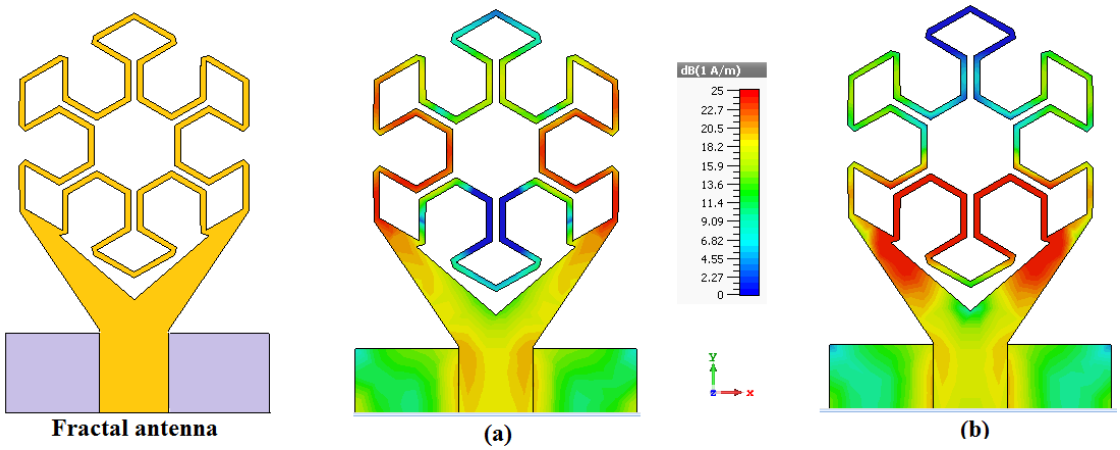

Figure 3.15: Fractal ring antenna structure and its currents distributions for $S_1 = 2mm$ at (a) 3.93GHz and (b) 4.44GHz

Effect of changing S_1

Figure 3.16 illustrates the simulated reflection coefficient result when the length S_1 varies from 1.4 mm to 2.0 mm with a step of 0.2 mm. It can be observed that as the value of S_1 increases, the first resonant frequency shifts slightly towards lower values side while the second operating band (for $S_1 = 1.8mm$ and $S_1 = 2.0mm$) decrease significantly. Moreover, it is noted that as the value of S_1 increases, the return loss at resonant frequencies deteriorates. Accordingly, the antenna operating frequencies can be controlled by mainly changing the value of the key parameter S_1 as confirmed in the current distributions at the resonant frequencies given in Figure 3.15.

3.4 Summary

The design procedure of a compact fractal ring antenna for dual-band operation has been proposed and discussed. In the first step, the design and study of circular patch antenna operating at 3.5 GHz is investigated. Then, it is modified to monopole configuration by

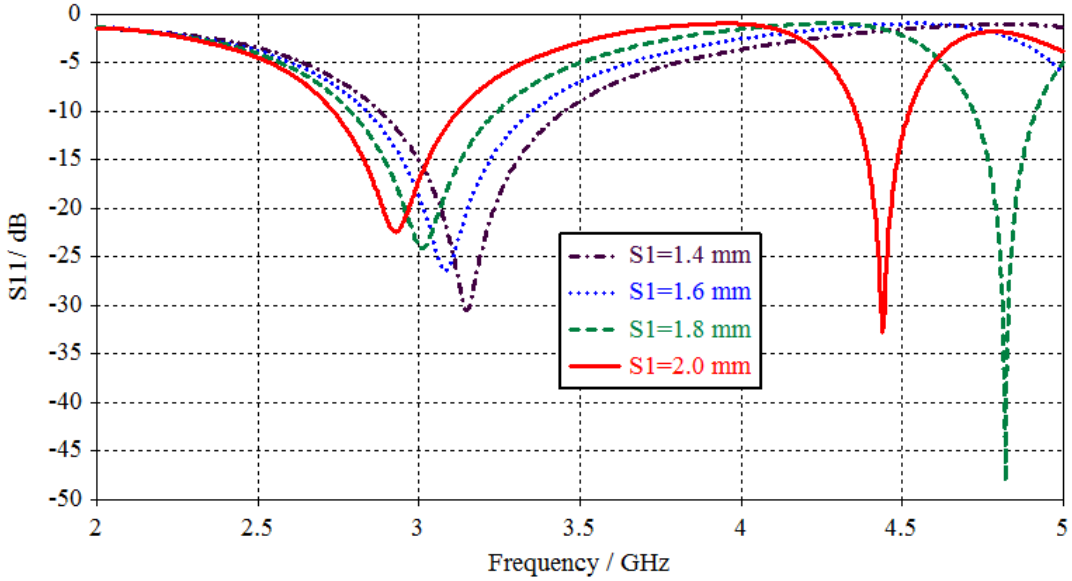

Figure 3.16: Simulated return losses for different values of S_1

ground plane truncation to downsize the antenna dimension and to widen its bandwidth. Hence, the resulted circular monopole antenna achieves 68% size reduction as compared to its patch configuration counterpart. The next step was to modify the circular monopole to an hexagonal monopole with a Y shaped fed line. The Y transmission line is used to improve the impedance matching at the resonant frequency of the antenna. At this stage, the hexagonal antenna has been loaded by a DMS hexagonal slot. Accordingly, the obtained hexagonal ring monopole antenna presents a lower resonant frequency as compared to a hexagonal monopole antenna which leads to antenna size reduction. The last step was to derive a fractal ring monopole antenna from the hexagonal ring monopole. The procedure of generation of the fractal ring has been explained and a comparison between hexagonal and fractal ring monopole antennas has been presented. Consequently, the fractal ring monopole antenna was very compact and can operate in dual band over the considered range of frequencies. This resulted fractal monopole antenna will be the basic design to develop more compact antennas operating in dual- and tri-band in the coming chapters.

Bibliography

[1] Vasa Radonić, Keith Palmer, Goran Stojanović, and Vesna Crnojević-Bengin. Flexible sierpinski carpet fractal antenna on a hilbert slot patterned ground. *International Journal of Antennas and Propagation*, 2012, 2012.

[2] Ankush Gupta, Hem Dutt Joshi, and Rajesh Khanna. An x-shaped fractal antenna

with dgs for multiband applications. *International Journal of Microwave and Wireless Technologies*, 9(5):1075–1083, 2017.

[3] Sarthak Singhal, Tushar Goel, and Amit Kumar Singh. Hexagonal tree shaped ultra–wideband fractal antenna. *International Journal of Electronics Letters*, 5(3):335–348, 2017.

[4] Shrivishal Tripathi, Akhilesh Mohan, and Sandeep Yadav. A compact octagonal-shaped fractal uwb antenna with sierpinski fractal geometry. *Microwave and Optical Technology Letters*, 57(3):570–574, 2015.

[5] Sarthak Singhal, Tushar Goel, and Amit Kumar Singh. Inner tapered tree-shaped fractal antenna for uwb applications. *Microwave and Optical Technology Letters*, 57(3):559–567, 2015.

[6] A Balanis Constantine et al. Antenna theory: analysis and design. *MICROSTRIP ANTENNAS, third edition, John wiley & sons*, 2005.

Chapter 4

Design of Miniaturized Dual Band Fractal Ring Monopole Antenna

Contents

4.1 Introduction

With the rapid development of modern wireless communication systems, the demand for antennas with compact size, lightweight, dual-band operation and high efficiency, capable to be embedded in diverse devices, has increased considerably. To achieve that, many research works have been conducted to design compact antennas which can operate in multiple bands and hence cover different communication applications [1], [2].

In this chapter, two novel compact dual-band monopole antennas with omnidirectional radiation pattern will be designed, fabricated and tested. First antennas is based on an appropriate combination of two coupled first-order hexagonal fractal rings designed in the previous chapter, one printed on the top side of the substrate whereas the second one embedded in the ground plane, along with Y-shaped feeding line, a dual-band operation as well as size reduction are achieved. The fractal rings perimeter and the dimensions of the feeding line are varied to obtain the desired resonant frequency bands which widely cover the bands

allocated to WLAN at 2.4 GHz and WiMAX at 3.5 GHz, simultaneously. Furthermore, an investigation will be performed in order to study the effects of mounting the proposed antenna on the side of a standard ground-plane (SGP) of laptop computer, on the antenna performance.

The second design consists of three slotted fractal rings combined effectively to caver two different bands dedicated RFID and GSM 1800. The parameters of the three fractal ring will be optimized through an extensive parametric study. The design and simulation will be carried out using CST microwave studio. The simulated and measured return losses and radiation patterns of the proposed antenna will be presented and discussed.

4.2 A Compact Dual-Band Planar Monopole Antenna using Fractal Rings and a Y-Shaped Feeding Transmission Line

4.2.1 Antenna structure and design procedure

Figure 4.1d shows the geometry of the proposed dual-band monopole antenna along with its elements in details. The proposed structure consists of two first-iterative hexagonal fractal rings, a Y-shaped transmission line and a U-shaped ground plane. On the top side of the substrate, is a fractal radiating ring fed with a Y-shaped transmission line while in the other side of the substrate is a second fractal ring, electromagnetically coupled with the first one, and a U-shaped ground plane. The detail of the fractal ring is illustrated in Figure 4.1d. The proposed structure is designed on a 1.6 mm thick FR-4 substrate with permittivity and loss tangent of 4.3 and 0.017, respectively. This substrate will be used for the design of all the structures which will be presented in this chapter and in the following chapters 5 and 6. The antenna dimensions are tuned by varying one parameter at a time and keeping the others as constants. The proposed design dimensions are listed in Table 4.1 .

Table 4.1: Geometrical dimensions of the proposed antenna

Parameter	L	L_1	L_f	W_f	W_1	S_1	S	W	θ	L_g	W_g	d	t
Value (mm)	18.9	5.2	4.1	3.5	6.2	1.65	6.5	13	30	4	13	2	0.3

The design process involves three different evolution stages as depicted in Figure 4.2. Initially, a simple hexagonal ring fed with a Y-shaped transmission line along with a U-shaped ground plane is designed, denoted as Ant.1. To downsize the antenna dimensions, instead of using a simple hexagonal shape, a first-iterative fractal hexagonal ring is introduced

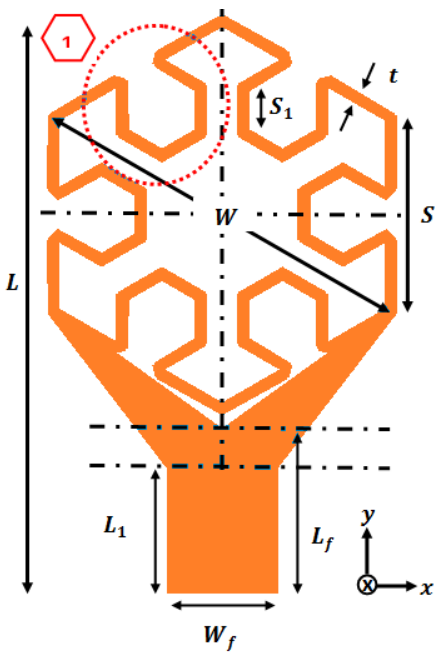

(a) Top view

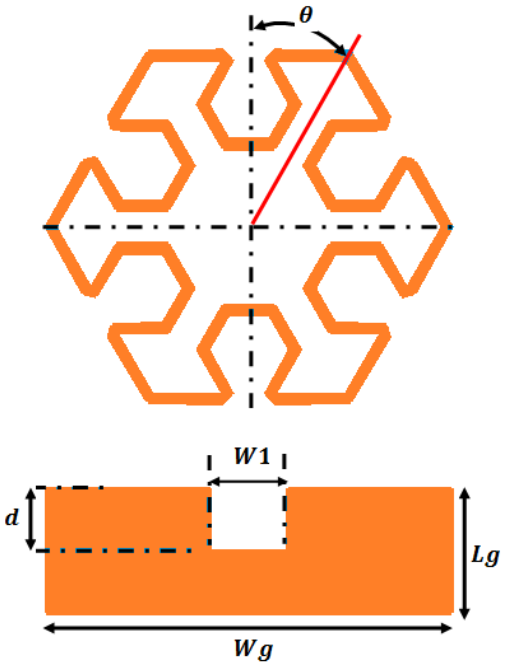

(b) Bottom view

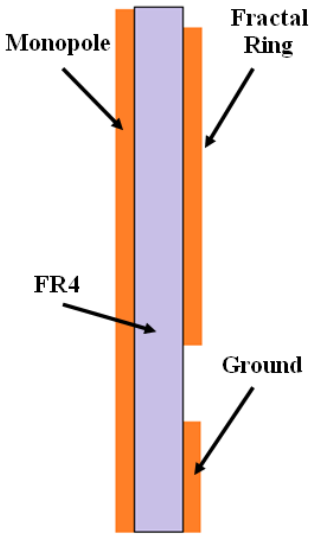

(c) Side view

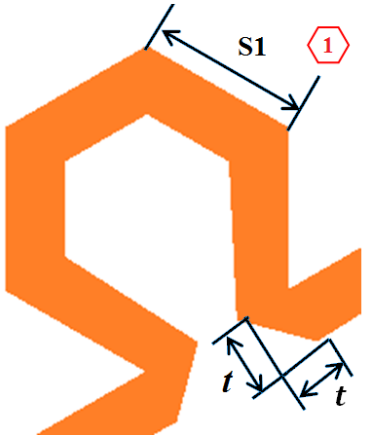

(d) Detail of the hexagonal fractal ring

Figure 4.1: Geometry of the proposed dual-band antenna

to derive Ant.2. Moreover, to achieve dual-band operation and to further reduce the antenna dimensions, a second fractal ring, with same dimensions as the radiating ring, is embedded in the ground plane to design the proposed antenna, denoted as Ant.3.

4.2.2 Simulation Results

Figure 4.3 shows a comparison of the simulated reflection coefficients of Ant.1, Ant.2 and Ant.3. From the results, it is observed that Ant.1 resonates at 4.19 GHz while Ant.2 resonates at 3.03 GHz. Thus, it can be concluded that by introducing the fractal radiating ring a shift

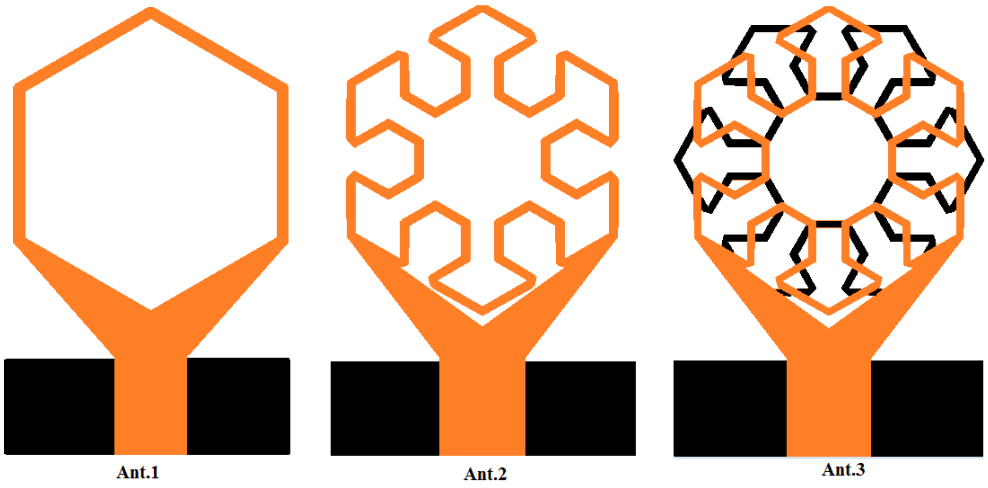

Figure 4.2: Geometry of different antennas involved in the design development.

of the resonant frequency from 4.19 to 3.03 GHz is observed. Accordingly, an antenna size reduction is achieved. Furthermore, by loading Ant.2 with a second fractal ring in the ground plane (Ant.3), an electromagnetic coupling between the two fractal rings is created leading to dual-band operation (2.45/3.5 GHz) and further reduction in antenna size in terms of the first resonant frequency value is achieved.

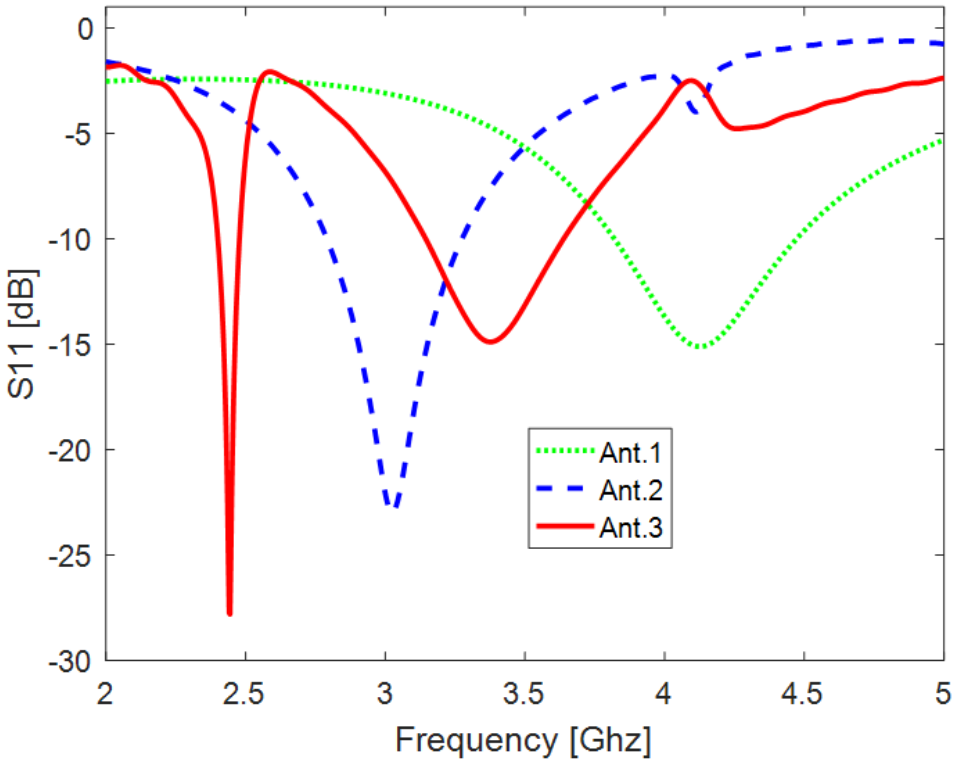

Figure 4.3: Return losses versus frequency for different antenna structures.

Figure 4.4a shows the results obtained through simulation of the return loss characteristic according to the change of $S1$ while all other parameters are kept constants. As the value of

$S1$ increases, both resonant frequencies shift to lower frequencies. Thus, by increasing $S1$, the electric current gets lengthened on the fractal radiating rings which causes the resonant frequency to decrease. It is clear that the two resonances are centered at the desired bands, 2.45GHz and 3.5GHz, with a good impedance matching when $S1$ equals to $1.65mm$.

The effect of varying the fractal rings width t on the return loss is shown in Figure 4.4b. It is observed that by increasing the parameter t, the two resonant frequencies shift to the higher frequencies. This is due to the decrease of the fractal ring inductance. For t equals to 0.3 mm, the two resonant frequencies are tuned to the desired bands.

The effect of varying the open slot depth etched in the ground plane d on the return loss is shown in Figure 4.4c. It can be seen that better impedance matching is achieved for the second band, without affecting the first one, by changing the parameter d. This good impedance matching is obtained for d equals to $2mm$.

Figure 4.4d illustrates the effect of changing the angle θ on the return loss. By increasing the value of the angle θ, the first resonant frequency shifts to the lower frequencies while the second one kept roughly constant. This shift is resulted from the change in the EM coupling between the fractal radiating rings. It is clear that the first operating band is centered at around 2.45 GHz for $\theta = 30°$.

Figure 4.4e shows the effect of varying the ground planelength (Lg) on the return loss. It is noticed from the results that the lower cut off frequency of the operating band shifts towards lower frequencies as the value of Lg decreases. Consequently, the second band broadens and the impedance matching improves. It can be concluded that for Lg equals 4 mm optimum results are obtained in terms of bandwidth and impedance matching for the second band.

Figure 4.4f shows the effect of varying the feedline width (Wf) on the return loss. It is found that by increasing the width Wf, the lower cut off frequency of the second band deceases with noticeable improvement of the impedance matching for the second band. For Wf equals to 3.5 mm, good impedance matching at both resonant frequencies is obtained.

To further investigate the operating mechanism of the proposed antenna, namely Ant.3, the current distributions are simulated at the two resonant frequencies of 2.45 and 3.48 GHz as depicted in Figure 4.5 . It can be observed that, at the first resonant frequency, the current is mostly concentrated on the two opposite sides of the fractal radiating ring as well as at the two opposite sides of the parasitic fractal ring embedded in the ground plane.

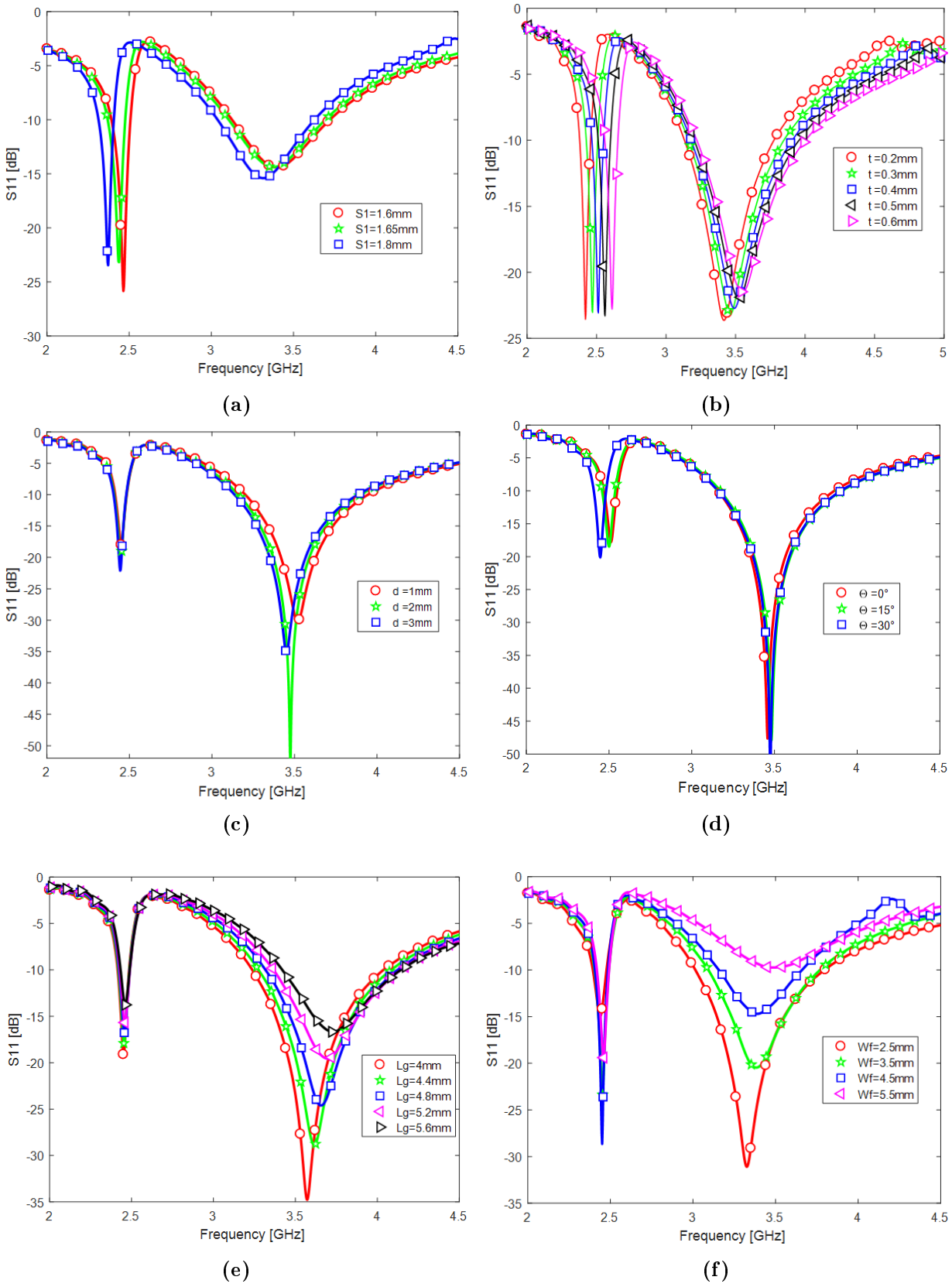

Figure 4.4: Return losses of the proposed antenna for different values of (a) S_1, (b) t, (c) d (d) θ, (e) Lg and (f) Wg

This confirms the fact that this first band is the result of the EM coupling between the two fractal rings. Consequently, the first resonant frequency can be controlled by changing

the circumference of the radiating rings. Concerning the current at the second resonant frequency, it is mainly concentrated in the Y-shaped feed line as well as in the two fractal rings. Therefore, this second resonance can be tuned by changing the dimensions of the feeding line and the perimeter of the radiating fractal rings.

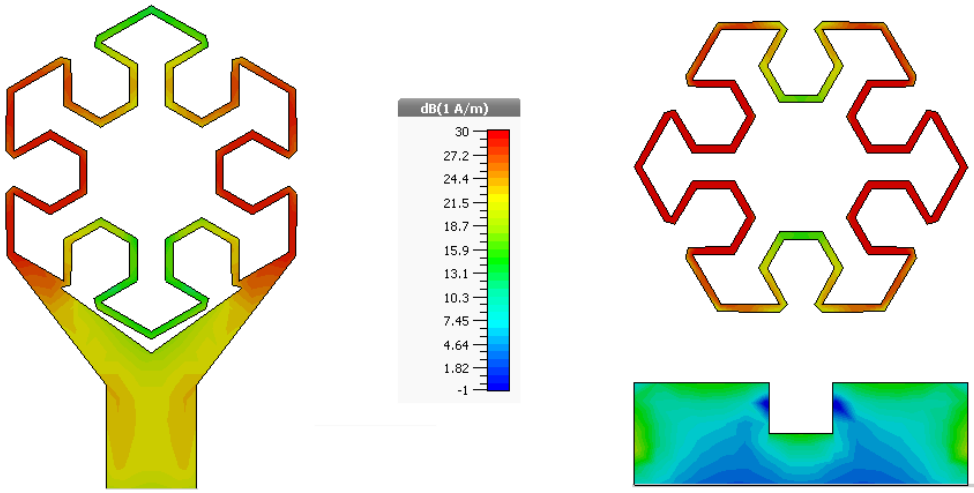

(a) at 2.45 GHz

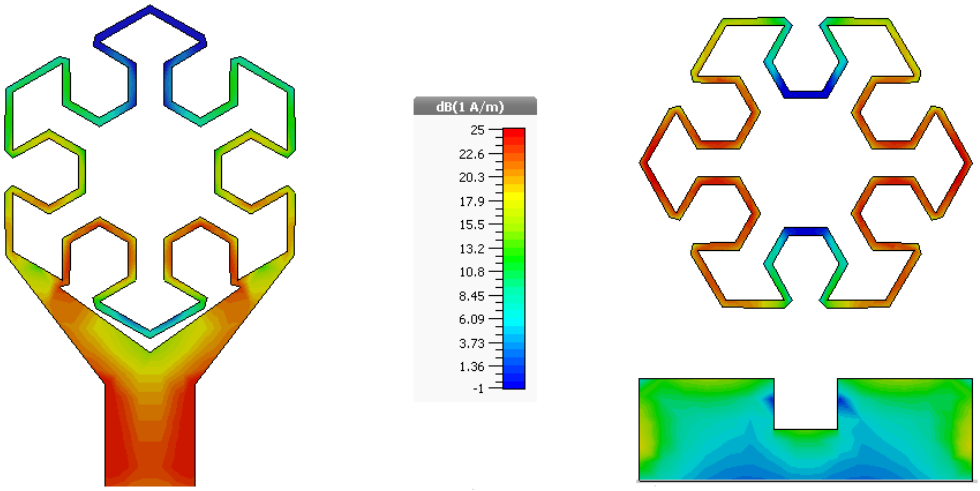

(b) at 3.5 GHz

Figure 4.5: Current distributions for the proposed antenna

4.2.3 Experimental Results

To validate the technical proposal, the proposed dual-band monopole antenna was fabricated and tested. Figure 4.6 shows the photograph of the fabricated prototype of the proposed dual-band antenna. The fabricated structure performances were measured using a vector network analyzer (VNA) operating in the frequency band from 100 KHz to 20 GHz. The measured and simulated return losses are depicted in Figure 4.7. It is observed that the measured and simulated results are in acceptable agreement. The measured 10-dB impedance

bandwidths are 300 MHz (2220-2520 MHz, 12.6%) and 1030 MHz (3320-4350 MHz, 26.8%) covering the 2.4 GHz WLAN and 3.5 GHz WiMAX bands, respectively. The slight deviation between the measured and simulated results is basically due to the manufacturing tolerances, the uncertainty on the thickness and dielectric relative constant of the substrate added to the SMA connectors quality.

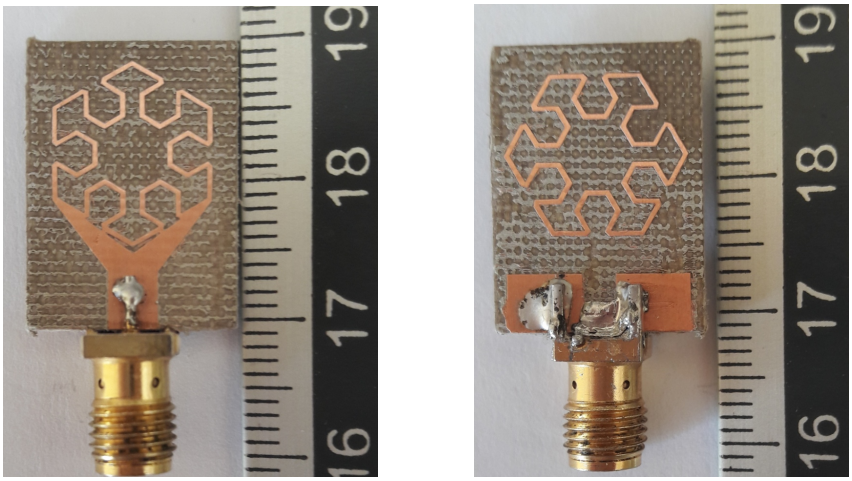

(a) Front View **(b)** Back view

Figure 4.6: Photograph of the fabricated dual-band antenna prototype

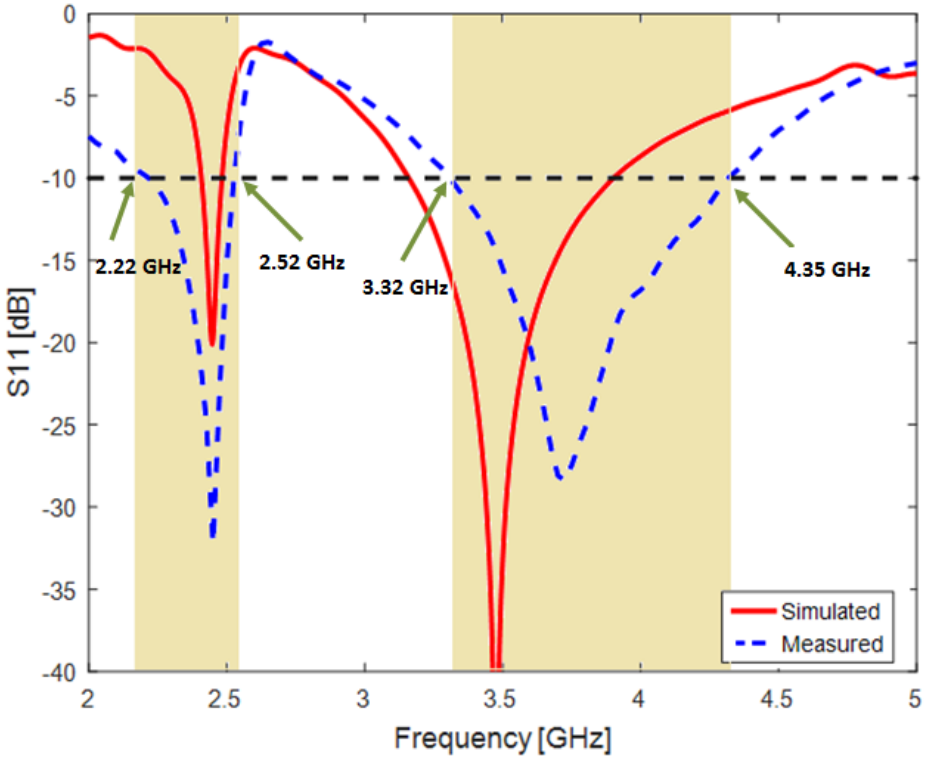

Figure 4.7: Simulated and measured return losses of the proposed antenna.

The radiation efficiency η of the proposed antenna was measured using the Wheeler cap

method [3], [4]:

$$\eta = \frac{Real(Z_{in}) - Real(Z_{wc})}{Real(Z_{in})} \tag{4.1}$$

where Z_{in} is the input impedance of the antenna and Z_{wc} is the input impedance of the antenna enclosed in a metallic sphere. At 2.45 GHz and 3.5 GHz, the measured radiation efficiencies using a metallic cylinder shown in Figure 4.8 are 91% and 97%, respectively. Therefore, these good radiation efficiencies at both operating bands make the proposed antenna suitable for the intended application.

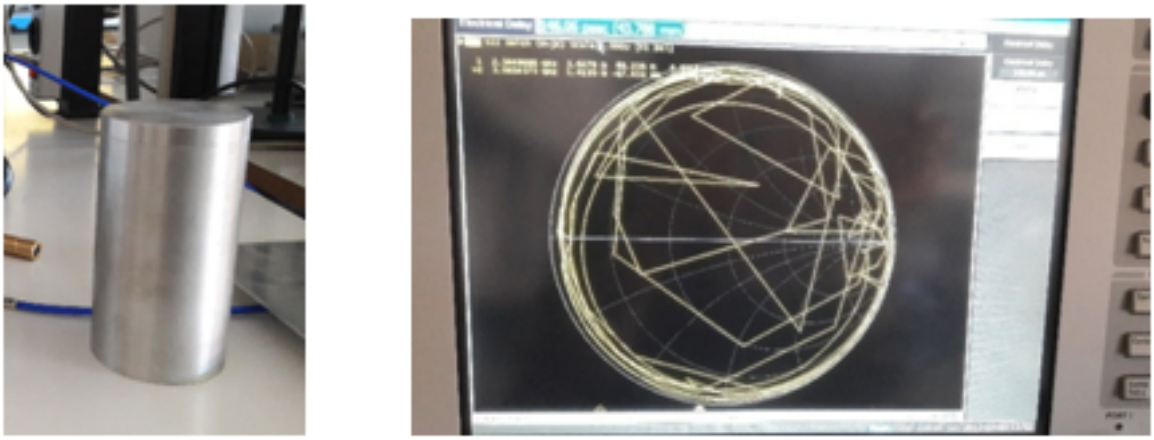

Figure 4.8: Cap (metalic cylinder) used to measure the efficiency and measured input impedance of the enclosed antenna

For practical applications, laptop and other portable devices, the proposed antenna was mounted on the side of a SGP of laptop computer as shown in Figure 4.9a. The reflection coefficient of the proposed antenna was simulated for different SGP sizes of laptop computer as illustrated in Figure 4.9b. From the results, it is clear that the antenna resonances are not affected by the SGP size even when it is reduced to 30x20 mm^2. Figure 4.10 shows the fabricated prototype of the proposed antenna, placed at 4.75 mm from the left corner of a copper SGP ($260mm \times 200mm$), along with its measured and simulated return losses. It is clearly seen that the simulated and measured results are in good agreement with slight difference especially in the second band where the measured return loss is better than 9 dB over the frequency band extending from 3 to 4.1 GHz. This deviation between the measured and simulated results is mainly attributed to the fabrication errors. Consequently, it can be concluded that the proposed antenna is a good candidate to be integrated into different standard of laptop computers.

The proposed antenna radiation patterns were also measured in an anechoic chamber

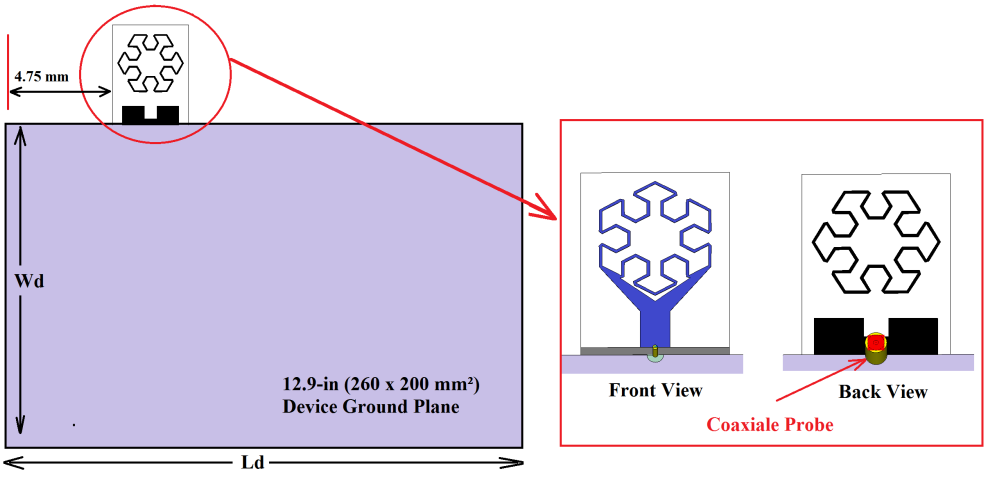

(a)

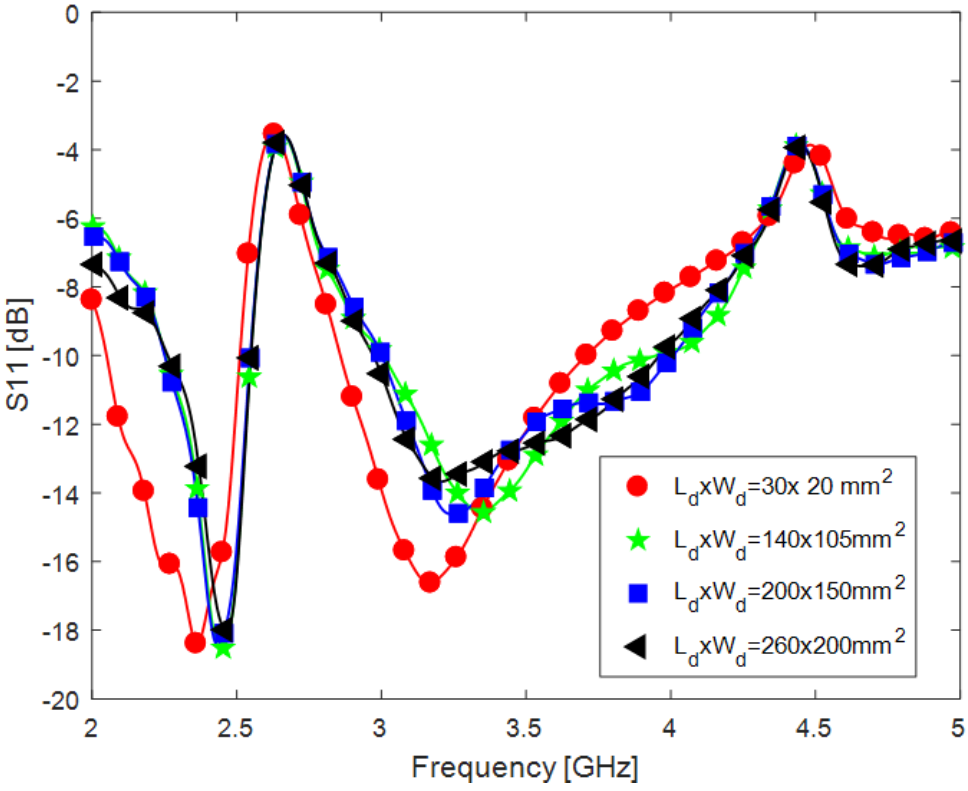

(b)

Figure 4.9: (a) Antenna attached to system ground plane of 12.9-in laptop computer and (b) Simulated return losses of the proposed antenna for different ground plane sizes

available in Universitat Politecnica de Catalunya (UPC). The normalized measured and simulated radiation patterns containing co-polarization E_θ and cross-polarization E_ϕ in the H-plane (x-z plane) and E-plane (y-z plane) are shown in Figure 4.11. It is clear that the measured and simulated results are in very good agreement. Moreover, the antenna exhibits an omnidirectional radiation patterns in the H-plane and monopole-like radiation patterns in the E-plane at both resonant frequencies. Accordingly, this confirms that the proposed

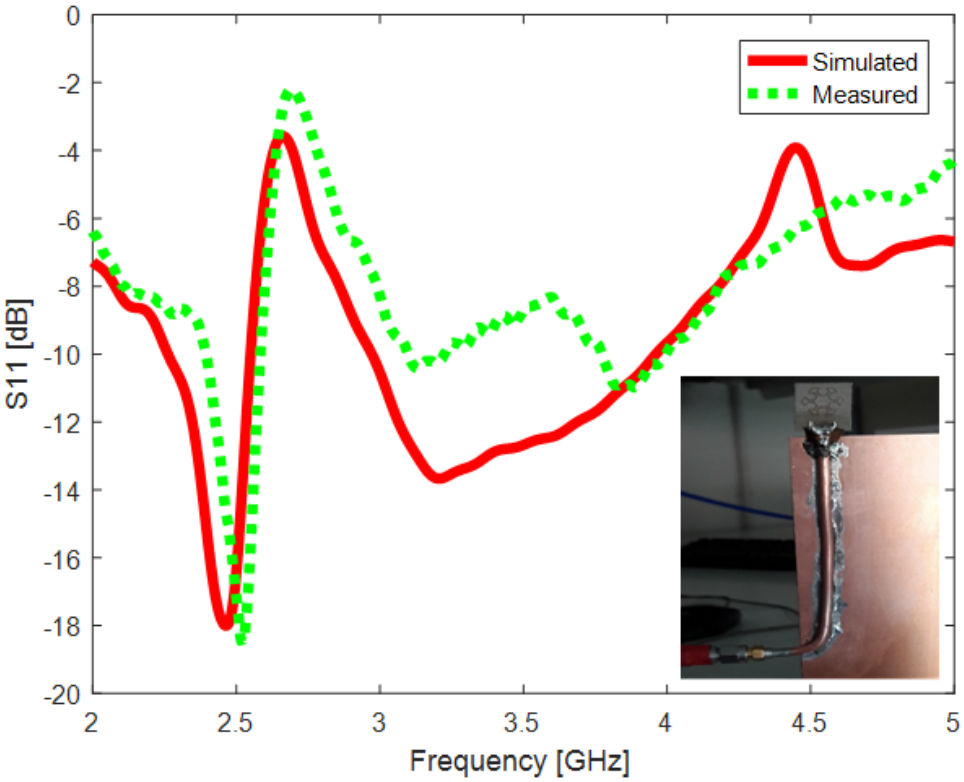

Figure 4.10: Simulated and measured return losses of the proposed antenna attached to system ground plane of 12.9-in laptop computer

antenna is well-suited for wireless communication applications.The slight difference between measured and simulated radiation patterns are attributed to perturbation in the radiation pattern introduced by the positioner during the measurement process. A comparison between the proposed antenna and other dual-band antennas reported in the literature is presented in Table 4.2. By comparing the reported antennas footprints , it is clearly seen that the proposed antenna has the smallest one and achieves significant size reduction in term of of free-space wavelength, λ_0^2 at the first resonance frequency. Moreover, in terms of impedance matching performance, the proposed antenna outperforms almost all the reported antennas.

4.3 Compact Dual Band Fractal Hexagonal Ring Monopole Antenna for RFID and GSM Applications

4.3.1 Antenna Structure

The second dual band antenna is designed to operate at two frequency bands allocated to RFID and GSM 1800 technologies. The structure covers entirely the RFID and GSM 1800 bands ([859-973MHz] and [1710-1886 GHz]). The developed microstrip line fed antenna con-

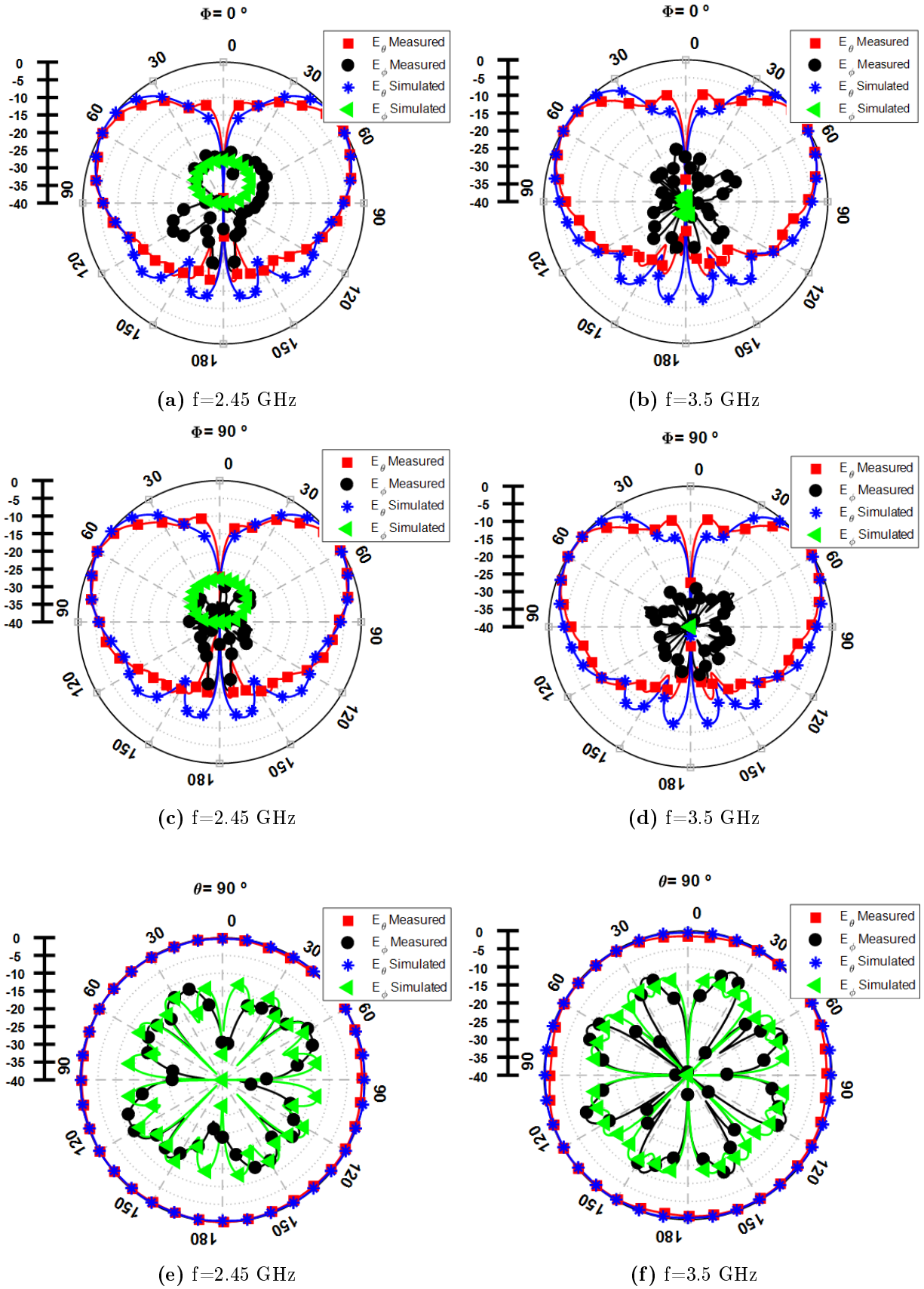

(a) f=2.45 GHz (b) f=3.5 GHz

(c) f=2.45 GHz (d) f=3.5 GHz

(e) f=2.45 GHz (f) f=3.5 GHz

Figure 4.11: Radiation patterns of the proposed antenna at different frequencies 2.45 and 3.5GHz

Table 4.2: Comparison between proposed antenna size along with application bands with other compact dual band antennas

Ref.	**Frequency (GHz)**	**Frequency ratio**	**Antennat Footprint**	**Bandwidth (%)**
[5]	3.5/5.5	1.57	0.068 λ_0^2	20.2%/24.8%
[6]	1.9/2.5	1.32	0.062 λ_0^2	5.8%/4.0%
[7]	2.4/3.5	1.46	0.026 λ_0^2	5.7%/6.3%
[8]	2.4/5.2	2.17	0.102 λ_0^2	10.3%/19%
[9]	2.4/3.5	1.46	0.024 λ_0^2	123.5%/24%
This current work	2.4/3.5	1.46	0.016 λ_0^2	12.6% /26.8%

figuration and details are shown in Figure 4.12 The design process is based on the work in [10] in which a slotted triangular monopole antenna suitable for a dual band RFID application is developed. Instead of slot loading, it has been observed that the approach based on fractal technology used in this work allows a further improvement in the antenna size reduction. For this purpose, the triangular shape is first replaced by a first-order hexagonal fractal ring. The antenna is printed on the FR-4 substrate with $\epsilon_r = 4.3$, $tan\delta = 0.0017$ and a thickness of $h = 1.6mm$.

When using one fractal ring as antenna radiator (the external ring), a tri-band structure is obtained. The first band is suitable for RFID applications ([0.896-0.937 GHz]). However, the two other bands ([1.196 -1.216 GHz]) and ([1.465 -1.496 GHz]) are not commercially useful. During the design process, it was observed that the fractal ring perimeter can be modified to finely tune only the resonant frequency in the RFID band. The two other frequencies depend mainly on the patch shape and, as opposed to the first resonance, they do not exhibit a direct dependence on the ring perimeter. Consequently, only the RFID band is controllable in the one fractal ring configuration. Nevertheless, this antenna, which can operate in the RFID band, realizes a size reduction of about 34 % ($70 \times 50 \times 1.6mm^3$) as compared to the antenna in [10]. To further reduce the antenna size and tune it to cover the GSM band, three slotted fractal rings are combined. The two identical inner rings have half size of that of the outer ring. Without slots, the antenna resonant frequency is the same as the one of the outer fractal ring, alone without the two smaller rings. In order to downsize the antenna dimensions, the electric current must be forced to flow from the outer ring to the inner one then, again to the outer one. Accordingly, slots are inserted to control the current path. The slots are located in the two opposite sides of the outer ring such that one slot is common to the outer and the inner rings. Consequently, the outer ring is loaded with

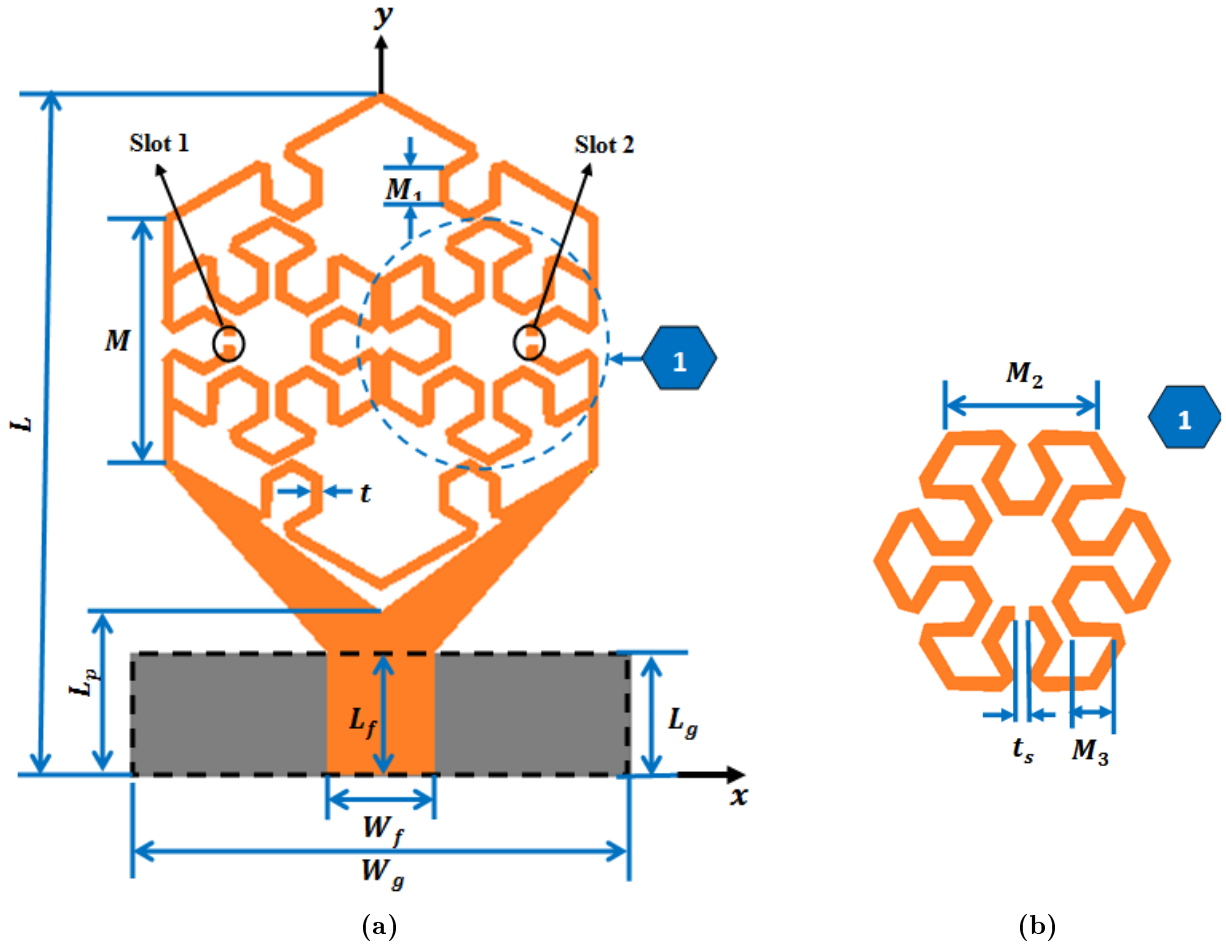

(a) (b)

Figure 4.12: (a) Geometry of the dual-band fractal ring monopole antenna (b) Details of the inner fractal ring

two symmetrical slots and the smaller rings are loaded with one slot. The final compact structure with dual band operation is shown in Figure 4.12 and its dimensions are listed in Table 4.3.

Table 4.3: Geometrical dimensions of the proposed antenna

Parameter	L	L_f	M	L_p	M_1	M_2	S	t_s	W_g
Value (mm)	61	15	20.5	6.5	2.8	10.25	6.5	1	41

4.3.2 Experimental and Simulation Results

Independent control of the antenna resonances in the design of multiple band antennas is a challenging task due to various technical limitations. Consequently, proposed antenna parametric analysis has been carried out and discussed. The effect of key geometrical parameters like the fractal rings dimensions will be observed through simulations and discussed in this section.

- **Effect of the radiating rings width**

The dependence of the reflection coefficient of the antenna on radiating rings width is shown in Figure 4.13 . It can clearly be seen that both resonant frequencies decrease with the increasing of the radiating rings width. In addition, better impedance matching for the two bands is achieved by increasing value of t. For t of 0.2mm, the two bands are centered at the desired frequencies of 0.934 and 1.75 GHz. Accordingly, antenna size reduction is achieved in term of first resonance.

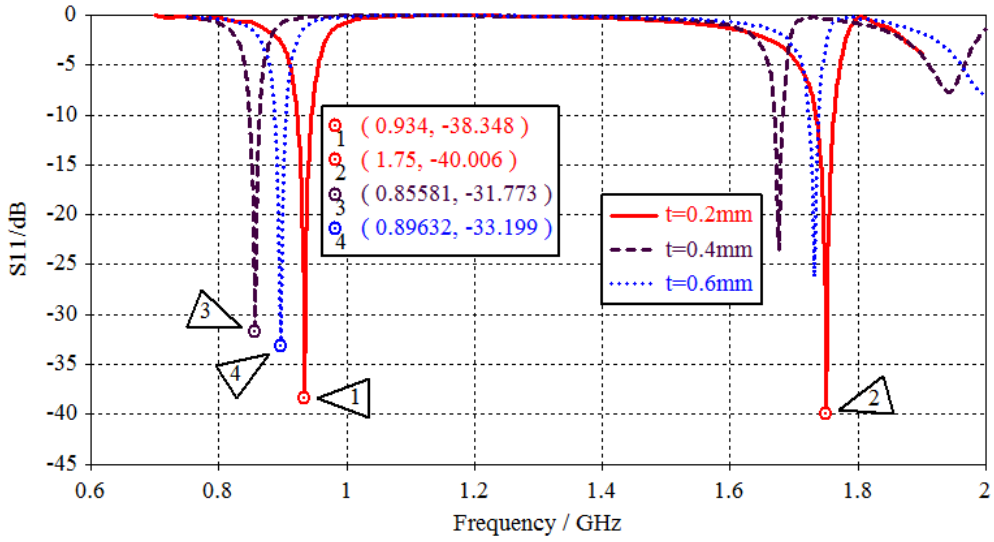

Figure 4.13: Simulated return loss for various t

- **Effect of the outer open loop side of the radiating ring**

Figure 4.14 shows the antenna return loss for different values of the open loop side $M1$ of the external fractal ring. It is clear that the values of M1 of 2.6, 2.7 and 2.9 mm assure dual band operation whereas for M1 of 2.9mm only one resonant frequency is obtained. In the case of dual band characteristic, it is noted that the change in the M1 value has no effect on the first resonance while by increasing its value, the second resonance is decreased. Thus, the parameter M1 is used to finely tune the second resonance.

- **Effect of the inner open loop side of the radiating ring**

The antenna return loss versus the open loop side $M3$ of the inner fractal rings is shown in Figure 4.15. It is observed that the parameter M3 has almost same effect on the antenna return loss as M1. However, for M3 values of 2.7, 2.8 and 2.9 mm assure dual band operation while for $M3$ of 2.6mm only one resonant frequency is obtained. Accordingly, the parameter M3 is used to control the second resonant frequency.

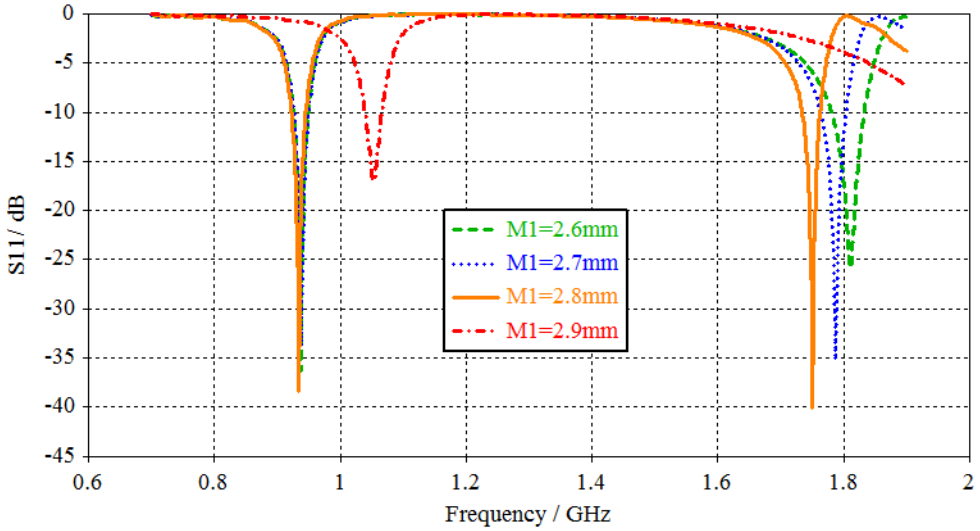

Figure 4.14: Simulated return loss for various M1

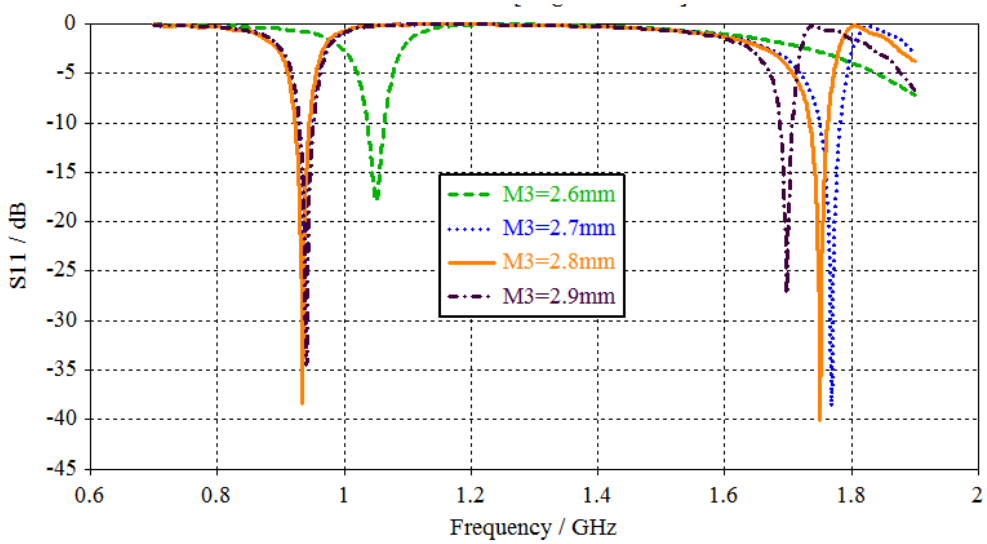

Figure 4.15: Simulated return loss for various M3

- **Effect of the external ring side**

Figure 4.16 shows the antenna return loss for different values of the external fractal side M. It is seen that by increasing M, the first resonant frequency decreases while the second resonance increases slightly. For M equal 20.5mm, the two band are centered at the desired frequencies.

To further investigate the operating mechanism of the proposed structure, the current distributions are simulated at the two resonant frequencies of 0.938 and 1.758 GHz as depicted in Figure. 4.17. It can be seen that, at the first resonant frequency, the current is mostly concentrated on the two inner fractal radiating rings as well as at the two opposite sides of the outer fractal ring. This confirms the fact that this first band is the result of the current

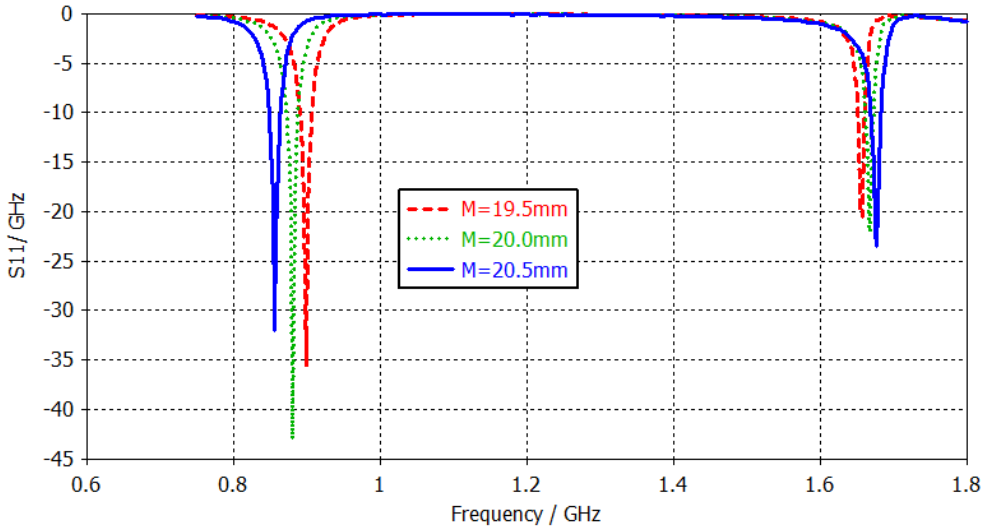

Figure 4.16: Simulated return loss for various M

flowing from the outer ring to the inner ring than again to the outer ring . Consequently, the first resonant frequency can be controlled by changing the circumference of the fractal rings. Concerning the current at the second resonant frequency, it is mainly concentrated in four corners of radiating structure including the outer and the inner rings.Therefore, this second resonance can be tuned by changing the dimensions of the radiating fractal rings.

The proposed dual-band monopole antenna was fabricated and tested. The photograph of the fabricated antenna is shown in Figure 4.18. The antenna external dimensions are $61.0 \times 41.0 \times 1.6 mm^3$ which yields a size reduction of about 53% as compared to the structure in [10].

The simulated and measured return losses are illustrated in Figure 4.19 which shows a good agreement between the measured and simulated results. The slight difference between the two graphs is attributed to various factors such as the substrate dielectric constant, fabrication accuracies and the quality of SMA connectors. Furthermore, the figure shows that the antenna operates at the two desired frequency bands allocated to the RFID and GSM 1800 application. The first operating band extends from 0.852 to 0.962 GHz whereas the second extends from 1.710 to 1.785 GHz covering the intended applications. Figure 4.20 illustrates the simulated radiation patterns in both E- and H- planes at the two resonant frequencies. As illustrated in Figures 4.20a and 4.20b, the antenna radiation pattern at 938 MHz is almost omnidirectional with a maximum directivity of 1.99 dBi (peak gain of 0.44 dB) in the direction $\theta = 180°$. While at 1.75 GHz, Figure 4.20c and 4.20d show that the antenna maximum radiation occurs in the directions $\theta = 0°$ and $\theta = 180°$ with a directivity

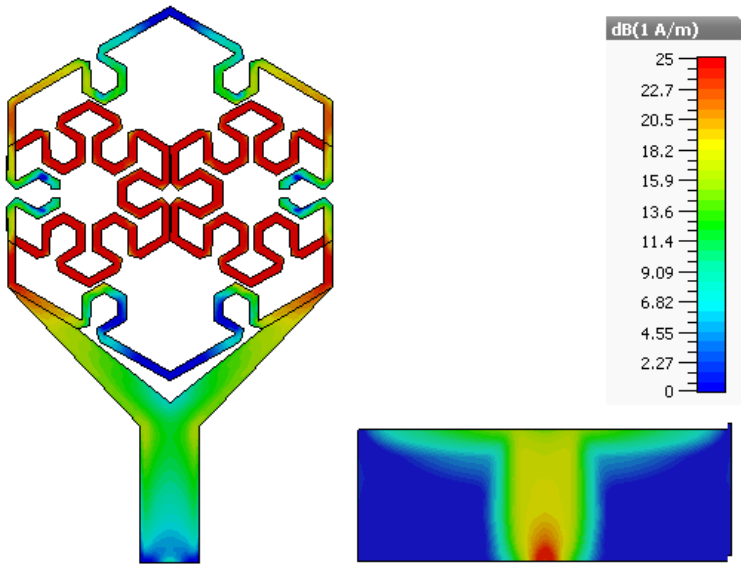

(a) at 0.938 GHz

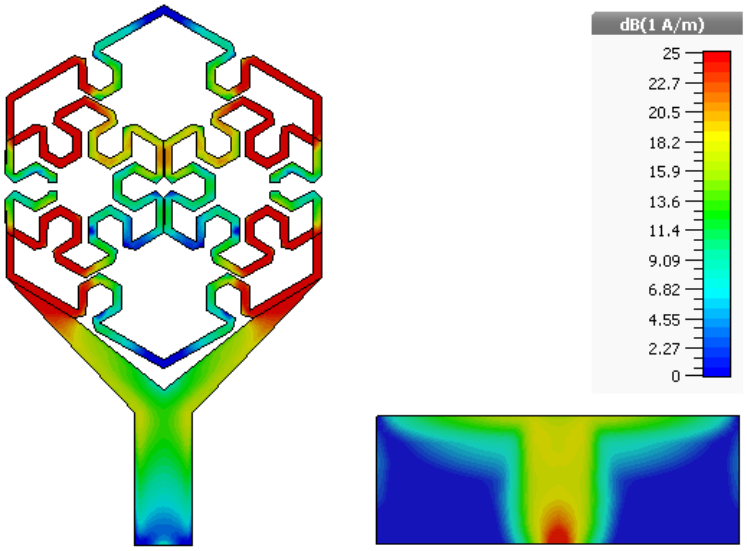

(b) at 1.758 GHz

Figure 4.17: Current distributions for the proposed antenna

of 2.27dBi (peak gain of 1.67 dB), greater than at the first resonance because of the higher antenna electrical length at this resonance. Accordingly, the pattern at this frequency covers particular zones more than others. Furthermore, the antenna achieves a good polarization purity with levels less than -40 and -26.5 dBi at respectively the first and second frequency in both E and H planes.

4.4 Summary

In this chapter, two dual band monopole antennas based on fractal shaped rings, using two identical rings and using a combination of three slotted rings have been presented . The new

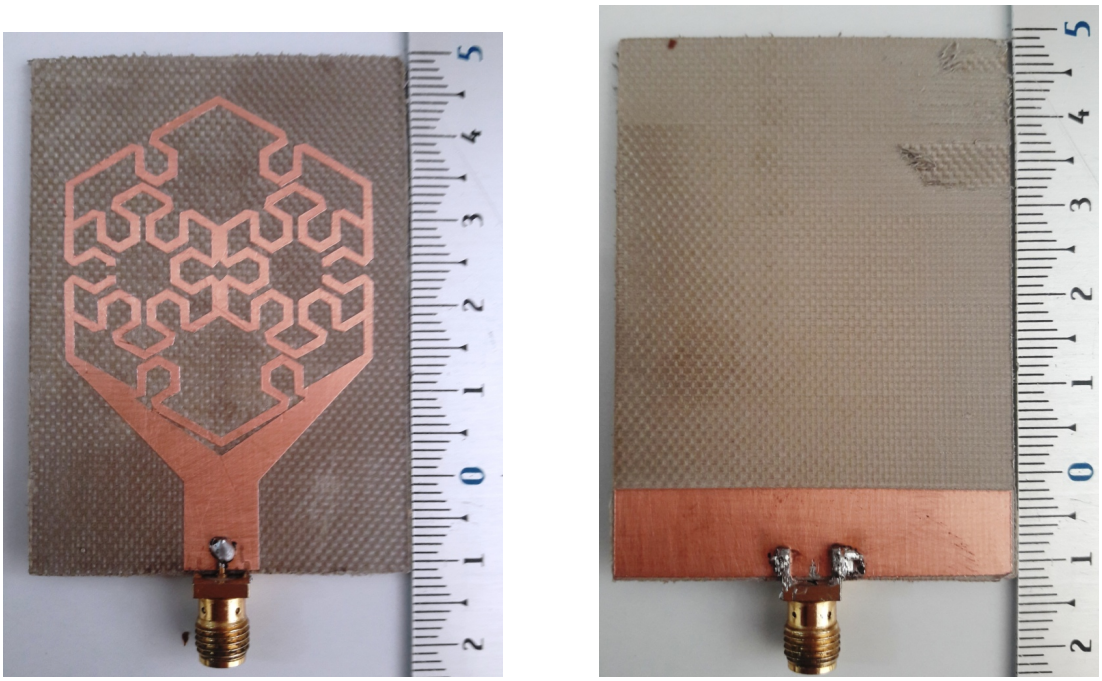

(a) Front View **(b)** Back view

Figure 4.18: Photograph of the fabricated dual-band antenna prototype

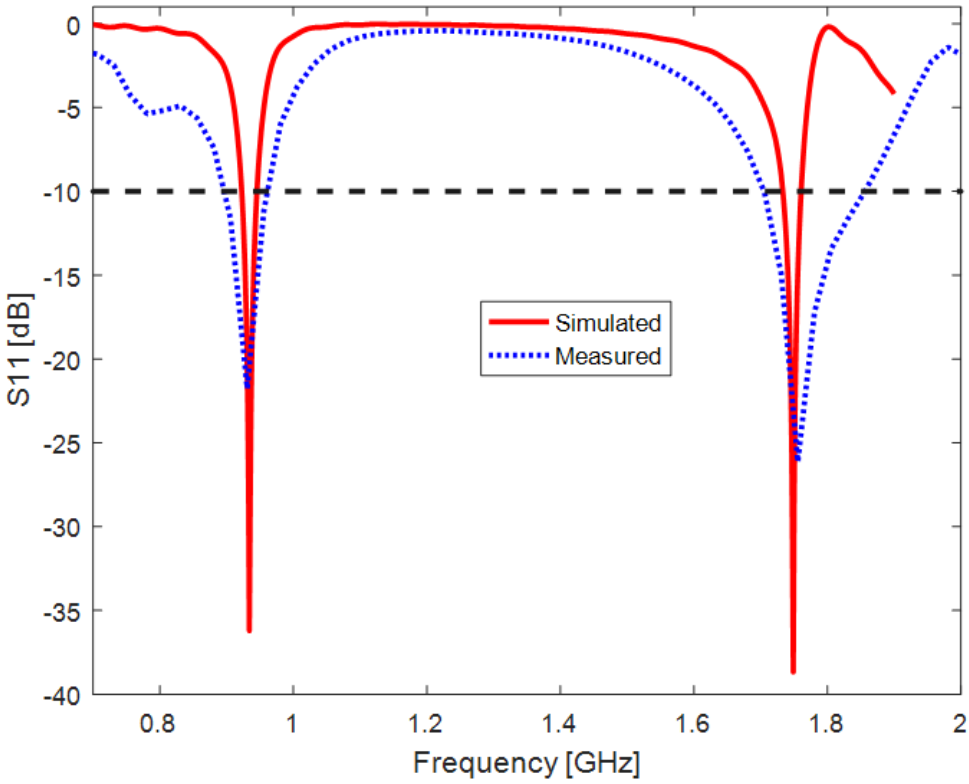

Figure 4.19: Simulated and measured return losses of the proposed antenna.

compact dual-band antenna has been designed to cover the WLAN/WiMAX applications. The simulation results have shown that adding a second fractal ring in the ground plane of the structure will create a lower resonance leading to antenna size reduction . In addition, the measured and simulated results have shown omnidirectional radiation pattern and good

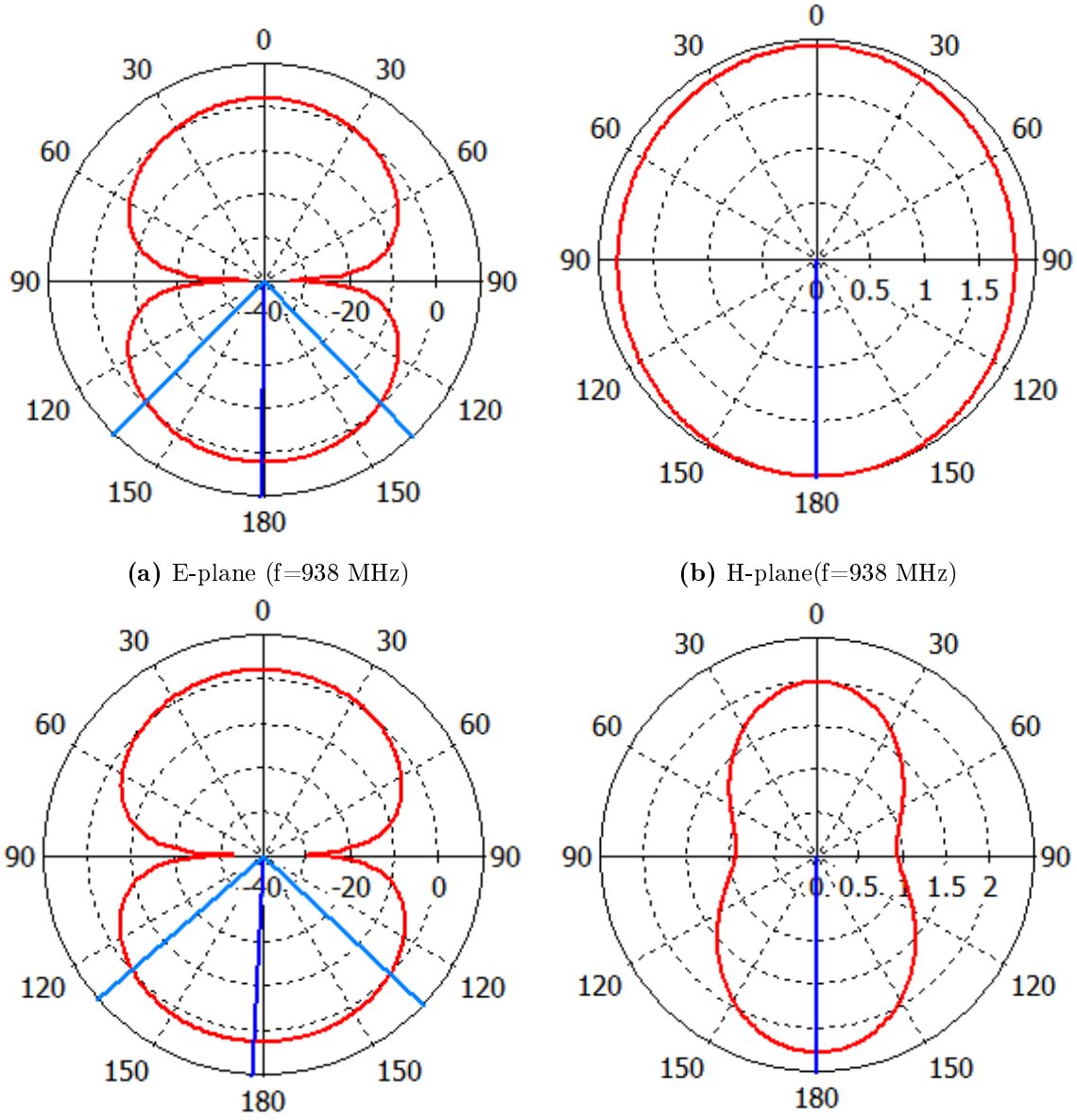

(a) E-plane (f=938 MHz)

(b) H-plane(f=938 MHz)

(c) E-plane(f=1.75 GHz)

(d) H-plane(f=1.75 GHz)

Figure 4.20: Radiation patterns of the proposed antenna at 938 MHz and 1.75 GHz

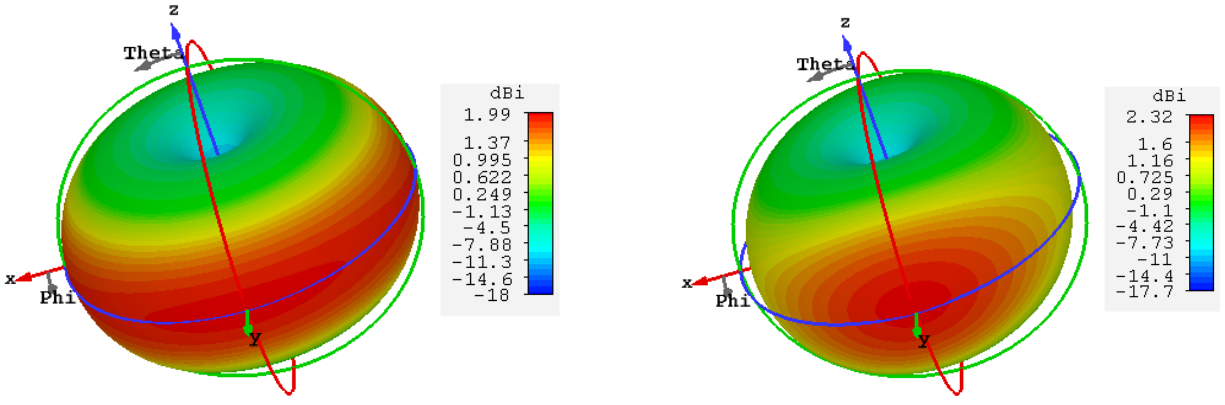

(a) f=938 MHz

(b) f=1.75 GHz

Figure 4.21: 3D radiation patterns of the proposed antenna

radiation efficiencies which makes the antenna well-suited for wireless application. Then, the antenna was mounted on SGP of a laptop computer in order to investigate its performance. The measured results have shown a satisfactory agreement with the simulated ones. The developed antenna with compact size of $18.9 \times 13mm^2$ has shown dual-band operation (it covers widely the bands allocated to 2.4 GHz WLAN and 3.5 GHz WiMAX) and good radiation patterns in both E and H-planes. Thus, these interesting characteristics make the proposed antenna suitable for the intended application. In the last section, a compact dual band hexagonal fractal ring monopole antenna for radio frequency identification (RFID) and GSM applications has been presented. At the first band, It exhibits a nearly omnidirectional radiation pattern while a directive radiation pattern is observed at the second band. Furthermore, the proposed antenna presented a significant size reduction (53%) as compared to the triangular dual band structure with an overall size of $61 \times 41 \times 1.6mm^3$. The proposed antenna was prototyped and tested and a good agreement has been observed between the simulated and measured return losses. Thepublications resulted from the work presented in this chapter are:

1. Djafri K, Challal M, Aksas R and Romeu J, *A Compact Dual-Band Planar Monopole Antenna using Fractal Rings and a Y-Shaped Feeding Transmission Line*, Frequenz: Journal of RF-Engineering and Telecommunications, 2018.

2. Djafri K, Challal M, Azrar A, Dehmas M, Aksas R, Mouhouche F. *Compact dual-band fractal hexagonal ring monopole antenna for RFID and GSM applications.* Microw OptTechnol Lett . 2018; $1 - 4$.

Bibliography

[1] K Fertas, H Kimouche, M Challal, H Aksas, R Aksas, and A Azrar. Design and optimization of a cpw-fed tri-band patch antenna using genetic algorithms. *ACES Journal-Applied Computational Electromagnetics Society Journal*, 30(7):754–759, 2015.

[2] K Fertas, H Kimouche, M Challal, H Aksas, and R Aksas. An optimized shaped antenna for multiband applications using genetic algorithm. In *IEEE-2015 4th International Conference on Electrical Engineering-ICEE*, 2015.

[3] Darioush Agahi and William Domino. Efficiency measurements of portable-handset antennas using the wheeler cap. *Applied Microwave and Wireless*, 12(6):34–43, 2000.

[4] Hosung Choo, Robert Rogers, and Hao Ling. On the wheeler cap measurement of the efficiency of microstrip antennas. *IEEE Transactions on Antennas and Propagation*, 53(7):2328–2332, 2005.

[5] Dhirgham K Naji. Compact design of dual-band fractal ring antenna for wimax and wlan applications. *International Journal of Electromagnetics and Applications*, 6(2):42–50, 2016.

[6] Taiwei Yue, Zhi Hao Jiang, Anastasios H Panaretos, and Douglas H Werner. A compact dual-band antenna enabled by a complementary split-ring resonator-loaded metasurface. *IEEE Transactions on Antennas and Propagation*, 65(12):6878–6888, 2017.

[7] Jagannath Malik, Amalendu Patnaik, and MV Kartikeyan. A compact dual-band antenna with omnidirectional radiation pattern. *IEEE Antennas and Wireless Propagation Letters*, 14:503–506, 2015.

[8] Jui-Han Lu and Hao-Shiang Huang. Planar compact dual-band monopole antenna with circular polarization for wlan applications. *International Journal of Microwave and Wireless Technologies*, 8(1):81–87, 2016.

[9] Praveen V Naidu. Printed v-shape acs-fed compact dual band antenna for bluetooth, lte and wlan/wimax applications. *Microsystem Technologies*, 23(4):1005–1015, 2017.

[10] M Dehmas, A Azrar, F Mouhouche, K Djafri, and M Challal. Compact dual band slotted triangular monopole antenna for rfid applications. *Microwave and Optical Technology Letters*, 60(2):432–436, 2018.

Chapter 5

Design of Miniaturized Triple Band Printed Monopole Antennas

Contents

5.1 Introduction

The electronic devices in the modern communication systems are required to be continuously smaller which has given rise to an important demand to design miniaturized antennas. Furthermore, more requirements in terms of multiband operation are needed. Consequently, several research works have been conducted to design compact multiband antennas which can support multiple communication applications such as WLAN and WiMAX technologies. To this end, several printed antennas with various geometries, selected for size reduction issue, have been reported. Triple band operation can be achieved by combining different resonators in one antenna [1]-[2] (where the geometry of each resonator is chosen to achieve maximum size reduction), loading the radiating patch with shaped slots [3]-[4], using metamaterial [5]-[6]. However, these reported antennas present large physical sizes.

In this chapter, two compact tri-band antennas will be presented. The first design is based on the ACS feeding technique to reduce the size while the second design is resulted

of interconnected two concentric fractal ring introduced in Chapter 3. The simulated and measured return losses and radiation patterns of the proposed antennas will be presented and discussed.

5.2 Compact ACS-Fed Triple Band Microstrip Monopole Antenna

5.2.1 Design Procedure

In this section, the design of a triple band ACS-fed monopole antenna is presented, where two different branches are used to create multiple resonances . The first one is a J-shaped strip connected to the exited strip and the other one is a simple open stub. The basic structure of this antenna is shown in Figure 5.1a . Four steps will be considered to design the proposed triple band antenna. The first one starts by an ACS-fed simple monopole antenna, then a small strip is connected perpendicularly to the end of the monopole antenna, next a J-shaped arm is connected and finally a simple rectangular branch is attached the structure. By extending the main exiting strip, as shown in Figure 5.1b (Ant.2), a resonance at 5.27 GHz is created without increasing the antenna length. The J-shaped branch is used as shown in Figure 5.1c (Ant3) to create the 2.51GHz resonance. The third resonant frequency is produced by connecting the rectangular branch as depicted in Figure 5.1d (Ant.4).

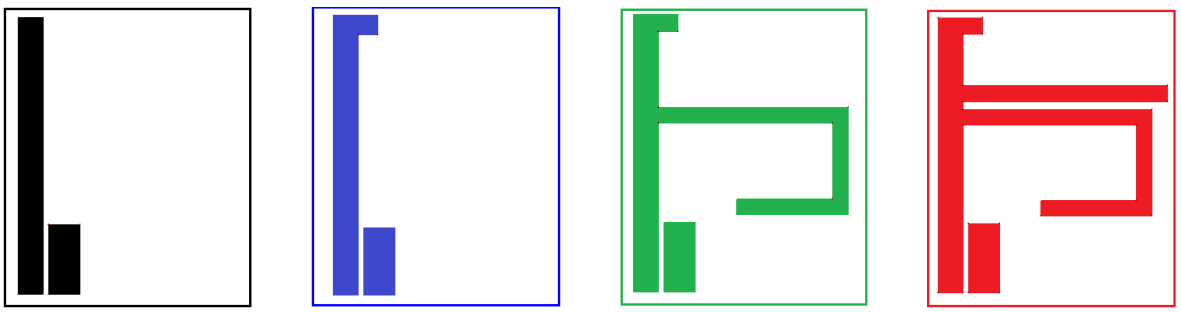

(a) Ant.1 **(b)** Ant.2 **(c)** Ant.3 **(d)** Ant.4

Figure 5.1: Design Evolution Steps of the Proposed ACS-fed Tri-band Monopole Antenna

The geometry of the final proposed ACS-fed tri-band antenna is shown Figure 5.2 (Ant.4). The ACS feed line has a signal strip width of 1.5 mm and a gap of 0.5 mm between the signal strip and the asymmetric ground plane. After an extensive simulation study with help of a powerful full wave simulator IE3D, the dimensions of the proposed antenna are determined and they are listed in Table 5.1. The radiating structure with ACS-fed line is printed in the same side of the substrate.

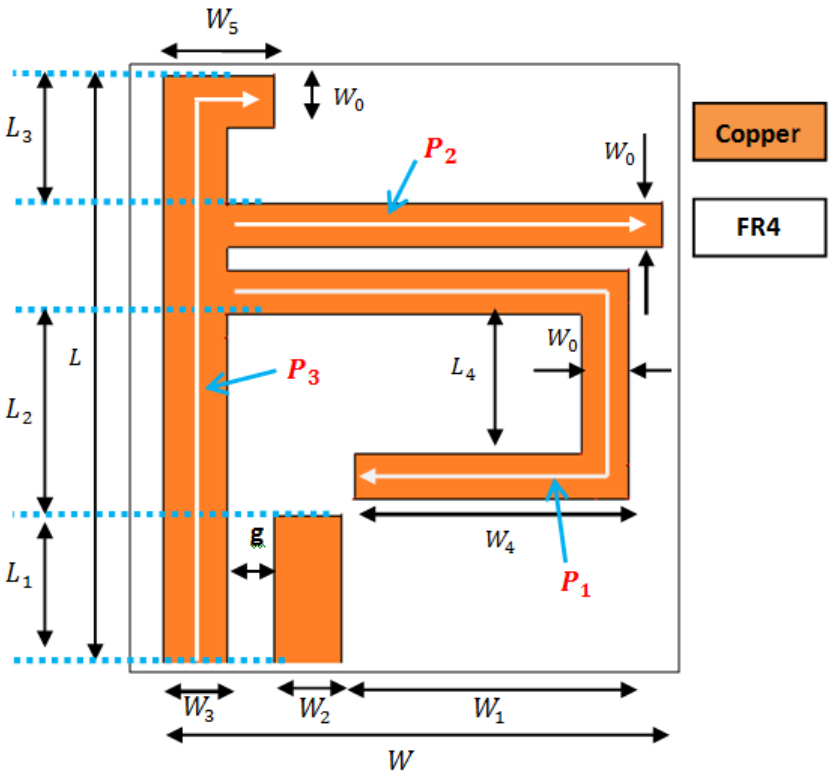

Figure 5.2: Geometry of the proposed ACS-fed tri-band antenna

Table 5.1: Dimensions of the proposed ACS-fed tri-band antenna (all dimensions are in mm)

Parameter	Value (mm)	Parameter	Value (mm)
W	17.5	L_1	5.4
W_0	1	L_2	6.3
W_1	9.7	L_3	4.3
W_2	2	L_4	4.8
W_3	1.6	P_1	25.9
W_4	9.1	P_2	13
W_5	2.8	P_3	15.7
L	14.6	g	0.5

5.2.2 Simulation Results

Figure 5.3 represents the simulated return losses of the antenna structures involved in the evolution study shown in Figure 5.1. Ant.1 has a single resonance which occurs at 5.46 GHz with a return loss of -9.5dB. To make the antenna operate at lower frequency, without increasing its dimensions, the monopole strip end is extended perpendicularly to obtain the second design Ant.2 as shown in Figure 5.1b. The obtained structure operates at 5.27 GHz with better impedance matching for -10dB return loss. By connecting the J-shaped strip Ant.3, a lower resonant frequency centered at 2.51GHz is created and the impedance matching at the second resonance is significantly improved. Besides the two resonances, a

third operating band centered at 3.5GHz is generated by attaching a rectangular strip to the antenna (Ant.4).

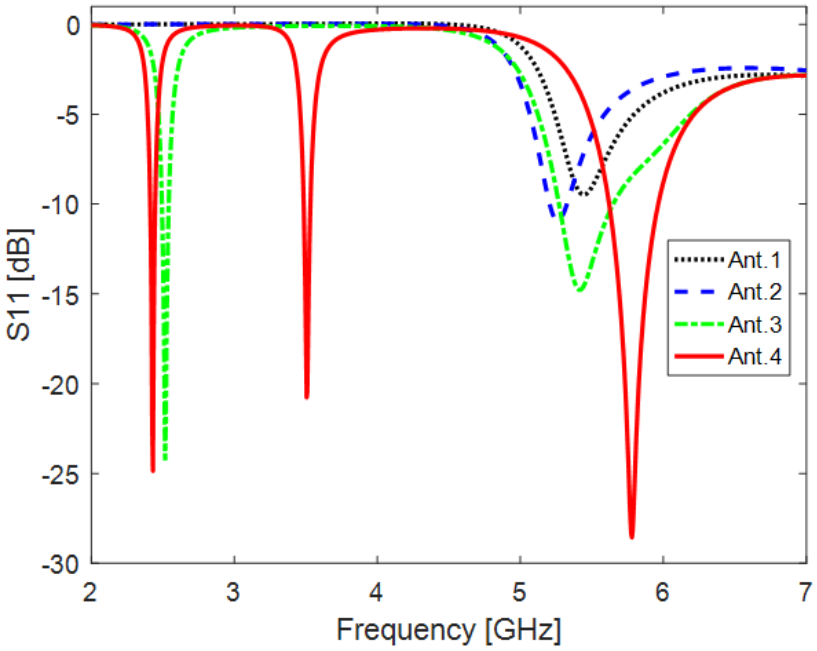

Figure 5.3: Simulated Return Loss (S11) Result of Various ACS-fed Antennas Involved in the Evolution Process

To further investigate the proposed antenna performance, a parametric study is carried out. Figure 5.4a shows the results obtained through simulation of the return-losses characteristics according to the changes in the J-shaped branch length P_1 while P_2 and P_3 are kept constants. As the length increases from 23.5 to 25.9mm, the frequency shifts towards lower frequencies. Furthermore, it can be seen that the reflection coefficient is quite well when $P1 = 25.9mm$. The simulated reflection coefficient for different sizes of the open stub branch P_2 is shown in Figure 5.4b. It is found that by increasing the length P_2 from 9 to 14 mm, the second resonant frequency shifts towards lower frequency side. The considered value of P_2 is 13 mm to obtain the centered resonant frequency at 3.5 GHz with good impedance bandwidth.Figure 5.4c shows the effect of varying the length of the main branch on the reflection coefficient. It is found that by increasing the length P_3, the upper frequency band deceases. For P_3 equal to 15.7mm, good performances are obtained in terms of impedance matching and resonant frequencies.

For better physical insight of the proposed antenna operating mechanism, the average current distributions are simulated at 2.43, 3.50 and 5.80 GHz as depicted Figure 5.5. It can

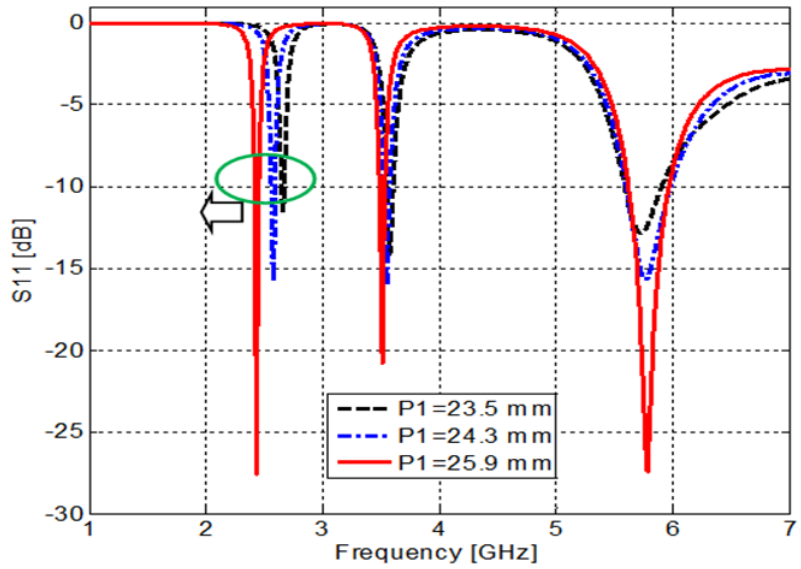

(a) P1 is varied while P2 and P3 are kept constants

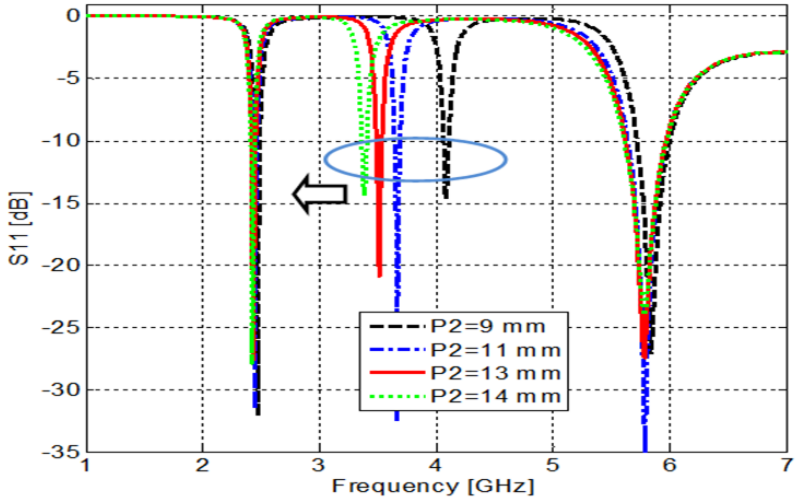

(b) P2 is varied while P1 and P3 are kept constants

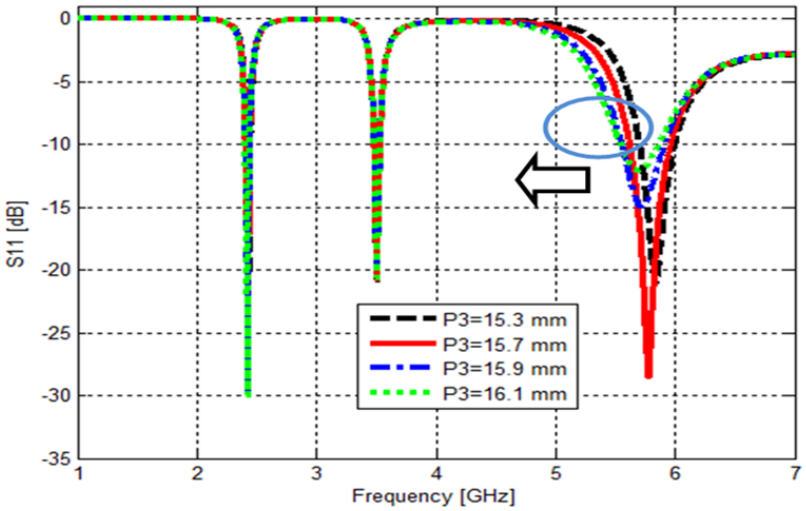

(c) P3 is varied while P1 and P2 are kept constants

Figure 5.4: Return losses of the proposed antenna

be observed that, for the first resonant frequency, the current is mostly concentrated in the J-shaped branch. Thus, the 2.45 GHz can be controlled by changing the length P_1 which is calculated by equation 5.1. For the second resonant frequency, the maximum current concentration is seen over the open stub. Consequently, the 3.5 GHz can be controlled by tuning the length of the open stub P_2 and its value can be calculated using equation 5.4. For the 5.8 GHz frequency, it can be noticed that large concentration of current is recorded at the main branch connected to the feed line, as well as on the other radiating branches due to the strong EM coupling between the branches contributing to the radiation.

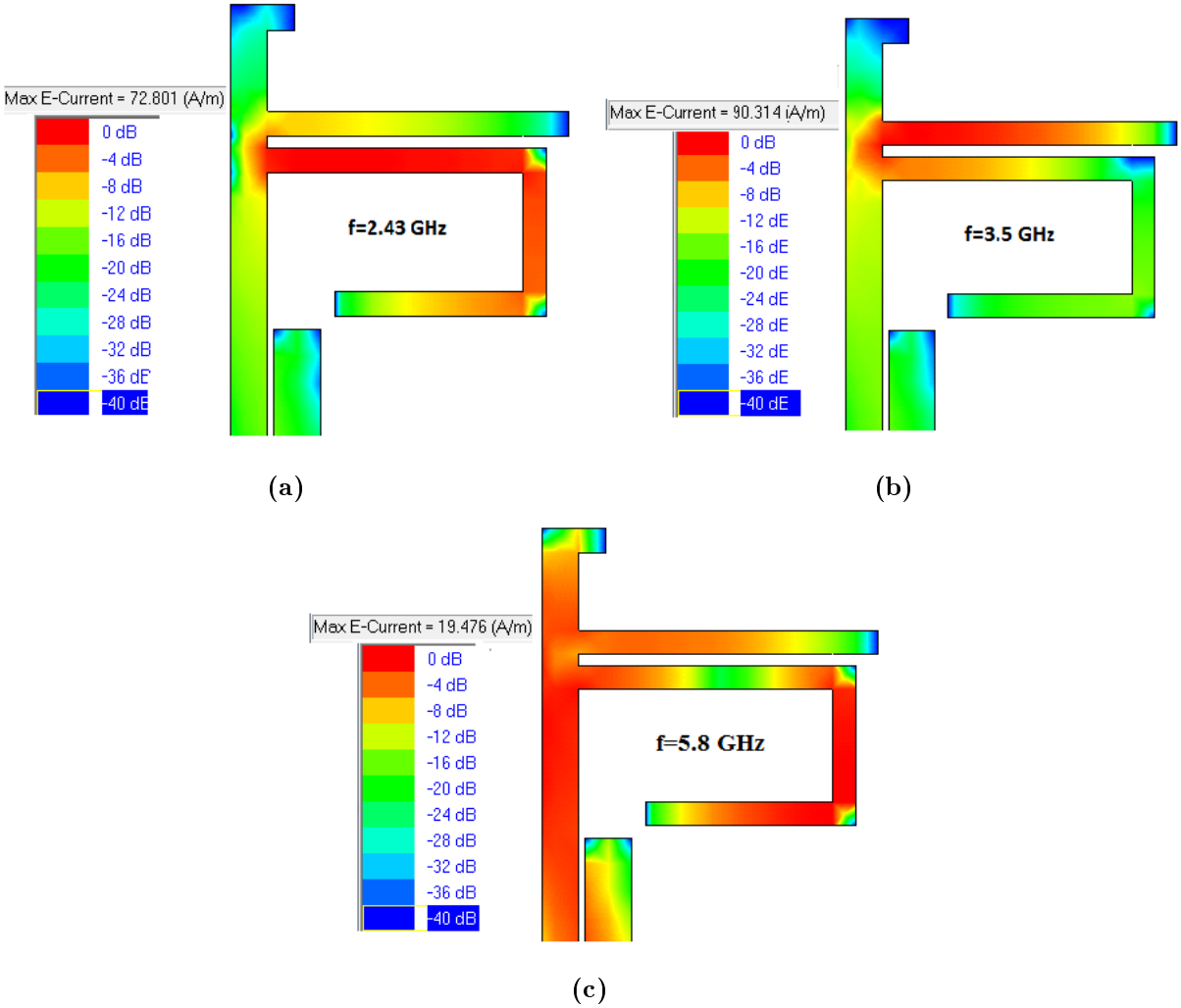

Figure 5.5: Average current distributions of the proposed antenna at 2.43, 3.5 and 5.8 GHz

The expression of the resonant frequencies (f_1, f_2 and f_3) are given by the following equations [7]:

$$f_1 = \frac{c}{3P_1\sqrt{\epsilon_{r,eff}}} \tag{5.1}$$

$$f_2 = \frac{c}{4P_2\sqrt{\epsilon_{r,eff}}} \tag{5.2}$$

$$f_3 = \frac{c}{2P_3\sqrt{\epsilon_{r,eff}}} \tag{5.3}$$

$$\epsilon_{r,eff} = \frac{\epsilon_r + 1}{2} \tag{5.4}$$

where c stands for the free space velocity and $\epsilon_{r,eff}$ is the effective permittivity of the substrate calculated using the equation 5.4.

The simulated radiation patterns of the tri-band proposed antenna at the three diverse resonant frequencies, namely 2.43 GHz, 3.5 GHz and 5.8 GHz, are shown in Figure 5.6. It is observed that the proposed antenna shows a dipole-like patterns in the E-plane (yoz) whereas in the H-plane (xoz), omnidirectional radiation characteristic is achieved for all resonant frequencies.

5.2.3 Fabrication and Measurement

The proposed tri-band monopole antenna is fabricated and tested. Figure 5.7 shows the photograph of the fabricated tri-band antenna.

The measured and simulated return losses of the proposed antenna are shown in Figure 5.8. The measured result indicates that the antenna has impedance bandwidths for 10-dB return loss of about 500 MHz (2.01-2.52 GHz), 230 MHz (3.48-3.71 GHz) and 1.2GHz (5.59-6.72GHz) which can be used for WIFI 2.45 GHz, WLAN 5.8 GHz and WIMAX 3.5 GHz (3.4-3.69 GHz). The slight difference seen between the simulated and the measured results is basically due to the manufacturing tolerances, the uncertainty on the thickness and dielectric constant of the substrate and the quality of the SMA connector. Furthermore, due to the small size of the antenna where the electrical size of the ground plane became small as compared to the wavelength. In this situation, the SMA connector and a part of the VNA connecting cable act as an additional ground plane [8]. Consequently, the current will flow back from the antenna to the connecting cable.

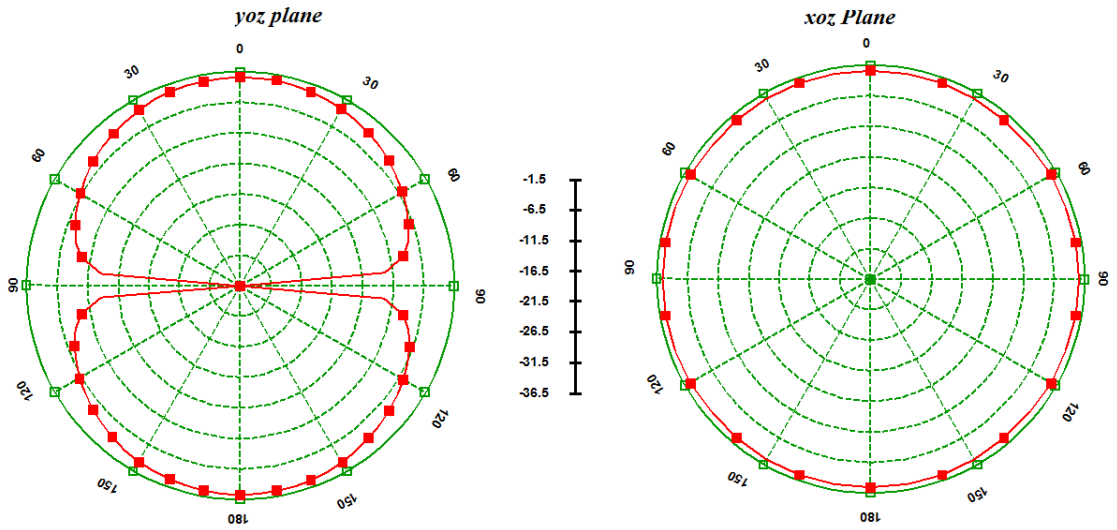

(a)

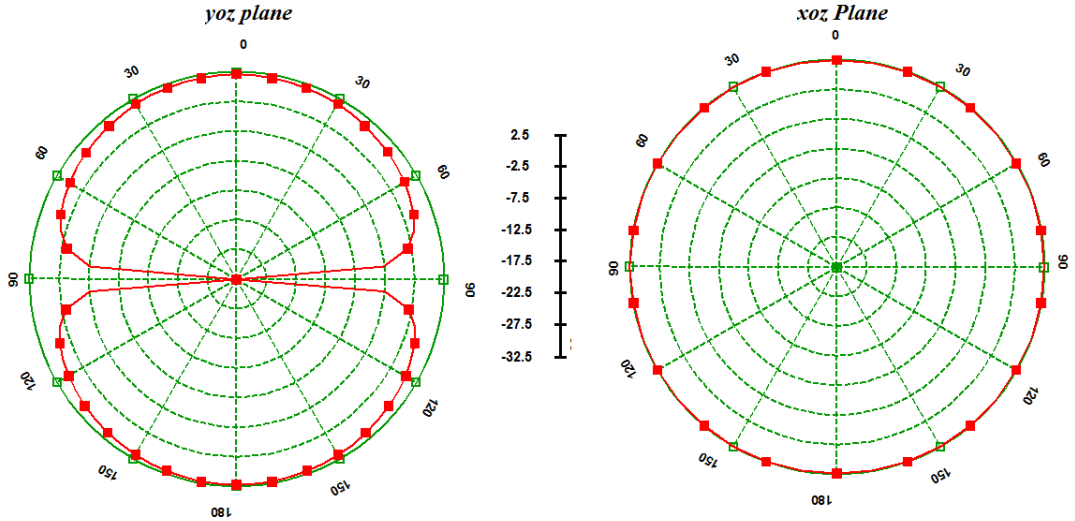

(b)

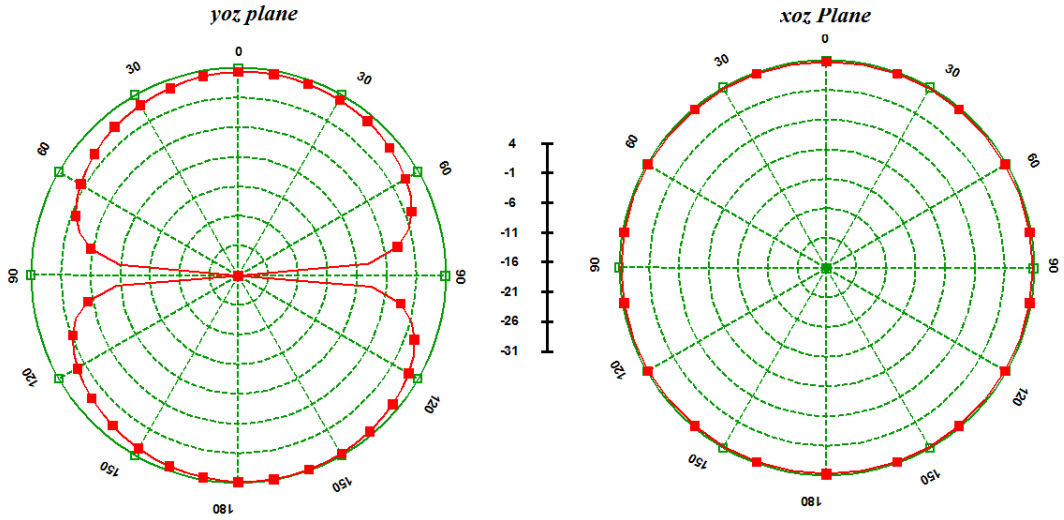

(c)

Figure 5.6: Radiation patterns at:(a) 2.43 GHz, (b) 3.5 GHz and, (c) 5.8 GHz

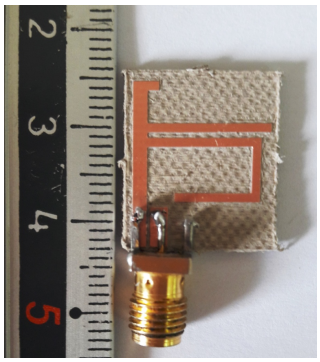

Figure 5.7: Fabricated tri-band antenna photograph

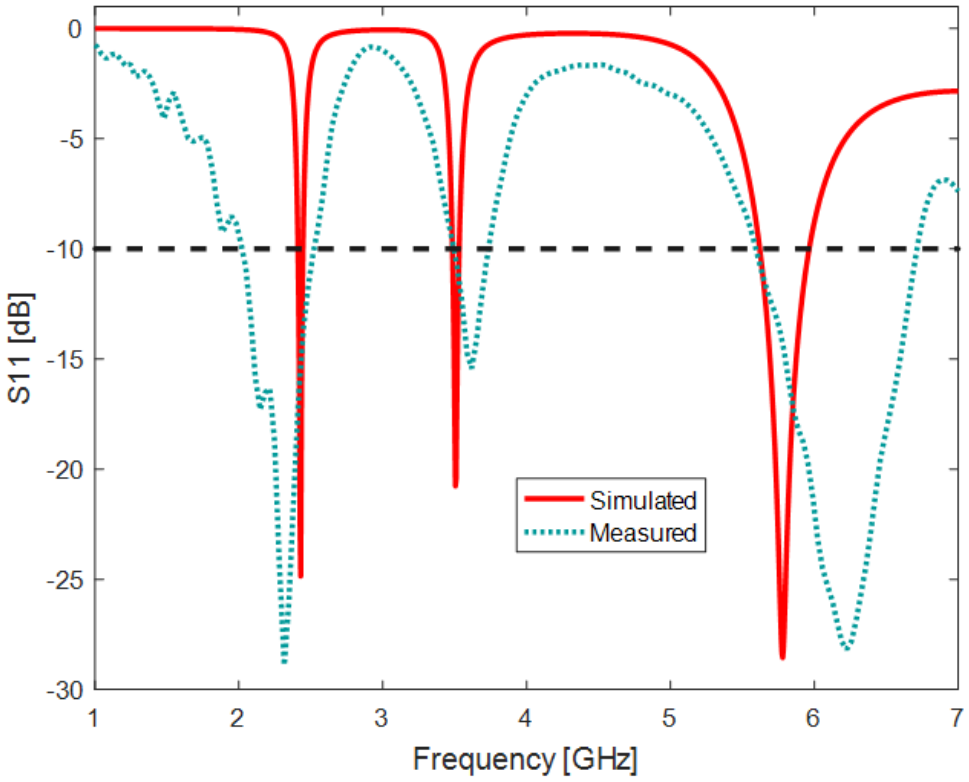

Figure 5.8: Simulated and measured return losses of the proposed antenna

5.3 Miniaturized triple band Concentric Hexagonal Fractal Rings based Microstrip Patch Antenna

The previous sections dealt with the design and development of compact ACS-fed antenna operating in three useful bands. In this section, a combination of two fractal rings is effectively used to design more compact tri-band antenna.

5.3.1 Design Procedure

In this section, the design of a triple band monopole antenna is presented, where two concentric fractal rings are used to create multiple resonances . The basic structure of this antenna is detailed in chapter 3 and it is shown in Figure 5.9a . Three steps will be considered to

design the proposed triple band antenna. The first one starts by an hexagonal fractal ring monopole antenna, then a second fractal ring is introduced at the center of the first fractal ring as shown in Figure 5.9b to design the second monopole antenna Ant.2 finally the two rings are connected to each other by a strip line , as can be seen in Figure 5.9c, to construct the proposed structure (Ant.3). The position of the connection strip is carefully chosen to create multiple useful operating bands.

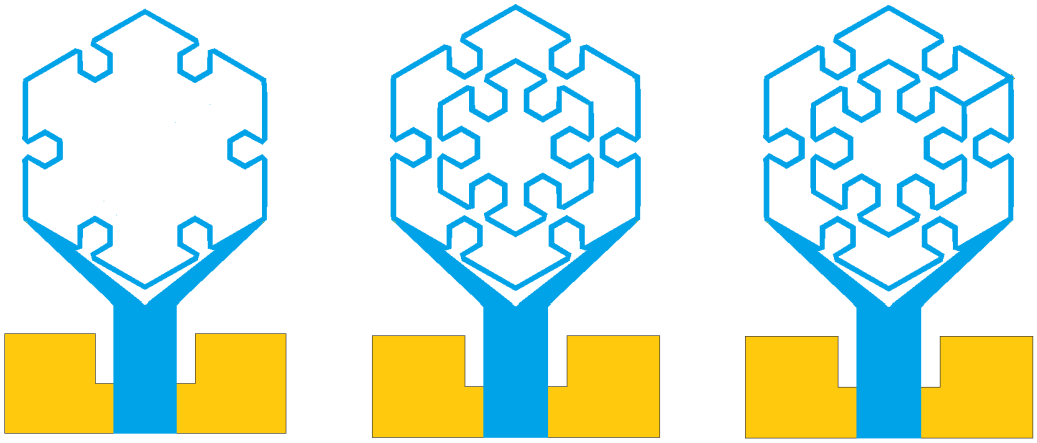

(a) Ant.1 **(b)** Ant.2 **(c)** Ant.3

Figure 5.9: Design Evolution Steps of the Proposed ACS-fed Tri-band Monopole Antenna

Figure 5.10 shows the geometry of the proposed two concentric fractal rings tri-band monopole antenna along with its dimensions. The proposed antenna with a planar size of only $9.3 \times 17mm^2$ is composed of a two connected concentric fractal shaped rings acting as a radiating element and a Y-shaped feed structure printed on the top side of the substrate and a partial ground plane embedded in the other side of the substrate. The fractal ring shape is selected for antenna miniaturization issue. The second fractal ring, which has same center as the first one, connected to the outer ring is used to generate multiple resonances and to achieve more compactness. Hence the resulted antenna resonates at three different frequencies covering the 2.4/5.6/5.8GHz GHz WLAN and 3.5GHz WiMAX bands. Furthermore, the slot etched in the ground plane is used to improve the impedance matching of the antenna. After an extensive simulation study, the geometrical parameters of the antenna were tuned and they are listed in Table 5.2. The antenna design and study is done with help of a powerful full wave electromagnetic simulator CST suite 2017.

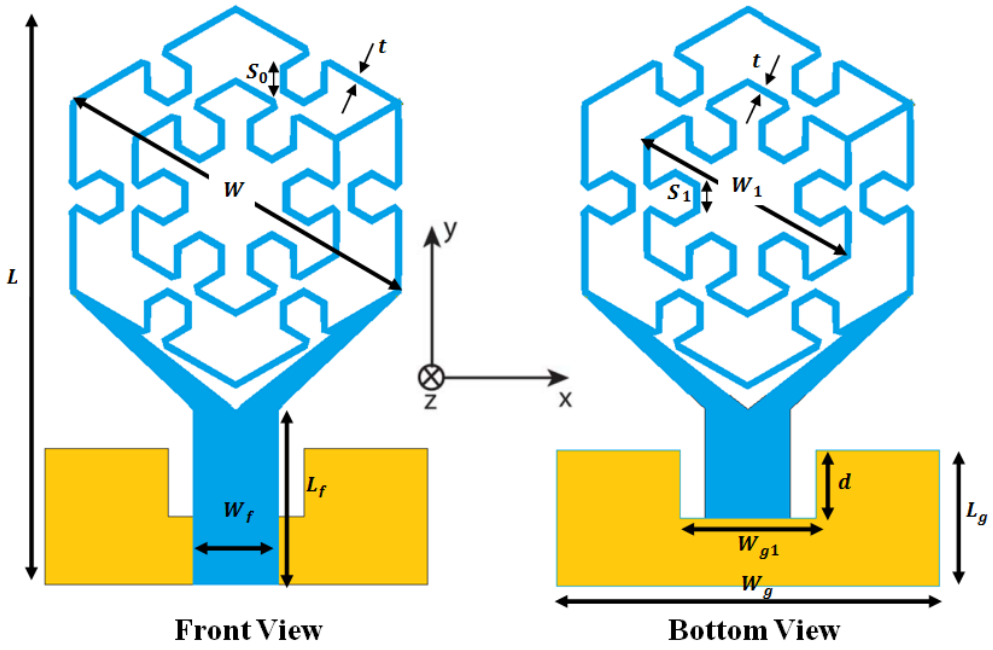

Figure 5.10: Geometry of the proposed antenna

Table 5.2: Geometrical dimensions of the proposed antenna

Parameter	Value (mm)	Parameter	Value (mm)
L	17	W	10.7
L_f	5.42	L_g	4
W_f	2.5	W_g	4.5
t	0.2	d	2
S_1	0.85	S_0	0.8
W_1	6.45	W_{g1}	2.5

5.3.2 Simulation Results

The three antennas involved in the design evolution illustrated in Figure 5.9 are simulated and their simulated return losses are plotted in Figure 5.11. Initially, a single band centered at 3.52 GHz is obtained for Ant.1. The introduction of the fractal radiating ring (Ant.1) increases the total current path length as a result of which Ant.1 resonant at 3.52GHz as illustrated in Figure 5.11. If the parameter S_1 is further increased to 2.7mm (maximum length before overlapping), the resonant frequency decreases and reach down to $3.26GHz$ (not able to reach the desired frequency: 2.45 GHz). Thus, the tuning of S_1 for the Ant.1 has a limitation and cannot shift the resonance as low as 2.45GHz. This is why a second fractal ring is introduced to create a resonance at 2.45GHz without increasing the antenna dimensions. By loading Ant. 1 with a second fractal ring to design Ant.2, the electromagnetic coupling (EM) between the two rings has led to dual band operation as well as fist resonance shift to 3.44GHz as can be seen in Figure 5.11. To achieve compact size and triple band

operation the two fractal rings are connected to each other by means of a strip line (Ant.3) as shown in Figure 5.9. It can be noted from this figure that the simulated 10-dB impedance bandwidths of the three operating bands are $2.43\%(2.43-2.49GHz)$, $23.1\%(3.25-4.10GHz)$ and $25.3\%(5.43-7.0GHz)$.

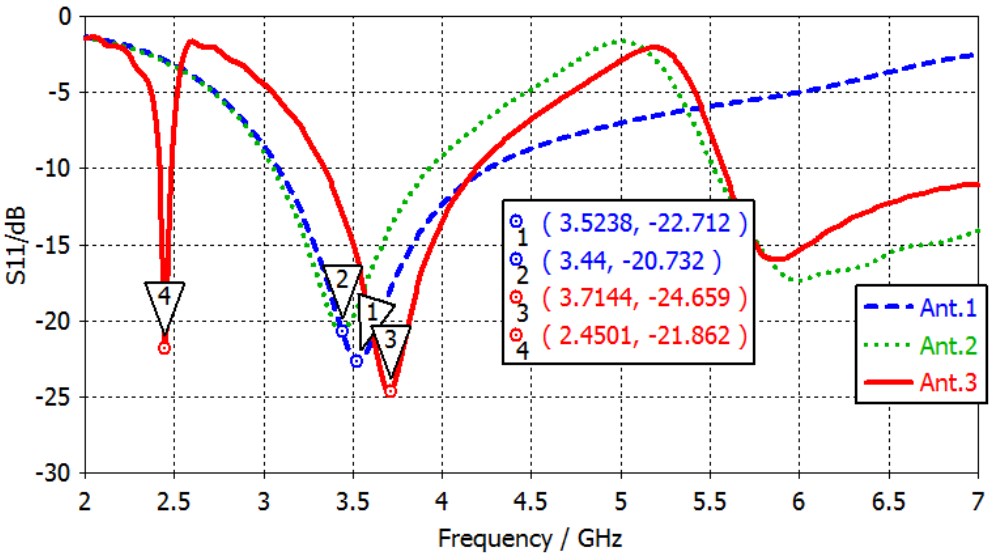

Figure 5.11: Return losses versus frequency of various antenna structures

The simulated return losses of the proposed antenna for different positions of the connecting strip are shown in Figure 5.12. It is clearly seen from the figure that the connection position affects significantly the antenna operating bands. When the connection is set at position $Z1$ as illustrated in Figure 5.12a, the antenna operates at two frequency bands centered at 2.43GHz and 3.92GHz. When the connection is established at position $Z2$ (Proposed antenna), three operating bands are obtained. However, if the connection is placed at position $Z3$, only two bands are exited whereas if the connection is placed at position $Z4$, one mode is exited. Consequently, good results, in term of multiband operation, are obtained when the connection is set at position $Z2$. It is worth to mention that the remaining positions of the connection are not considered in the study due to the structure symmetry.

The simulated return losses of the proposed antenna when the side length of the small hexagonal open ring S_0, for the first iteration, of the external fractal ring is changed are presented in Figure 5.13. It is clearly seen from the results that by increasing S_0 from 0.6 to 0.9mm with a step of 0.1mm, the three operating bands are significantly affected. For the first resonance, by increasing the value of S_0, the resonant frequency shifts to lower frequencies. As for the second band, the lower cut-off frequency is slightly shifted to lower frequencies whereas the upper cut-off frequency sifts significantly to higher frequency resulting in bandwidth

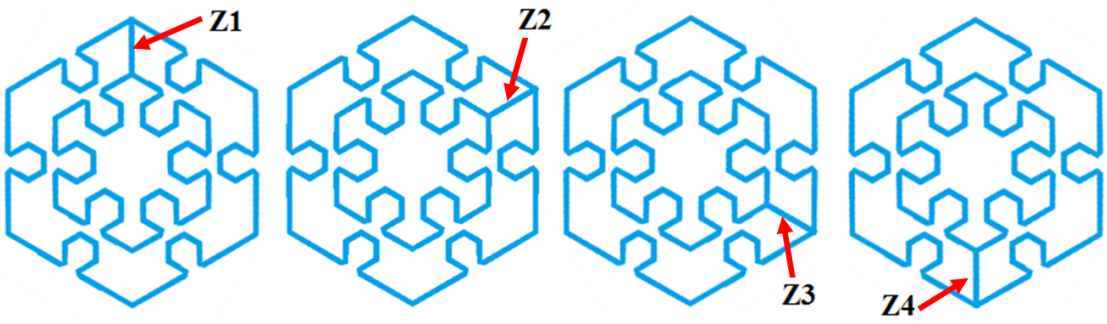

(a)

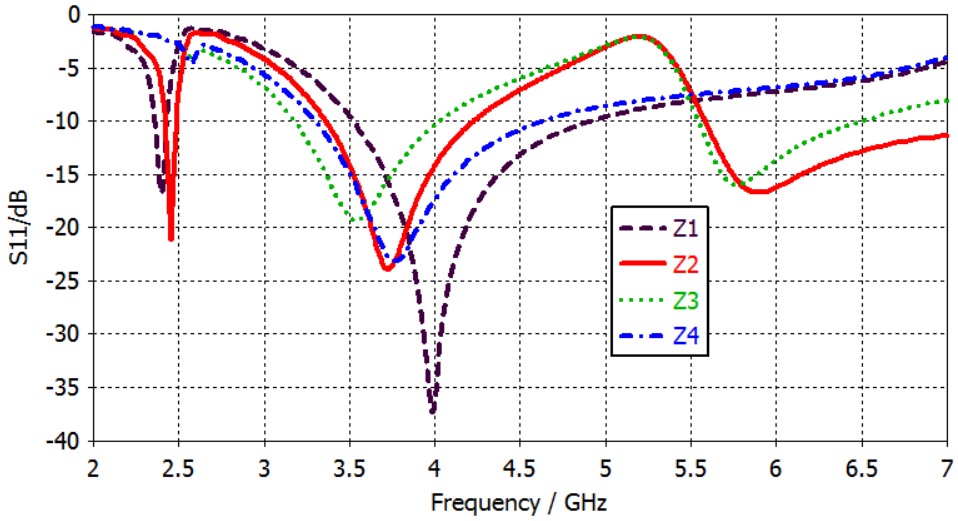

(b)

Figure 5.12: (a) Position of the connection strip and (b) effect of the position of the connecting strip on the return loss.

widening. For the third band, significant shift of the lower cut-off frequency is observed when S_0 is decreased. Consequently, it can be concluded that good results are obtained for $S_0 = 0.8mm$.

The effect of changing the parameter S_1 on the antenna return losses characteristics is depicted in Figure 5.14. It can be observed from the figure that by increasing the value of S_1, the lower cut-off frequency of the third band is shifted towards higher frequency, the first resonance is also slightly increased while the higher cut-off frequency of the second band increases. Hence, It can be concluded that good results are obtained for $S_1 = 0.85mm$.

To further understand the operating mechanism of the proposed antenna, the current distribution at the three resonant frequencies are simulated and presented in Figure 5.15. At the first resonant frequency, the current is mostly concentrated on the two fractal rings. Thus this resonance can be finely tuned by changing the parameters of the radiating rings. Large current concentration is seen at the vicinity of the connection strip and on the feedline at the second resonance. Accordingly, this resonance can be controlled be changing the outer

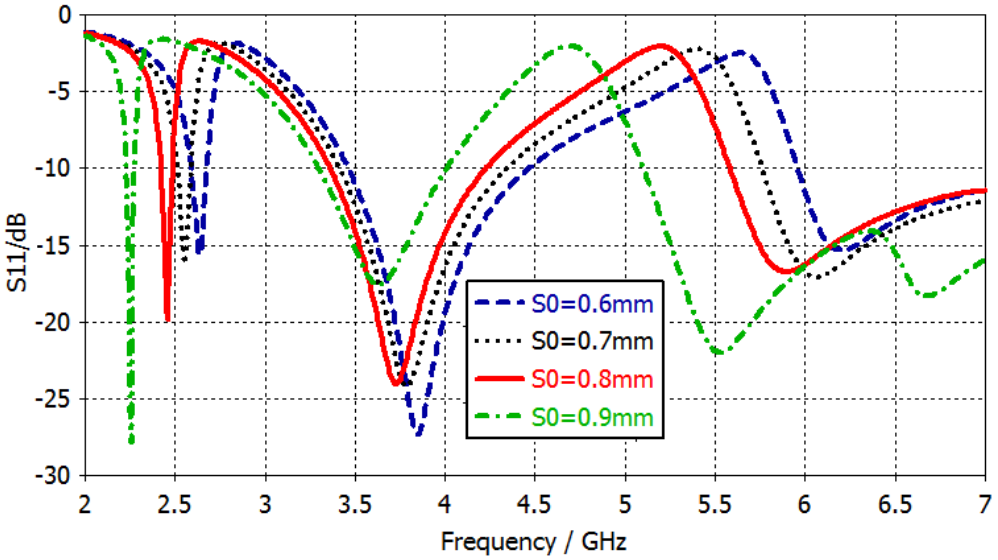

Figure 5.13: Effect of S_0 on the return loss

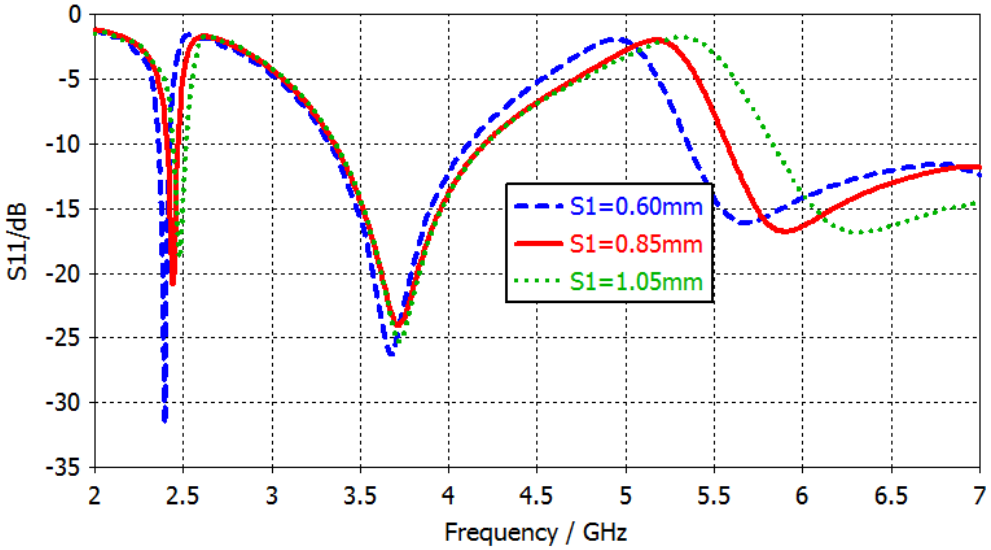

Figure 5.14: Effect of S_1 on the return loss

ring dimensions. At the last operating frequency of 5.8 GHz, high concentration of current occurs on the feedline and on the two fractal rings. this band can be controlled by changing the fractal rings configuration and dimension.

5.3.3 Fabrication and Measurements

Figure 5.16 shows the photograph of proposed antenna. The simulated and measured return losses results of the antenna are illustrated in Figure 5.17 . It can be observed that the simulated and measured results are in good agreement, showing a tri-band operation with measured 10-dB impedance bandwidths of 686 MHz (1814 – 2500 MHz, 31.8%), 1770 MHz (2967 – 4737 MHz, 45.9%) and 1461 MHz (5539 – 7000 MHz, 23.3 %). The slight difference

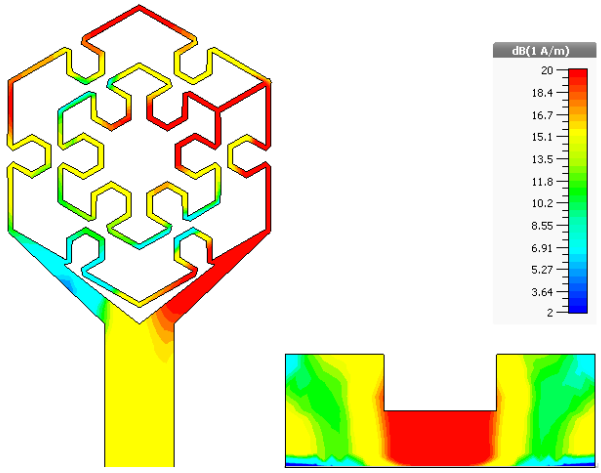

(a) $f = 2.45GHz$

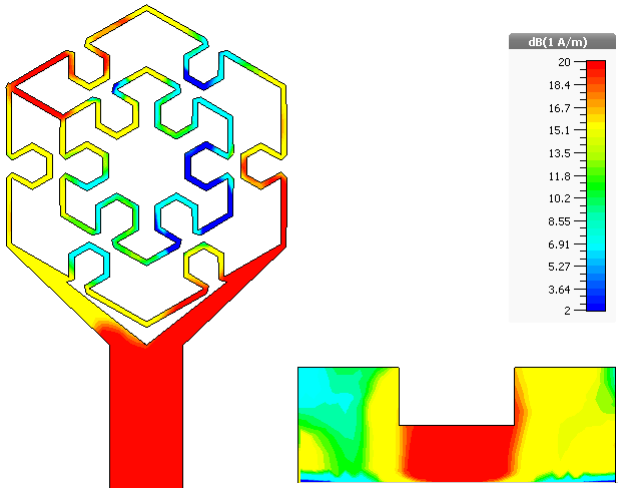

(b) $f = 3.7GHz$

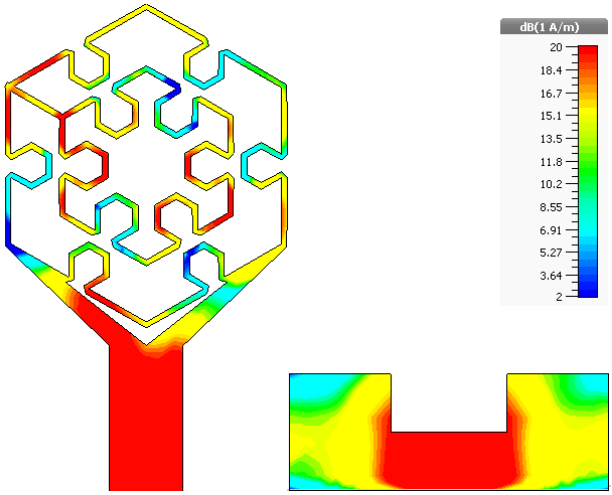

(c) $f = 5.8GHz$

Figure 5.15: Simulated current distribution at different resonant frequencies

between the measured and simulated results may be due to the tolerance of fabrication unit and soldering of the SMA connector. The obtained bandwidth covers widely the WLAN (2.4, 5.6 and 5.8 GHz) and WiMAX (3.5 GHz) applications.

The antenna radiation patterns were measured in an anechoic chamber available at

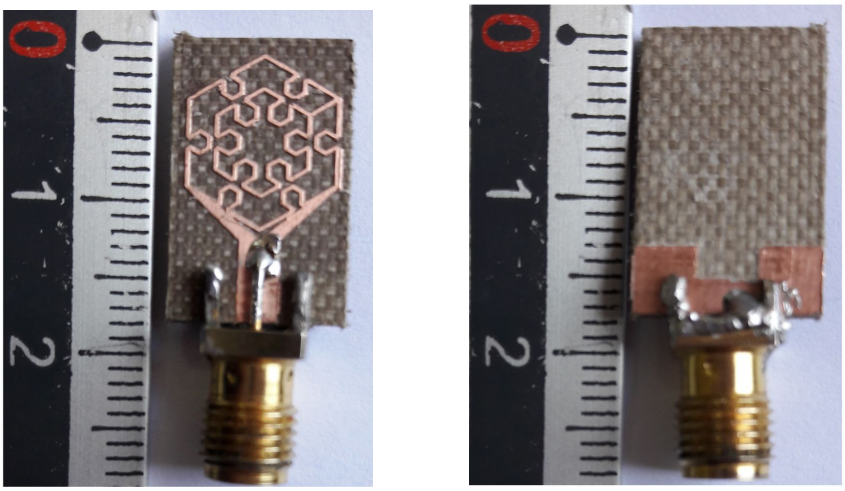

(a) Front View **(b)** Back view

Figure 5.16: Photograph of the fabricated tri-band antenna prototype

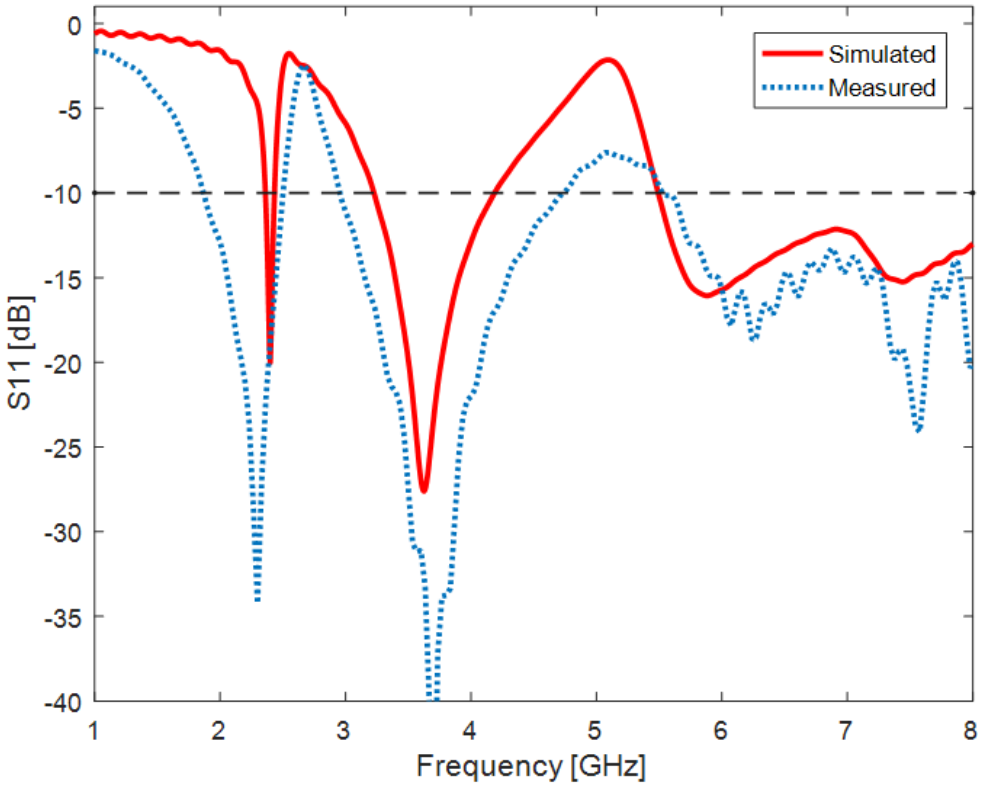

Figure 5.17: Simulated and measured return losses of proposed antenna

USTHB university (Figure 5.18). The simulated and measured radiation patterns of the proposed antenna in the E and H planes at different frequencies (2.45, 3.5 GHz, and 5.8 GHz) are plotted in Figure 5.19. It is seen that the simulated and measured results are in good agreement. The slight deviation seen between the simulated and measured radiation patterns is mainly due to then positioner during the measurement process. For all frequencies, the antenna has a monopole-like radiation pattern in the E-plane and an omnidiretional radiation pattern in the H-plane which make it well-suited for the intended applications. The

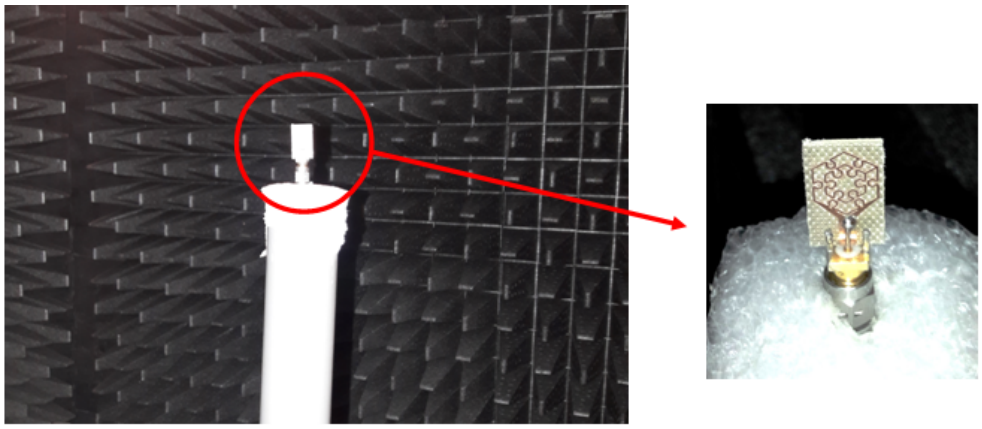

Figure 5.18: Antenna placed in the anechoic chamber

simulation peak gain of the proposed antenna at 2.45 GHz is 3.75 dB, at 3.5GHz is 0.71dB while the peak gain at 5.8 GHz is 0.12 dB.

A comparison between the proposed antennas and other antennas reported in the literature is presented in Table 5.3. By comparing the reported antennas footprints, it is clearly seen that the proposed antennas have the smallest one. Consequently, It can be concluded that the proposed antennas achieves significant size reduction. Moreover, In terms of impedance matching performance, the proposed antennas outperform almost all the reported antennas.

Table 5.3: Comparison between proposed antenna size along with applications bands with other compact antennas

Ref.	**Antenna Size** (mm^2)	**Antenna Footprint**	**Operating bands**
[2]	23×20	$0.027\lambda_0^2$	2.39-2.52 GHz-3.3-4.47 GHz-5.15-6.0GHz
[3]	18×22	$0.022\lambda_0^2$	2.27-2.50 GHz-3.28-3.81 GHz-4.91-5.98GHz
[5]	35×38	$0.048\lambda_0^2$	1.78-1.84 GHz-2.34-3.86 GHz-5.75-5.87GHz
[4]	18×18	$0.022\ \lambda_0^2$	2.51-2.62 GHz-3.42-3.5 GHz-5.68-5.96GHz
[9]	32×12	$0.026\lambda_0^2$	2.36-2.70 GHz, 3.35-2.74 GHz and 5.01-6.12GHz
[10]	38×20	$0.051\lambda_0^2$	2.32-2.51GHz, 3.05-3.95GHz and 5.4-5.85GHz
[7]	17.2×30	$0.034\lambda_0^2$	1.75-2.0GHz, 3.2-3.5 GHz and 5.0-6.8GHz.
[11]	21×33	$0.046\lambda_0^2$	2.39-2.51GHz, 3.26-4.15 and 5.0-6.43GHz
[12]	17.6×30.3	$0.035\lambda_0^2$	2.16-3.61GHz-3.36- 3.72GHz and 4.98-5.87GHz
[13]	21×19	$0.027\lambda_0^2$	2.24-2.55GHz and 4.64-5.39GHz
[14]	14.7×26	$0.025\lambda_0^2$	2.2-2.52GHz and 3.3-4.2GHz
[15]	51×33.4	$0.113\lambda_0^2$	2.4-2.5 GHz-3.4-3.6 GHz-5.2-5.5GHz
1st Antenna	14.6×17.5	**0.017** λ_0^2	2.01-2.52 GHz-3.48-3.71 GHz-5.59-6.72GHz
2nd Antenna	9.3×17	**0.0105** λ_0^2	1.84-2.50 GHz-2.97-4.74 GHz-5.54-7.00 GHz

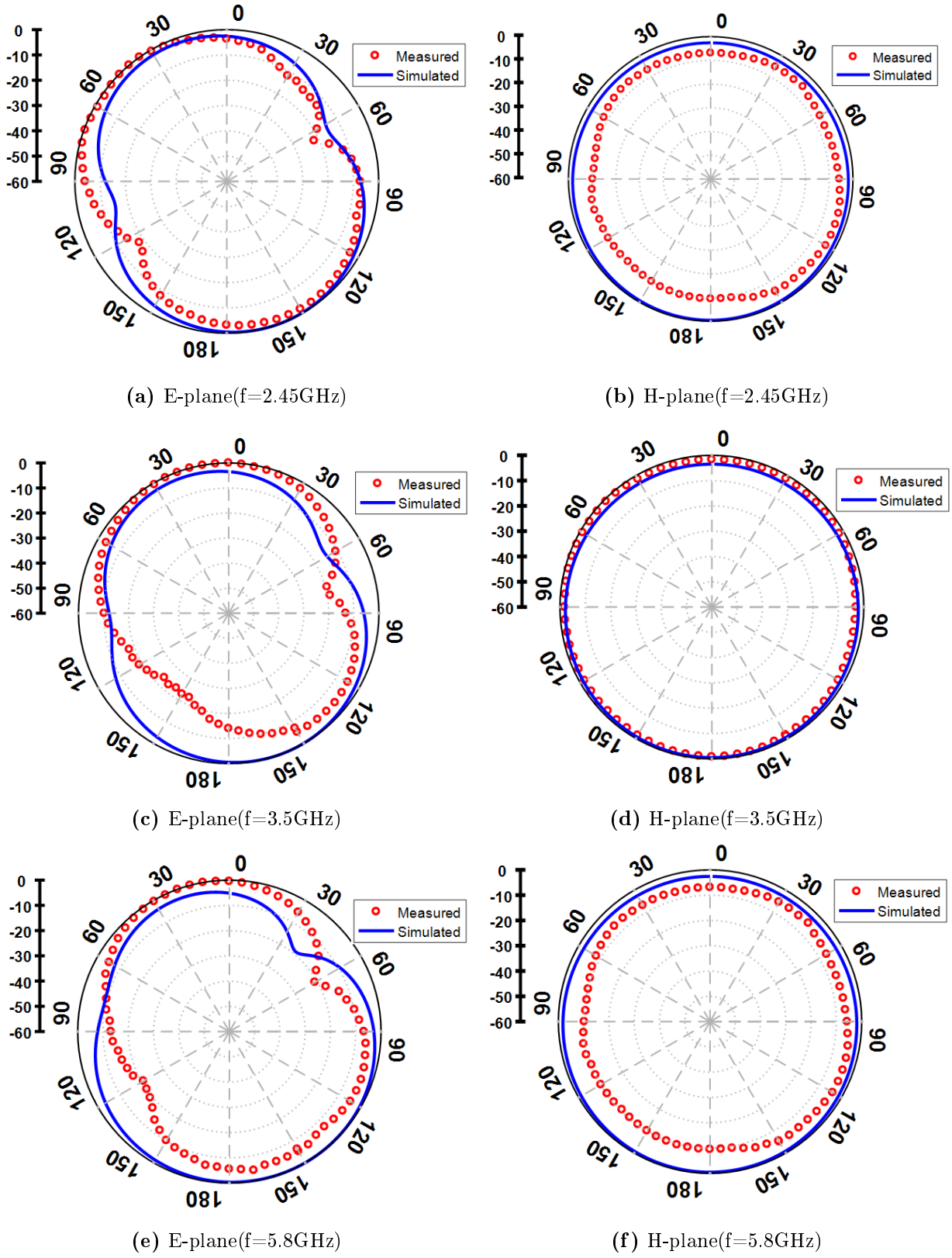

(a) E-plane(f=2.45GHz)

(b) H-plane(f=2.45GHz)

(c) E-plane(f=3.5GHz)

(d) H-plane(f=3.5GHz)

(e) E-plane(f=5.8GHz)

(f) H-plane(f=5.8GHz)

Figure 5.19: Radiation patterns of the proposed antenna at 2.45 GHz,3.5 GHz and 5.8 GHz

5.4 Summary

In this chapter, two compact tri-band microstrip antennas have been presented, fabricated and measured. The first proposed antenna has a very simple patch shape, ACS feeding

structure and compact size of $14.6 \times 17.5mm^2$. The three resonant frequencies have been realized by connecting two different branches to the monopole exciting strip. By changing the length of the branches, the operating bands can be easily tuned to the desired frequencies. The second proposed antenna consists of two concentric fractal radiating rings fed with a Y-shaped microstrip line. By connecting the two fractal rings a tri-band operation along with size reduction have been achieved. The proposed antenna has exhibited omnidirectional radiation patterns in the three operating bands. Furthermore, the measured results of the proposed antenna with compact size of $9.3 \times 17mm^2$ have shown good agreement with the simulated ones. All measured results demonstrate that the two proposed antennas are suitable for WLAN and WiMAX applications. The following is the list of publications resulted from the work presented in this chapter:

1. Djafri K, Challal, Dehmas M, Mouhouche F and Aksas R,*A Compact ACS-Fed Tri-band Microstrip Monopole Antenna for WLAN/WiMAX Applications*, Advanced Electromagnetic Journal 2018.

2. Djafri K, Challal M, Aksas R, Mouhouche F and Dehmas M, *Miniaturized Concentric Hexagonal Fractal Rings based Microstrip Patch Antenna for WLAN/WiMAX Application*, **Accepted** in Radioengineering Journal, Nov 2018.

The previous chapters deal with the conception and design of compact antennas dedicated for wireless applications. In the following chapter, a compact antenna design for medical application will be developed and discussed.

Bibliography

[1] Mohammad Alibakhshikenari, Bal S Virdee, and Ernesto Limiti. Triple-band planar dipole antenna for omnidirectional radiation. *Microwave and Optical Technology Letters*, 60(4):1048–1051, 2018.

[2] Wajid Zaman, Hamza Ahmad, and Haris Mehmood. A miniaturized meandered printed monopole antenna for triband applications. *Microwave and Optical Technology Letters*, 60(5):1265–1271, 2018.

[3] Vivek Kumar Pandit and AR Harish. A compact cpw-fed tapered monopole triple-

band antenna for wlan/wimax application. *Microwave and Optical Technology Letters*, 60(9):2298–2303, 2018.

[4] Tanweer Ali and Rajashekhar C Biradar. A triple-band highly miniaturized antenna for wimax/wlan applications. *Microwave and Optical Technology Letters*, 60(2):466–471, 2018.

[5] Cheng Zhu, Tong Li, Ke Li, Zi-Jian Su, Xin Wang, Hui-Qing Zhai, Long Li, and Chang-Hong Liang. Electrically small metamaterial-inspired tri-band antenna with meta-mode. *IEEE Antennas and Wireless Propagation Letters*, 14:1738–1741, 2015.

[6] Pratyush Pushkar and Vibha Rani Gupta. A metamaterial based tri-band antenna for w i max/wlan application. *Microwave and Optical Technology Letters*, 58(3):558–561, 2016.

[7] Praveen V Naidu and Akshay Malhotra. A small asymmetric coplanar strip fed tri-band antenna for pcs/wimax/wlan applications. *Microsystem Technologies*, 23(1):13–22, 2017.

[8] L Liu, YF Weng, SW Cheung, TI Yuk, and LJ Foged. Modeling of cable for measurements of small monopole antennas. In *Antennas and Propagation Conference (LAPC), 2011 Loughborough*, pages 1–4. IEEE, 2011.

[9] Le Kang, Hao Wang, Xin Huai Wang, and Xiaowei Shi. Compact acs-fed monopole antenna with rectangular srrs for tri-band operation. *Electronics Letters*, 50(16):1112–1114, 2014.

[10] Xueshi Ren, Steven Gao, and Yingzeng Yin. Compact tri-band monopole antenna with hybrid strips for wlan/wimax applications. *Microwave and Optical Technology Letters*, 57(1):94–99, 2015.

[11] Wei Hu, Ying-Zeng Yin, Peng Fei, and Xi Yang. Compact triband square-slot antenna with symmetrical l-strips for wlan/wimax applications. *IEEE Antennas and Wireless Propagation Letters*, 10:462–465, 2011.

[12] Mohammed Lamsalli, Abdelouahab El Hamichi, Mohamed Boussouis, Naima Amar Touhami, and Tajeddin Elhamadi. Genetic algorithm optimization for microstrip

patch antenna miniaturization. *Progress In Electromagnetics Research*, 60:113–120, 2016.

[13] V Deepu, R Sujith, S Mridula, CK Aanandan, K Vasudevan, and P Mohanan. Acs fed printed f-shaped uniplanar antenna for dual band wlan applications. *Microwave and Optical Technology Letters*, 51(8):1852–1856, 2009.

[14] Praveen V Naidu. Printed v-shape acs-fed compact dual band antenna for bluetooth, lte and wlan/wimax applications. *Microsystem Technologies*, 23(4):1005–1015, 2017.

[15] Adrian Bekasiewicz and Slawomir Koziel. Miniaturized uniplanar triple-band slot dipole antenna with folded radiator. *Microwave and Optical Technology Letters*, 60(2):386–389, 2018.

Chapter 6

Design of a Compact Antenna for a Microwave Colonoscopy System

Contents

6.1 Introduction

The goal of this chapter is to design an antenna element to be used in antenna array for a colonoscopy application. A colonoscope is a long, thin, flexible tube with a camera and a light on the end. The tube is inserted into the rectum to look at the inside of the colon. This tool is used during a common diagnostic and screening procedure called a colonoscopy.Then, the tool must be small, flexible to move easily and safely inside the colon. Furthermore, the antenna array must ensure full coverage of the colon inside and the number of its elements must be power of two for switching and resolution reasons. In addition, the antenna array must be cylindrical to fit the tool geometry with maximum dimensions of: diameter of 22.3mm and height of 30mm and it must operate in the frequency range from 5GHz to 8.0 GHz [1]. To meet the above mentioned requirements, the number, postion and configuration of the antenna array must be carefully chosen. This chapter will discusses in details the design of a compact microstrip antenna that meet the requirements of the considered application.

6.1.1 Array of Sixteen Elements

The proposed array consists of sixteen identical cavity-backed U-slot elements fed by sixteen L-shape microstrip lines. The elements are arranged in two rows of eight elements each. One row is used for transmission and the other for reception. The elements are wrapped around a conducting cylinder with sixteen recessed cavities. As illustrated in Figure 6.1, antenna elements on the same row were separated by metallic walls of a width of 1 mm while transmission and reception rows were separated by a metallic disk of a thickness of 4 mm and a diameter of 23.2 mm. For feeding convenience, each antenna element was backed by an open cavity such that the cavity comprises only three metallic walls. Accordingly, no metallic wall was present in the feeding side of each antenna element [2] [3].

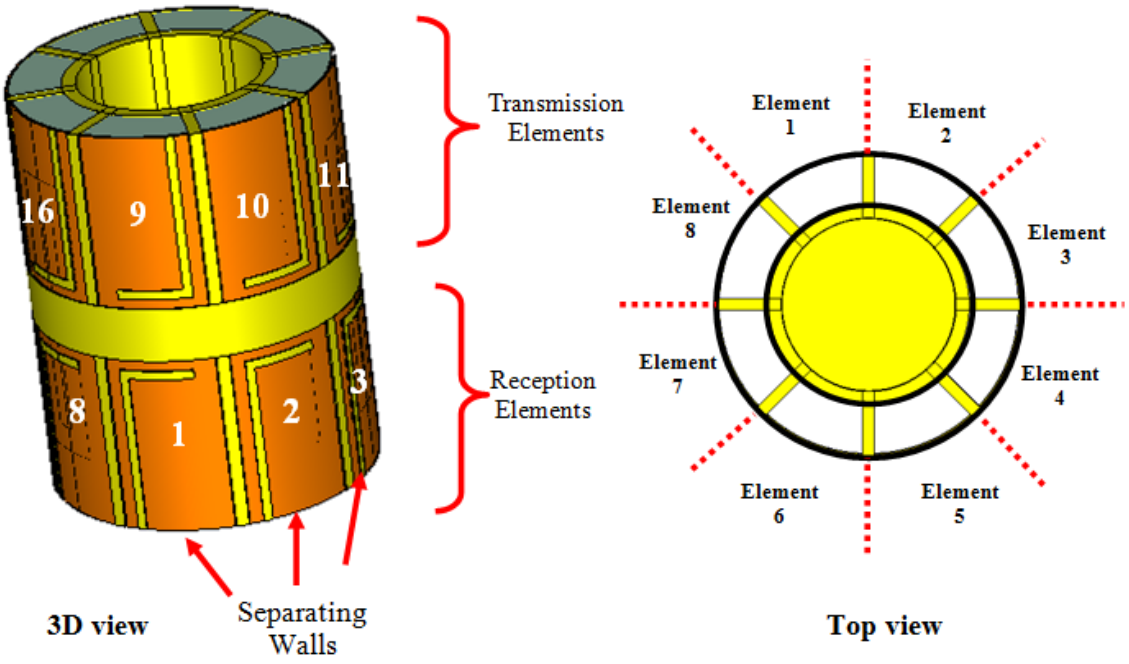

Figure 6.1: Geometry of the cylindrical U-slot antenna array

6.2 Microstrip-Fed U-Slot Baked by a Cavity

The proposed antenna element used in the applicator is a cavity-backed U-slot fed by an L-shape microstrip line. The U-shaped slot is selected to meet the reduced size requirements of the intended application. Besides, the slot antenna is backed by a cavity to enhance the isolation between array elements. The slot is printed on RT/Duroid 5880 substrate having a relative permittivity of 2.2 and a thickness of 0.127 mm. The substrate is very flexible and thus could be easily conformed onto a cylindrical surface. An L-shape microstrip line

Table 6.1: Proposed antenna dimensions (all dimensions are in mm)

Parameter	Value (mm)	Parameter	Value (mm)
L	14	P_1	1.0
g_1	1.75	P_2	0.1
g_2	1.0	P_3	0.7
g_3	0.75	W_s	1.8
g_4	4.55	W_p	0.65
L_s	7.7		

printed on the back side of the substrate was used to excite the slot. The cavity was filled by a lossy foam with relative permittivity of 2.1 as illustrated in Figure 6.2a. The size of the cavity is $13 \times 8.16 mm^2$, which is shown by the external dashed rectangle in Figure 6.2b, and the cavity depth is 4 mm. After an extensive simulation study with help of a powerful full wave simulator CST, the optimized dimensions of the proposed antenna are determined and are listed in Table 6.1.

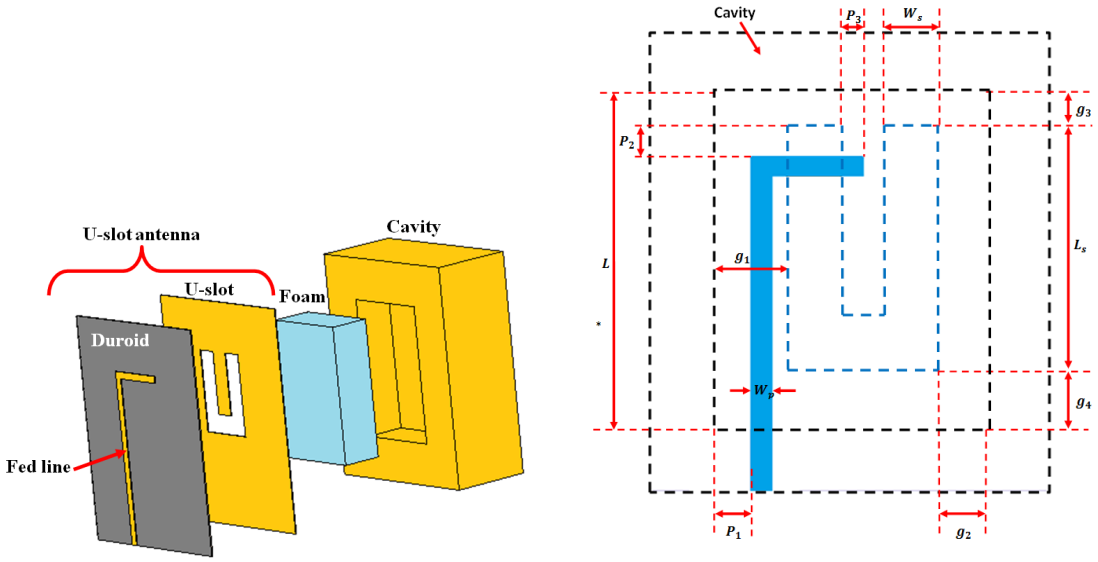

(a) **(b)**

Figure 6.2: Geometry of the cavity-backed U-slot antenna element (a) perspective view (b) slot antenna geometry

6.2.1 Simulation Results

To further understand the operating mechanism of the U-slot antenna, the effect of the cue parameters on the reflection coefficient is studied. The effect of varying the value of $P3$ on the reflection coefficient is depicted Figure 6.3a. By increasing the value of $P3$ from 0.6mm to 0.9mm by a step of 0.1mm, the impute impedance matching is greatly affected. It can be concluded from the results that better impedance matching is achieved for $P3 = 0.7mm$.The

variation of the slot width on the antenna return loss is depicted in Figure 6.3b. It can be seen from the figure that by changing the value of W_s from 1.4 to 2.0 mm, the antenna resonant frequency shifts towards high frequency side. For $W_s = 1.8mm$T better impedance matching in obtained.

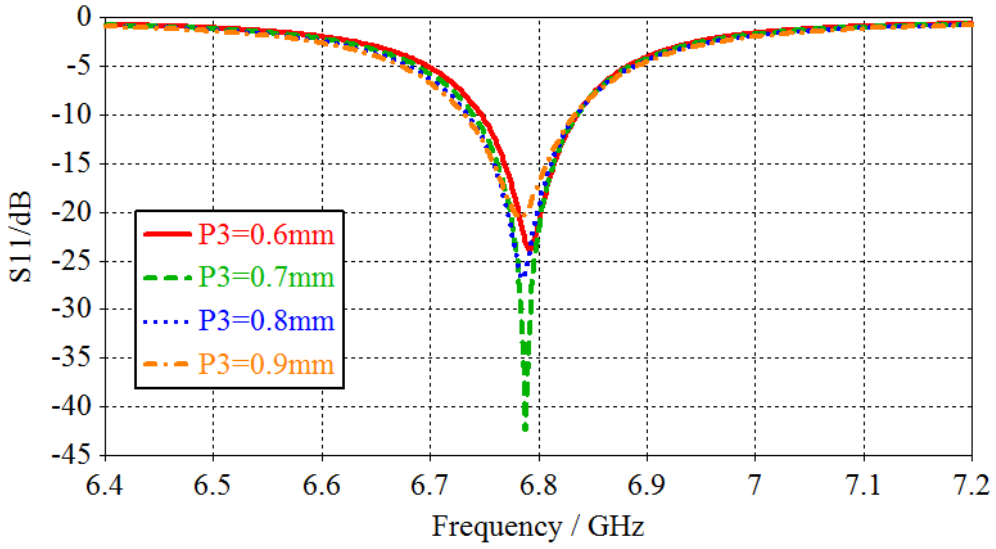

(a)

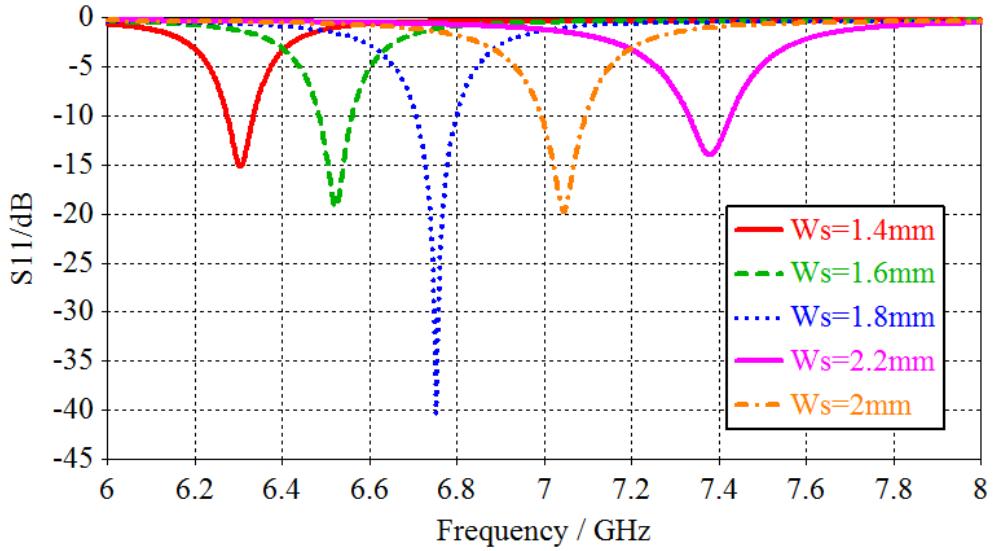

(b)

Figure 6.3: Variation on the return loss versus frequency,(a) Effect of varying P4 and (b) Ws on the return loss

The effect of changing the value of the gap g_4 , separating distance between the bottom cavity wall and the horizontal part of the U-slot, on the reflection coefficient is illustrated in Figure 6.4a. By increasing the value of g_4 the length of the resonant slot decreases which give rise to antenna resonance frequency increasing. It is clealy seen from the figure that optimum results are obtained for $g_4 = 3.9mm$. The effect of changing the fed lie width W_p on the the reflection coefficent characteristic is depicted in Figure 6.4b. It is seen from the

results that by increasing the value of the W_p from 0.45mm to 0.75mm the antenna return loss is greatly affected. It can be concluded that good impedance matching is achieved for W_p equal to 0.65mm.

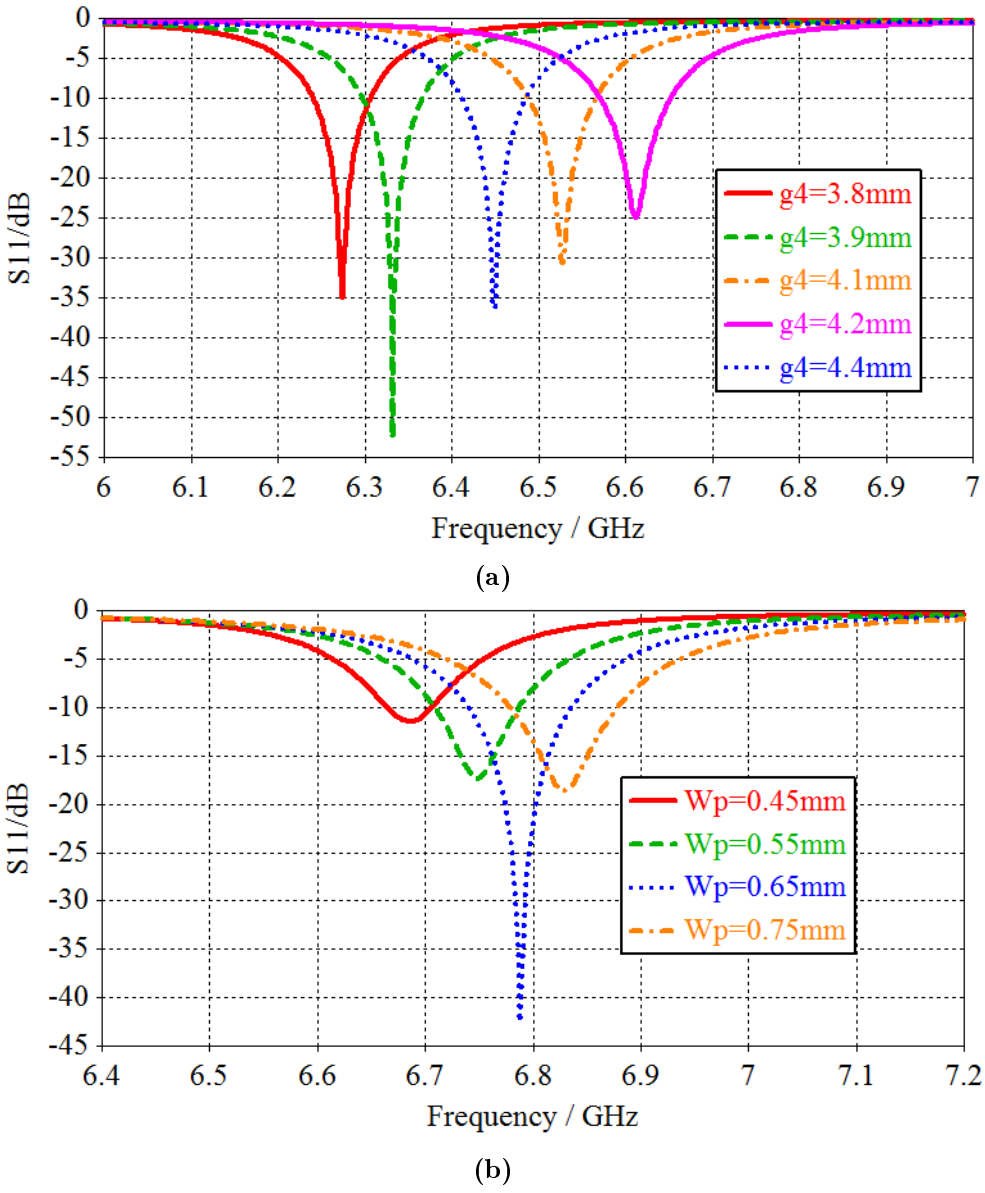

Figure 6.4: Variation on the return loss versus frequency. (a) g4 and (b) Wp on the return loss

In order to understand the behavior of the designed antenna, the surface current distribution is simulated at the resonant frequency 6.788 GHz as depicted in Figure 6.5. As can be seen from the figure, the current is mainly concentrated along the edges of the U-Slot and the feed line. Accordingly, the antenna resonant frequency can be controlled by changing the slot dimensions as well as the fed line parameters.

Figure 6.6 describes the simulated radiation patterns in the E-plane ($xoz - plane$) and H-plane ($yoz - plane$) at the center frequency of 6.788 GHz. It shows that this slot antenna

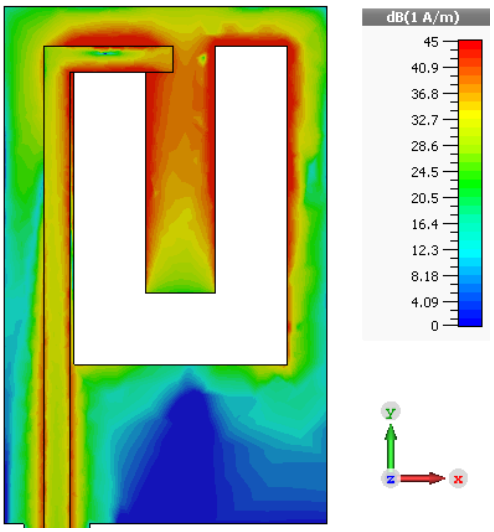

Figure 6.5: Current distribution at 6.788 GHz

has a unidirectional radiation pattern with a gain of 3.4 dB. The simulated 3D radiation pattern at the resonant frequency is shown in Figure 6.6c.

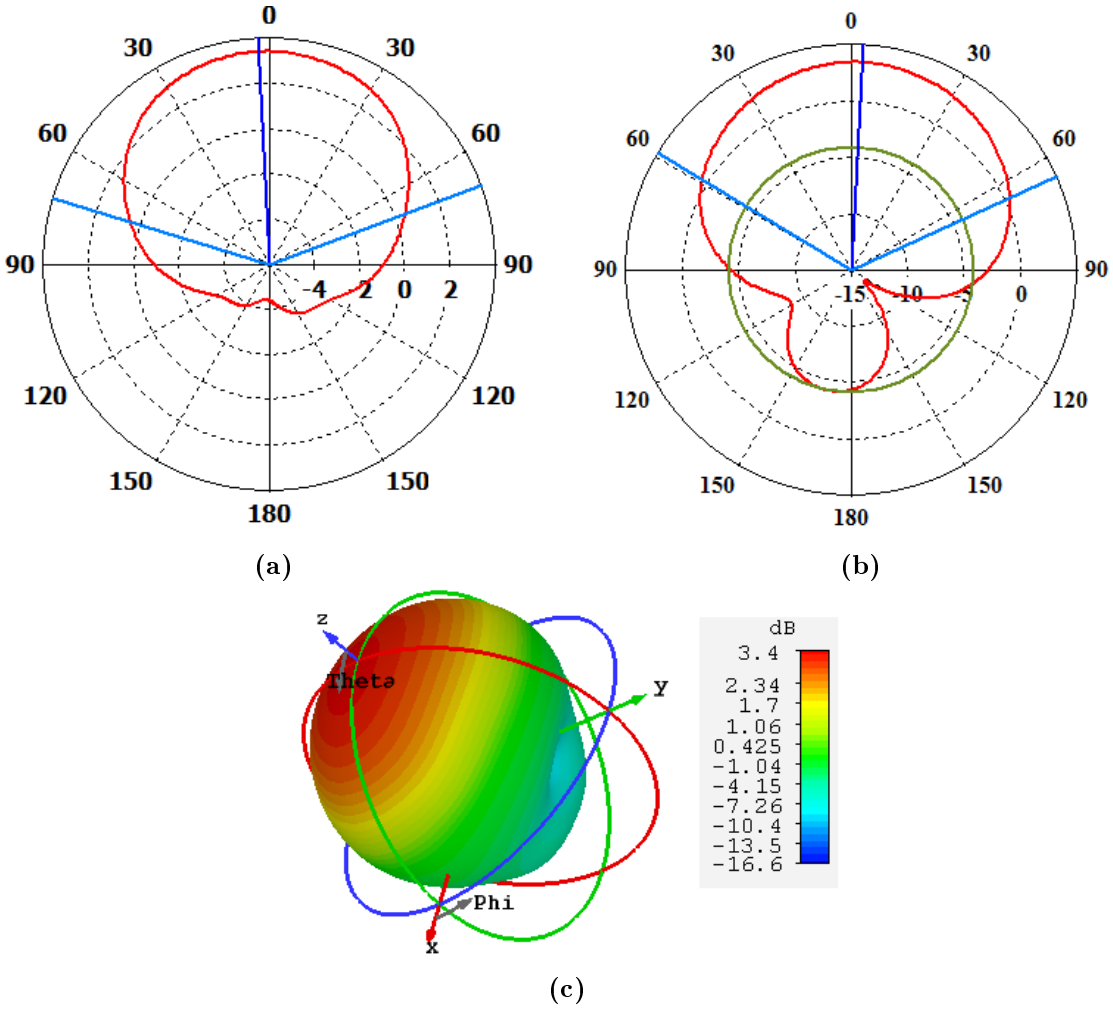

Figure 6.6: Simulated radiation pattern (a) E-plane, (b) H-plane and (c) 3D presentation

6.2.2 One Antenna Element with Colon Tissue

is designed to operate inside the human colon. Consequently, the presence of colon tissue must be considered in the analysis. The simulated reflection coefficients for different distances D between the antenna and the colon tissue are presented in Figure 6.9. It can be observed that the antenna input impedance matching is affected by the presence of the biological tissue. The minimum level of the input reflection coefficient is less than -10 dB for all simulated distances. Furthermore, the antenna resonant frequency decreases slightly as the distance between the antenna and the colon tissue increases.

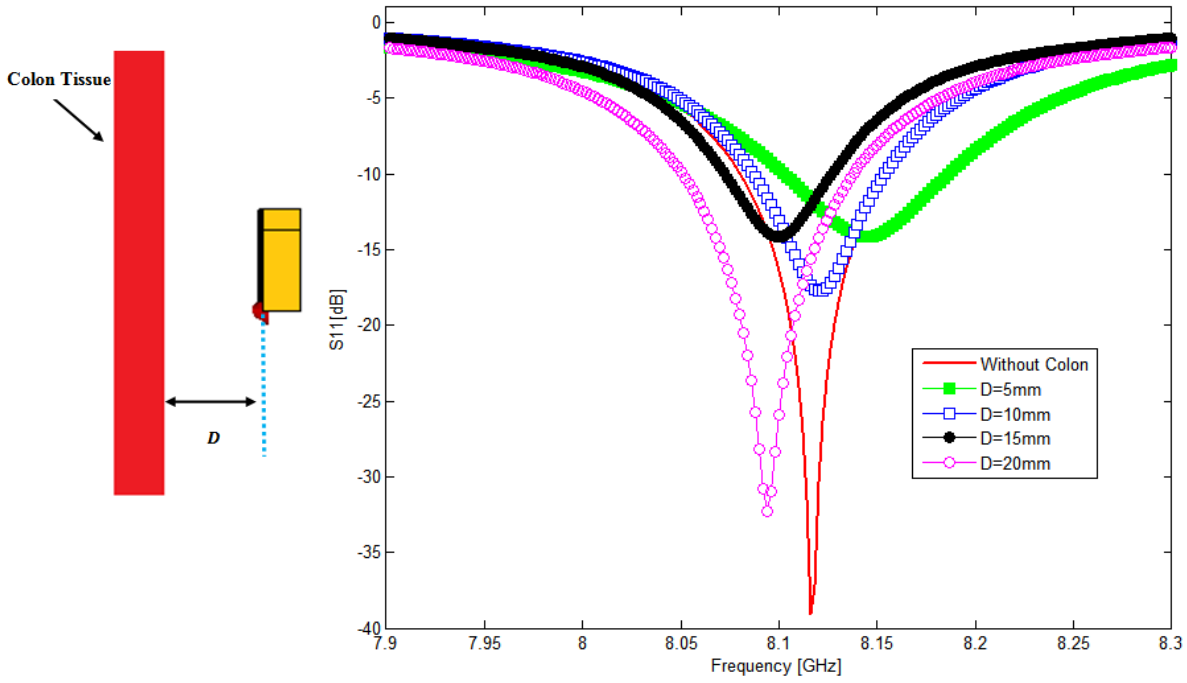

Figure 6.7: (a) Separating distance D between antenna element and colon tissue (b)Simulated reflection coefficient of one antenna element for different values of D

6.2.3 Array of Two Antenna Elements

Since the antenna array will be used in switched-beam mode, the isolation between antenna elements is crucial. Accordingly, two configurations of two adjacent antennas are investigated as shown in Figure 6.8. The first configuration consisted of two adjacent antenna elements, one used for transmission and the other for reception, namely transmission-reception configuration. In the second configuration two adjacent antenna elements were located in the same

row dedicated either for transmission or for reception, namely side by side configuration.

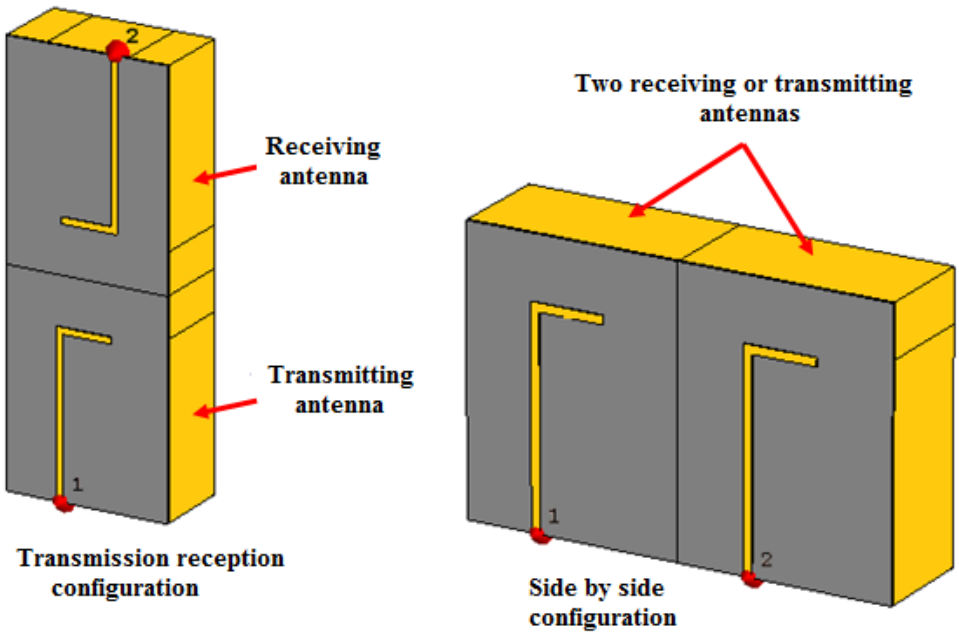

Figure 6.8: Studied antenna configurations: transmission-reception configuration (left), and side by side configuration (right)

The simulated return loss ($S11$) and the mutual coupling ($S21$) of the transmission-reception configuration with and without colon tissue for different distances D (6.9a from colon tissue is illustrated in Figure 6.9b. It is clear from the figures that these parameters are affected by the presence of the colon tissue. As the distance D between the antennas and the colon wall increases, the input impedance matching is improved. Also, the antenna resonant frequency decreases slightly as D increases. The antenna return loss is less than -15 dB for all simulated values of D, and the coupling between two antennas is always lower than -12 dB denoting an acceptable isolation between elements. As expected, the isolation improves as the distance between the antenna and the colon wall increases.

For the side by side configuration, the simulated return loss and the mutual coupling with and without colon tissue for different distances D are presented in Figure 6.9a. Similarly to the previous configuration, the antenna matching and the resonant frequency are affected by the presence of the colon tissue. In this case the antenna reflection coefficient is lower than -10 dBand the isolation is lower than -15 dB for all assumed values of D.

6.2.4 Fabrication and Measurement

Two identical antennas have been fabricated, one working as a transmitter and the other as a receiver. The antennas were connected to a two-port commercial Agilent performance net-

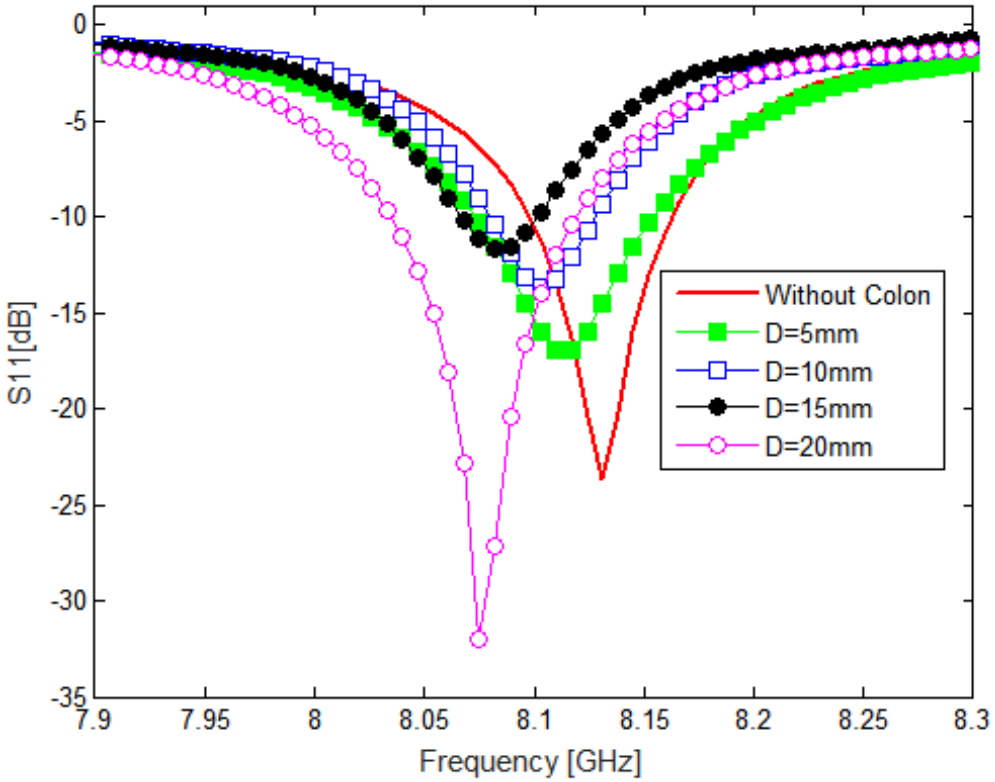

(a)

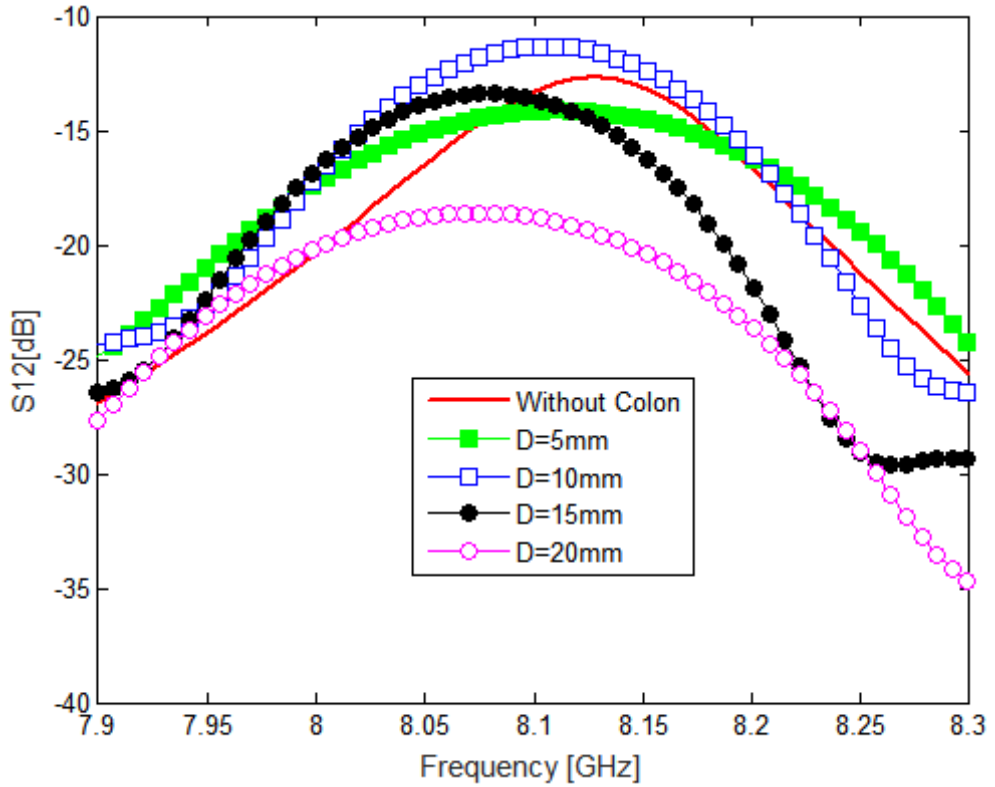

(b)

Figure 6.9: (a)Simulated return loss and (b) mutual coupling (bottom) for different values of D for transmission-reception configuration

work analyzer (PNA) with flexible coaxial cables to measure the S-parameters. Figure 6.11 shows a picture of the fabricated antennas. Figure6.12 shows the measured and simulated return loss for one antenna element without colon tissue. A slight difference can be observed between the measured and simulated return loss. This shift can be attributed to fabrication errors and a small displacement between the substrate and backing cavities [25].

The measured and simulated return loss and isolation for the transmission-reception configuration are illustrated in Figure 6.13. It can be observed that the simulated and measured results exhibit a good agreement. The small difference between them is possibly due to fabrication errors. The measured isolation is lower than -30dB while the simulated one is lower than -17 dB. This difference may be produced by the presence of two metal walls between the transmitting and receiving antennas in the fabricated applicator, whereas only one wall existed in the simulations. The measured isolation is lower than -25 dB for the transmission-reception configuration.

6.3 Summary

In this chapter, a U-slot cavity backed antenna element for endoscopy application is presented. The antenna is designed to operate at a frequency of 8.1GHz. Also, the proposed antenna is designed and optimized through parametric study to suit the restrictions of the application in terms of operating frequency as well as size. Furthermore, the isolation between two adjacent element have been studied since the proposed antenna is designed to operate in an array of sixteen elements wrapped around a cylinder. The simulated and measured results have shown very good agreement which validate the proposed design. The work presented in this chapter is published in:

1. Guardiola M, **Djafri K**, Challal M, Miguel A, Ballester G, Fernandez-Esparrach G, Camara O and Romeu J, *Design and Evaluation of an Antenna Applicator for a Microwave Colonoscopy System*, IEEE Transactions on Antennas Propagation, Jan.2019.

Bibliography

[1] Marta Guardiola, Santiago Buitrago, Glòria Fernández-Esparrach, Joan M O'Callaghan, Jordi Romeu, Miriam Cuatrecasas, Henry Córdova, Miguel Ángel González Ballester,

and Oscar Camara. Dielectric properties of colon polyps, cancer and normal mucosa: ex vivo measurements from 0.5 to 20 gh z. *Medical physics*, 2018.

[2] Quan Li and Zhongxiang Shen. Inverted microstrip-fed cavity-backed slot antennas. *IEEE antennas and wireless propagation letters*, 1(1):98–101, 2002.

[3] Weihua Tan, Leong Chuan Lee, and Zhongxiang Shen. A circularly polarized microstrip-fed t-slot antenna array on a conducting cylinder. *IEEE Antennas and Wireless Propagation Letters*, 5(1):507–510, 2006.

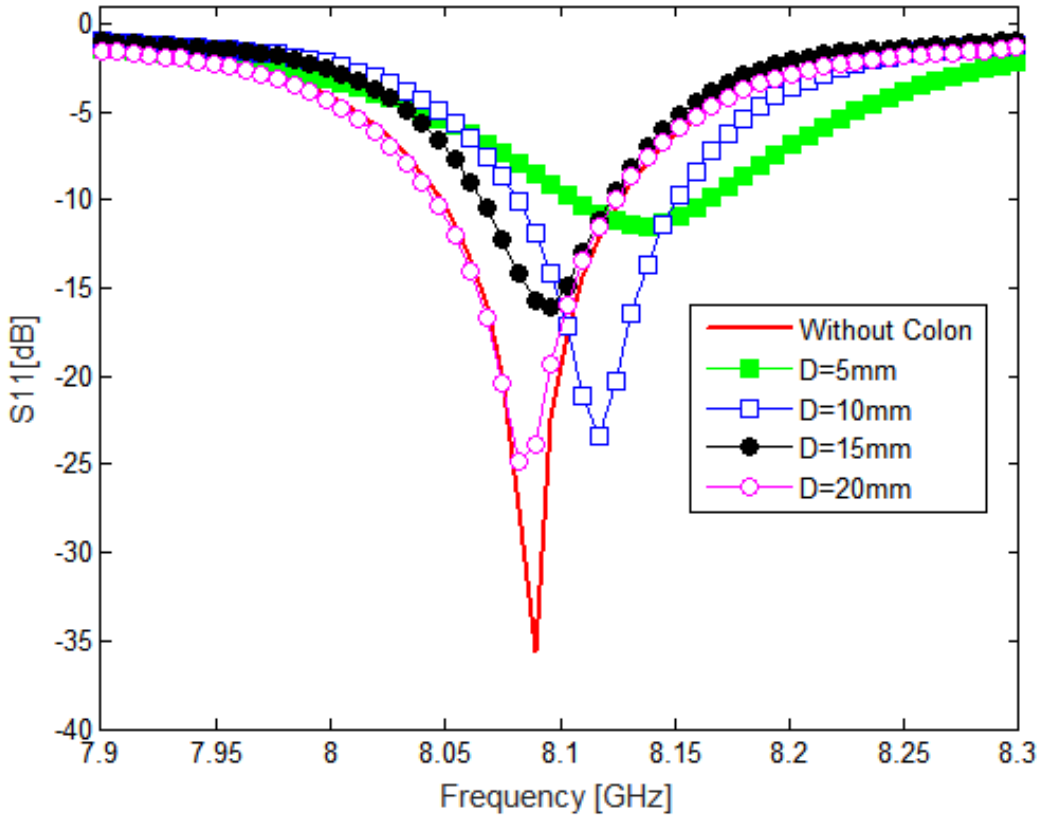

(a)

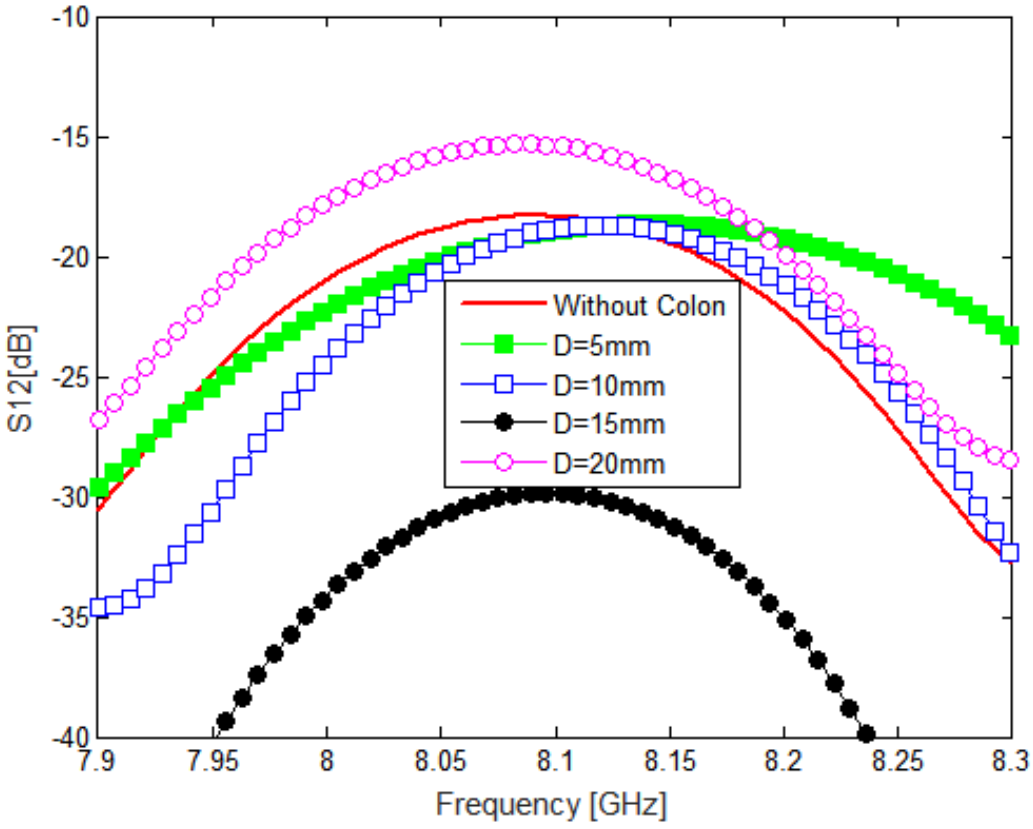

(b)

Figure 6.10: (a)Simulated return loss and (b) mutual coupling (bottom) for different values of D for side by side configuration.

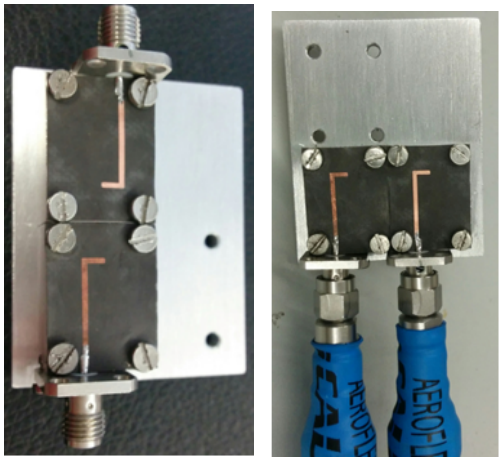

(a) **(b)**

Figure 6.11: Photograph of the realized antennas: (a) Transmission reception and (b) side by side configurations

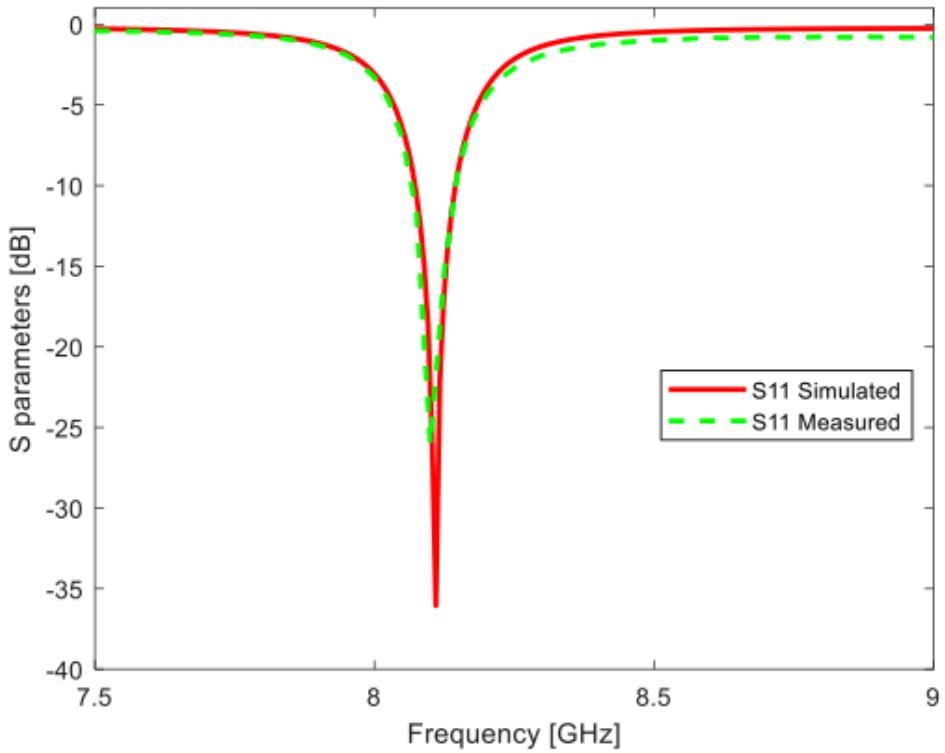

Figure 6.12: Simulated and measured return loss for one antenna element without colon tissue.

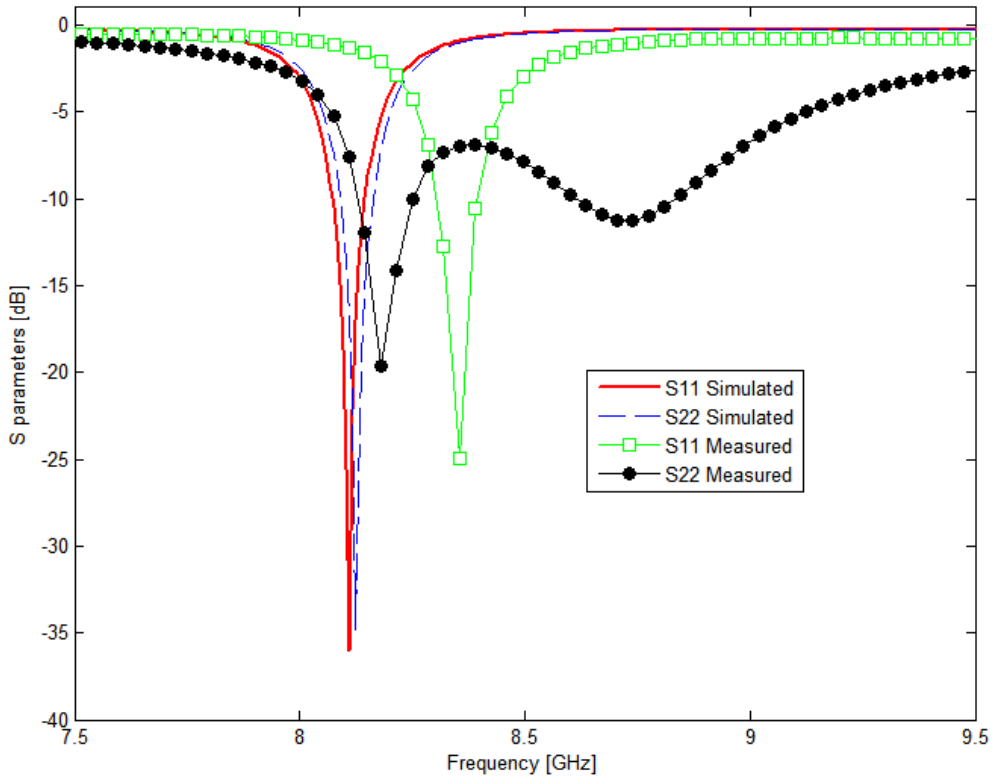

(a)

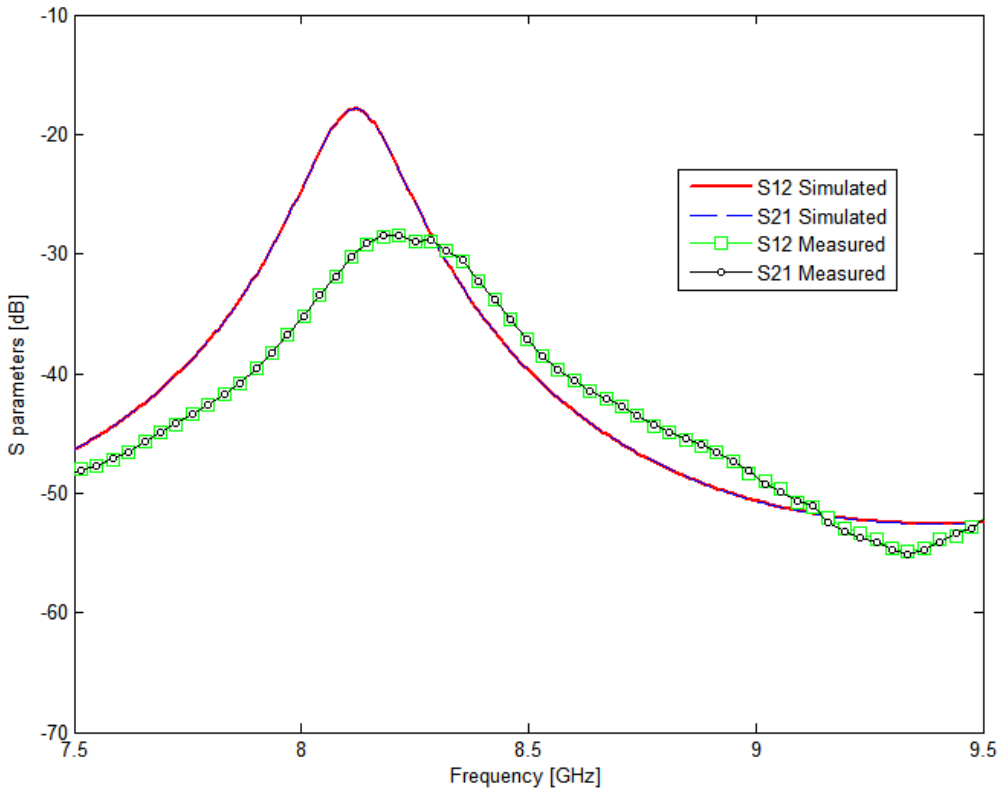

(b)

Figure 6.13: (a) Simulated and measured return loss and (b) isolation (bottom) for transmission-reception configuration without colon tissue.

Chapter 7

Conclusions and Suggestions for Further Work

Contents

This research work focuses on study, design, fabrication and measurement of miniaturized microstrip antennas. Different microstrip antennas for wireless applications have been proposed. In the first part, two designs of dual band miniaturized monopole antennas have been proposed. The first antenna design covers the 2.4 WLAN and the 3.5 GHz WiMAX band with a compact size while the second design covers two bands allotted to the RFID and GSM applications. The second part deals with the design of triple band miniaturized antennas. Two different designs have been proposed, both of them cover the 2.4.8 GHz WLAN and 3.5GHz WiMAX bands. In the last part, a miniaturized antenna structure for colonoscopy has been investigated. The proposed antenna meet the requirements of size of the intended application. All the proposed compact microstrip structures have been simulated, investigated, tested and compared to the previous published works.

7.1 Conclusions

In this thesis , new compact microstrip antennas have been studied , designed and tested for wireless and medical applications. These include first-order hexagonal fractal ring monopole antenna with a parasitic element, combination of three slotted fractal ring based monopole , concentric two fractal ring connected by a strip line monopole , and asymetric coplanar strip monopole and a U-slot microstrip fed antenna baked by a cavity for colonascopy application. For better insight of the multiband behavior and the operating mechanism, the

designed antennas have been investigated in details. The simulated S-parameters and current distributions on the radiating structure at different resonant frequencies have shown the dependence of the antenna shape and dimensions on the operating frequencies. Parasitic resonator embedded either within the radiator or in the ground plane to create multiband characteristic and achieve size reduction has shown satisfactory results in terms of antenna miniaturization and multiband behavior. Accordingly, the proposed designs are very compact and operate in dual and triple bands commercially useful which makes them well-sweated for the intended applications.

The first designed antenna consists of a first-order hexagonal fractal radiating ring coupled electromagnetically with a second fractal ring embedded in the ground plane. The resulted structure operates in dual band covering the 2.4 WLAN and 3.5GHz WiMAX applications. The radiation pattern of the antenna is omnidirectional for both operating bands. Furthermore, the antenna is very compact with an overall dimension of only $L \times W = 18.9 \times 13.3mm^2$ with a radiation efficiency of 91% and 97% at the first and second resonance respectively. The two bands can be tuned at any desired frequencies by controlling the geometrical parameters of the fractal radiating rings. The design has been simulated and tested connected to different standards of laptop ground planes and has shown very satisfactory results. In addition, to design a compact antenna and tune it to cover the RFID and GSM bands, three slotted fractal rings have been effectively combined. Two small identical fractal rings have been inserted inside the outer one to reduce the antenna size. Furthermore, the three rings have been loaded with slots such that the current is forced to flow from the outer ring to the inner one then again to the outer one. Hence, the current path have been effectively lengthened to achieve maximum size reduction and dual band operation tuned to the intended applications. This antenna structure has a compact size of $61 \times 41mm^2$n and exhibits an omnidirectional pattern in both operating bands. Consequently, the proposed antenna is perfectly suiteble for wireless application with a compact size and omnidirectional antenna pattern.

Two triple band compact antennas has been also proposed . The first design consists of a simple monopole strip connected to two branches in order to create multiple resonances. It has been fed using ACS technique to reduce the antenna overall size. The geometry of the branches have been chosen carefully to ensure compactness and to tune the resonances at the desired band namely WiFi 2.45 GHz, WiMAX 3.5GHz and 5.8 GHz WLAN. The first branch

has been chosen to look like a J-shape directed to the asymmetric ground plane whereas the second has been an open stub. The first resonance has been found to be controlled mainly by the length of J-shaped branch while the second resonant frequency which is centered at 3.5 GHz has been strongly dependent on the open stub length. The last resonance has been dependent on the main strip dimension of the monopole antenna. Furthermore the antenna has shown an almost omnidirectional radiation patterns at the three resonances with peak gains of -1.5 dB, 2.5dB and 4dB. Besides, the antenna has a very compact size of $14.6 \times 17.5mm^2$ which makes it a good candidate for wireless application. The second tri-band antenna has been designed using two concentric first-order hexagonal fractal rings connected to each other. This obtained topology has been found to operate in three ban covering the the 2.4GHz WLAN, 3.5 dB WiMAX and 5.6/5.8GHz WLAN applications. Omnidirectional patterns have been obtained at the resonant frequencies. Furthermore , the measured results of the antenna with a very compact size of $9.3 \times 17mm^2$ have shown good agreement with the simulated ones.

Furthermore, a compact antenna element has been designed and tested for colonoscopy application. Due to the restriction of size of the intended application, the proposed antenna consisted of a U-slot printed in the ground plane fed by an inverted L-shaped microstrip line. The shape of the slot is so chosen for miniaturization issue. The proposed antenna has been designed to operate in an array configuration of sixteen elements thus the isolation between element must be considered. For better isolation between the array elements, the antenna element has been backed by a cavity. The proposed design with dimensions of $14 \times 8.1mm^2$ has satisfied the requirements of the application and it has been tested. The simulated and measured results have shown good agreement which makes the proposed design an excellent candidate for colonoscopy application.

7.2 Suggestions for further work

The rapid development of wireless communication systems has given rise to a growing demand for compact multiband antennas. Thus, the design of the antenna must be improved. The following points discuss some possible future research directions for the work reported in this thesis:

- New size reduction techniques must be investigated to meet the requirement of size

and bands of the nowadays communication systems.

- The gain of the compact antenna should be improved using metamatrials.
- Investigate the use of the proposed designs for MIMO application.
- Implement and test the antenna array of sixteen elements for colonoscopy.